ABSTRACT

Title of Document: DENDRITIC INTEGRATION AND RECIPROCAL INHIBITION IN THE RETINA

William N. Grimes, Ph.D., 2008

Directed By: Professor Robert Walker, Department of Chemical Physics

The mammalian retina is capable of signaling over a vast range of mean light levels (~10^{10}). Such a large dynamic range is achieved by segregating signals into contrasting pathways and utilizing excitatory and inhibitory neural circuits. The goal of this study was to elucidate subcellular mechanisms responsible for shaping dendritic computation and reciprocal inhibition within the retinal circuitry.

Amacrine cells make up a unique class of inhibitory interneurons which lack anatomically distinct input and output structures. Although these interneurons clearly play important roles in complex visual processing, there is relatively little known about the ~30 subtypes. A17 amacrine cells have been shown to shape the time course of visual signaling *in vivo*. Intuition might suggest that a wide field (~400 µm) interneuron, such as A17, would provide long range lateral inhibition or center surround inhibition. However, using multi-disciplinary approaches, we have uncovered multiple mechanisms which underlie dendritic integration and synaptic transmission in A17 that allow it to respond with a high degree of synapse specificity.

Additionally, these mechanisms work in concert with post-synaptic mechanisms to extend the dynamic range of reciprocal inhibition in the inner retina.

DENDRITIC INTEGRATION AND RECIPROCAL INHIBITION IN THE RETINA

By

William N. Grimes

Dissertation submitted to the Faculty of the Graduate School of the
University of Maryland, College Park, in partial fulfillment
of the requirements for the degree of
Doctor of Philosophy
2008

Advisory Committee:
Professor Robert Walker, Chair
Jeffrey Diamond, Ph.D., NIH Advisor
Professor Michael Coplan
Professor Marco Colombini, Dean's Representative
Professor Michael Losert
Wei Li, M.D., Ph.D.

Dedication

I would like to dedicate this body of work to my family. Although not physically present, their love and support played a critical role in helping me to complete this eventful and enriching chapter of my life.

Table of Contents

List of Tables

List of Figures

Chapter 1: Introduction

Introduction to Interdisciplinary Neuroscience

Physicists have had many essential roles in shaping the field of neuroscience. From the invention of the patch clamp technique (for recording electrical responses in single neurons) and two-photon microscopy, to the discovery of quantized synaptic transmission (neurotransmitters are released in discrete packets), physicists have made a tremendous impact by applying their in depth understanding of the fundamental laws that govern nature and a high level of quantitative rigor. Why have physicists been drawn to the field of neuroscience? The answer is simple: The most sophisticated computer on earth is right inside our own skull, yet its incredible complexity keeps us from fully understanding its inner workings. Due to this high level of complexity physicists have incorporated a plethora of interdisciplinary techniques into their repertoire because using a single technique or discipline is simply not sufficient.

My dissertation research aims to address some very fundamental questions about basic computation and the subcellular mechanisms which underlie this computation in the visual system. Because of the system's high level of complexity questions are focused to particular levels (i.e. single connections between neurons - synapses, single cell computation or complete intact circuitry) and multi-disciplinary

approaches have been incorporated to elucidate their answers. This body of work focuses on the retina, and in particular I ask how biophysical membrane properties of individual neuron classes shape signaling within the neural circuitry. The research focuses on night vision or *scotopic vision*, our ability to see under very dimly lit situations. In fact, it has been demonstrated that we can perceive the absorption of single photons (Hecht, 1942). Under these conditions, photons are very scarce but the retina manages to reproducibly detect these photons using distinct and specialized ultra-sensitive circuitry, composed of unique neurons which signal to one another via combinations of excitatory and inhibitory synapses. The scotopic circuitry is termed the rod pathway because the individual neurons which absorb single photons and transduce the signal into an electrical response are called *rod photoreceptors*. Here, I will not focus on this well documented phenomenon but instead will focus on processing of the rod-driven signal by second and third order neurons in the rod pathway (Figure 1). We will discuss the literature-to-date describing the synaptic signaling between these second and third order neurons, biophysical membrane properties of individual neuron types, multi-neuron circuitry and physiological paradigms. After a thorough introduction to the system, the structure and function of the A17 amacrine cell (one of the third order neurons) is assessed using combinations of two-photon calcium imaging, electrophysiology, pharmacology and computational approaches. My specific aim is to study the mechanisms which underlie excitatory synaptic transmission, reciprocal inhibition and dendritic integration within the A17 amacrine cell in an attempt to gain insight into its role in visual processing.

Figure 1

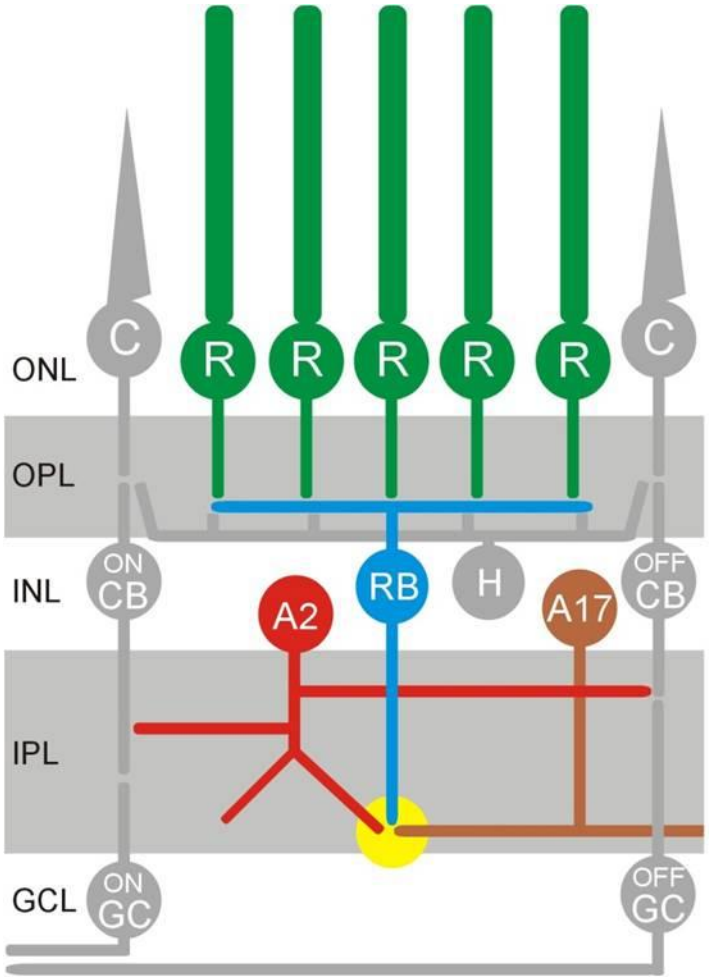

Error! Reference source not found.. Schematic of the neural circuitry of the rod-pathway. Approximately 25 rod photoreceptors converge onto a single type of rod bipolar (RB) cell. The RB cell transmits the graded response into the inner plexiform layer (IPL) where it makes synaptic contacts the AII (A2) and A17 amacrine cells. While the A17 provides reciprocal inhibition to shape the time course of glutamate release form the RB cell, the AII conducts the feed forward signal onto the brain through the cone bipolar (CB) cells. Yellow circle indicates the primary synapse discussed herein.

Rod pathway structure and function

Sensory systems of the central nervous system have the fundamental challenge of needing to maintain sufficient sensitivity (signal to noise) while avoiding saturation of the signaling capacity of the individual cellular components within the circuitry. Adaptation at various locations within the neural circuitry provide critical gain controls that enable signals to be discerned from dynamically changing noise levels (partially attributable to convergence in the circuitry). Due to its well-established circuitry and accessibility, the mammalian retina is an ideal system for studying the relationship between the physiology of individual neuronal components and circuit function. This highly evolved, biological light detector is capable of converting both the spatial and temporal aspects of the imposed light signal into a format the brain can interpret. Subsequent higher order processing of this signal gives rise to conscious perception of the visual world. The retina is also highly adaptive and can produce functional outputs in response to the large range of mean physiological light levels we experience in the visual world on a daily basis (~10-12 orders of magnitude). Individually insufficient, a single photoreceptor cell, rod or cone, has a dynamic range of only two orders of magnitude in response to a flash of light (this means an individual photoreceptor response saturates when a flash of light is greater than two log unit above the mean (background) light level; reviewed by Shapley, 1997). The discrepancy between the limited cellular response and the wide response range necessary for diurnal (day and night) vision is partially mitigated by exploiting differences in subcellular photoreceptor properties (i.e. intrinsic noise levels which gives rise to sensitivity ranges and adaptation). The distinct spectral and sensitivity

properties of individual photoreceptors, along with their unique circuitries, allow the retina to utilize specific neuronal circuits (with some overlapping components) for general ranges of mean light levels, i.e. daylight, twilight and starlight conditions. While the cone-driven pathway mediates photopic (daylight/daytime) vision, the rod-pathway is almost entirely responsible for scotopic (starlight/night) vision. The rod pathway is optimized for reliability and maximal sensitivity (Baylor *et al.*, 1979; Baylor *et al.*, 1984; Doan *et al.*, 2006), not for spectral range and acuity. The remainder of this introduction will focus primarily on the circuitry and cellular components of the rod pathway (Figure 1).

Upon stimulation (by as little as one photon) the rod hyperpolarizes its membrane potential and slows the tonic release of the excitatory neurotransmitter glutamate onto the postsynaptic rod bipolar cell (RBC, this is the one and only second order neuron in the rod pathway; Kolb and Nelson, 1983). Through this synaptic connection, the RBC is subsequently depolarized in a graded manner (analog response), resulting in relatively proportional output (i.e. neurotransmitter release). The RBC output primarily drives AII and A17 amacrine cells (third order neurons in the rod pathway) in the inner plexiform layer (IPL) via excitatory glutamatergic chemical synapses (Kolb and Famiglietti, 1974). Although these two cells are both classified as amacrine cells, functionally and morphologically (structurally) they are very different. The rod pathway does not make a direct connection to the output cells (ganglion cells) of the retina. Instead, it passes its signal through 'on' and 'off' cone bipolar cells ('on' cells respond to light onset whereas 'off' cells respond to light offset) and their associated ganglion cells. The signal is transmitted to the 'borrowed'

cone pathway via the AII amacrine cell (Figure 1). The AII feeds its 'on' signal forward, making sign-conserving (depolarized cell produces a depolarized response in the next cell in the circuitry) gap junction (electrical) synapses onto 'on' cone bipolar cell terminals and sign-inverting chemical (glycinergic) synapses onto 'off' cone bipolar cells. In contrast, the A17 amacrine cell provides negative feedback to the presynaptic RBC through an inhibitory (GABAergic) synapse (Nelson and Kolb, 1985; Hartveit, 1999; Chavez *et al.*, 2006). Not only has this synapse been theorized to be the ideal location for gain control in the rod pathway (Dunn *et al.*, 2006; Dunn and Rieke, 2006), but is also thought responsible for setting the time course of contrast adaptation (Manookin and Demb, 2006). This introduction will primarily focus on reviewing previous literature concerning synaptic signaling at the RBC/AII/A17 dyad connection, biophysical properties of AII and A17 amacrine cells at the single cell level, and participation of AII and A17 in the rod-driven network. Additional focus will aim at identifying remaining questions about these particular topics and potential experiments for addressing them.

The Rod Bipolar Cell Dyad

As mentioned above, the rod bipolar cell makes a sign-conserving excitatory synaptic dyad with AII and A17 cells (Figures 1 and 2). Understanding the physiology of AII and A17 requires an understanding of the functional input from the RBC. The RBC bouton (nerve terminal) contains a specialized thin structure attached to the presynaptic membrane that extends perpendicularly into the cytoplasm. This structure, known as the *ribbon*, has many tiny neurotransmitter-filled vesicles tethered

in rows along its length (reviewed by Lagnado, 2003 and Sterling and Matthews, 2005). Also found in the cochlea (of the ear), ribbons are thought to be fundamental to analog central nervous system (CNS) pathways. The rate of vesicle fusion at a ribbon synapse depends on the strength of the membrane depolarization. However, previous work at the RBC ribbon synapse has shown that strong sustained depolarizations, leading to high concentrations of presynaptic intracellular calcium, result in transient excitatory postsynaptic currents (EPSCs) in AII amacrine cells (Singer and Diamond, 2003). This non-linear effect on the temporal aspects of electrical signaling is partially accounted for by the depletion of a readily releasable pool (RRP) of transmitter filled vesicles (see glossary). The RBC's RRP is thought to be the bottom most row of vesicles that are attached to both the ribbon and the presynaptic membrane. The RRP of vesicles can be depleted in ~4 ms but requires nearly 4 s to refill (Singer and Diamond, 2006). This fast release and slow recovery results in a form of short term synaptic depression (weakening of the signal transfer) which might be important for gain adjustment at light levels too low to cause rod adaptation (a known phenomenon). Other reports have demonstrated that quantal transmission (of neurotransmitter-filled vesicles) from the RBC obeys binomial statistics (Singer *et al.*, 2004), an observation first used in 1954 by biophysicists to correctly describe quantized synaptic transmission at the neuromuscular junction (Del Castillo and Katz, 1954). This approach led to the conclusion that the rod bipolar cell ribbon synapse is capable of coordinated multi-vesicular release (MVR; Singer *et al.*, 2004). This means that multiple rather than single docked vesicles are prompted to exocytose simultaneously upon stimulation. This might provide the AII with a

method for discriminating a single photon response from the noise attributed to convergence in the rod circuitry.

In summary, AII and A17 amacrine cells receive a quantized, excitatory input which is proportional to the RBC's graded membrane potential. A strong sustained RBC depolarization elicits a large transient postsynaptic response which decays to a smaller steady state component. The large transient component of the response correlates to a fast depletion of the readily releasable pool of transmitter filled vesicles whereas the steady-state component reflects a balance between depletion and replenishment of the pool. Additionally, evidence for coordinated MVR at the RBC might suggest that postsynaptic amacrine cells can readily distinguish between single and double events.

Figure 2

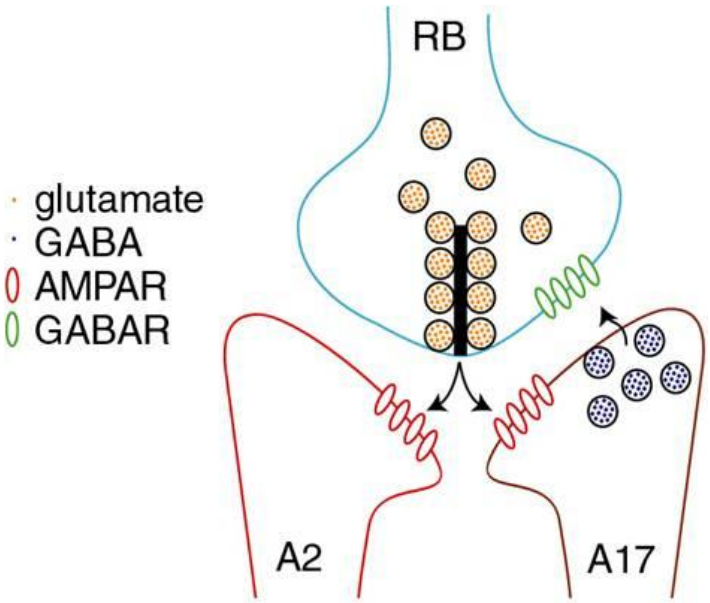

Figure 2. Schematic for RBC dyad synapse.

The RBC feeds its excitatory transmitter (glutamate: orange) forward onto the postsynaptic amacrine cells. Upon stimulation A17 provides a reciprocal negative feedback signal (GABA: blue) to the RBC.

AII amacrine cell

Unlike the majority of CNS neurons, amacrine cells lack distinct axons. Without a standard specialized output region, amacrine cells must incorporate unorthodox approaches to derive functional outputs. Identifying biophysical properties of single cell membranes, static and active conductances, and intracellular calcium dynamics is important for understanding a cell's physiology and contributions to network processing. An example of AII morphology is shown in Figure 3. In general, the AII cell body lies in the innermost portion of the inner nuclear layer (INL) and has a single dendritic stalk extending into the inner plexiform layer (IPL). Between sublaminas 2 and 3 this dendritic stalk branches into arboreal dendrites that terminate in sublamina 5 (where RBCs make their synapses). Electron microscopy studies have shown that arboreal dendrites in sublamina 5 receive excitatory input from RBC ribbon synapses (Famiglietti and Kolb, 1975). Futhermore, this excitatory synapse uses specialized AMPA receptors (AMPARs; see glossary; Singer and Diamond, 2003) which have faster kinetics, larger single channel conductances, are highly permeable to calcium ions and, at other synapses, may be involved in synaptic plasticity (Plasticity is phenomenon in which synapses, or connections between cells, are strengthened or weakened. This is thought to be the basis for memory formation. reviewed by Isaac *et al.*, 2007). To date no forms of plasticity observed in the inner retina have been correlated with expression of functional calcium permeable AMPARs (CP-AMPARs).

Additionally, so-called lobular appendages extend for short distances from the single dendritic stalk in sublaminas 1 and 2. Although these structures have been

reported to receive a small number of inputs from 'off' CBCs (Strettoi *et al.*, 1992), electron microscopy studies have shown that these lobular appendages contain transmitter filled vesicles and make inhibitory synaptic contacts onto 'off' CBCs (Famiglietti and Kolb, 1975). The AII amacrine cell can range from 20-70 μm in diameter and 50-100 μm in length and the sites of excitatory input and inhibitory output are typically >20μm apart (Figure 3). In addition, vesicular neurotransmitter release is calcium dependent at all chemical synapses in the CNS. Considering this information, it is unlikely that calcium influx through CP-AMPARs alone leads to increases in intracellular calcium at the lobular appendages sufficient for triggering transmitter release. To overcome this obvious dilemma, AIIs likely fire propagating action potentials (aka spikes) which traverse the AII's surface area and trigger voltage-gated calcium channels (VGCCs) in the lobular appendages. Typically, calcium influx through VGCCs located close (<200 nm) to the release machinery results in vesicular transmitter release. Independent reports have confirmed that AIIs fire spikes in response to glutamate application at the arboreal dendrites (Tamalu and Watanabe, 2007; Veruki and Hartveit, 2002a). Spikes are a result of fast sodium channel activation (fast membrane depolarization), fast sodium channel inactivation (initial repolarizing of the membrane), and potassium channel activation (speeds repolarization and produces afterhyperpolarizations and/or refractory periods). Additionally, L-type voltage-gated calcium channels, specifically $Ca_v1.3_{\alpha1}$, have been localized to the lobular appendages of AIIs (Habermann *et al.*, 2003). L-type channels, with very slow inactivating kinetics, have been associated with graded potential neurons and tonic transmitter release. Overall, finding L-type VGCCs,

instead of fast inactivating VGCCs, at the inhibitory output synapses of AII is surprising in light of several experimental observations regarding temporal characteristics of the AII response. Sustained RBC depolarization leads to large but transient responses in the AII suggesting a speeding of the rod signal (Singer and Diamond, 2003; Nelson, 1982). Additionally, the rising phase of light evoked responses recorded in AII are nearly twice as fast as those recorded in the presynaptic RBCs and get faster with increased light intensities (Nelson, 1982). The AII responds physiologically by generating spikes frequencies that are proportional to the concentration of glutamate applied indicating that AIIs could transmit high frequency information (Tamalu and Watanabe, 2007). Together these results would suggest that at the AII output synapse onto 'off' CBCs, rod signaling is *slowed* by the integration of action potential patterns by slowly inactivating L-type VGCCs. If true, temporal properties of the incident signal could get converted into correlated amplitudes, not unlike a time-to-amplitude converter.

As previously mentioned, AIIs also make gap junctional (electrical synapses) connections with 'on' CBCs as part of the feed forward signaling of the rod pathway (Kolb and Famiglietti, 1974). Often found in clusters, functional gap junctions are formed between pairs of neurons consist of two complimentary connexin proteins. When the Connexin36 gene is deleted in a transgenic mouse, rod responses are no longer transmitted to the on ganglion cells (Deans *et al.*, 2002), thus playing an essential role in rod signaling. Tracer coupling studies have revealed that gap junctions between AIIs and 'on' CBCs are modulated by nitric oxide and cyclic GMP agonists (agonists are pharmacological reagents which activate a particular reaction

whereas antagonists are compounds which block a particular reaction; Mills and Massey, 1995) and could act physiologically to expand or contract the spatial extent of the electrically coupled network. One or both of these compounds could be used to switch off the AII to 'on' CBC network under photopic conditions. This is important because large networks of electrically coupled cells would compromise the higher acuity enabled by higher photon absorption rates. Paired whole-cell recordings from the two cells have revealed several fundamental biophysical properties of the AII to CBC gap junction in rat (Veruki and Hartveit, 2002b). Under light adapted conditions measurements of total gap junction conductance under voltage clamp were relatively large (~1.2 nS). However, due to differences in input resistances (proportional to the cell's total membrane surface area) of the two cells (R_{CBC}~2.5xR_{AII}), potential changes in the AII produce larger potential changes in the 'on' CBCs than in the reverse direction. Both the coupling coefficient and phase of the response are dependent on input frequency and are significantly altered over 10Hz (therefore acting as a low-pass filter; Veruki and Hartveit, 2002b).

AIIs also form direct gap junctions with one another to form an additional electrical network that is also dynamically modulated by biochemical signaling. Under scotopic conditions, when photons are extremely scarce, AII coupling is weak producing a smaller network. Reducing static conductances could act to maximize the transfer function of individual AIIs. Under mesopic conditions (the range of light conditions between photopic/daytime and scotopic/night conditions; typically associated with dusk) , coupling of AII-AII network is enhanced. This allows for summation (synchronized depolarizing inputs often add to produce stronger

depolarizations) of synchronous activity and reduced sensitivity to asynchronous background noise (Bloomfield and Volgyi, 2004). Dopamine release in the IPL under photopic light conditions is responsible for triggering the cascade of events that leads to the uncoupling of the AII network (Hampson *et al.*, 1992).

In summary, AII amacrine cells are responsible for the feed forward signaling of the RBC response. This could be accomplished by converting inputs into spikes and dividing the signal into 'on' and 'off' channels via gap juctions with 'on' CBCs and inhibitory synapses with 'off' CBCs, respectively. AIIs also form their own gap junctional network. The strength of its coupling is dependent on mean light levels and specifically, the neurotransmitter dopamine is responsible for its uncoupling.

Figure 3

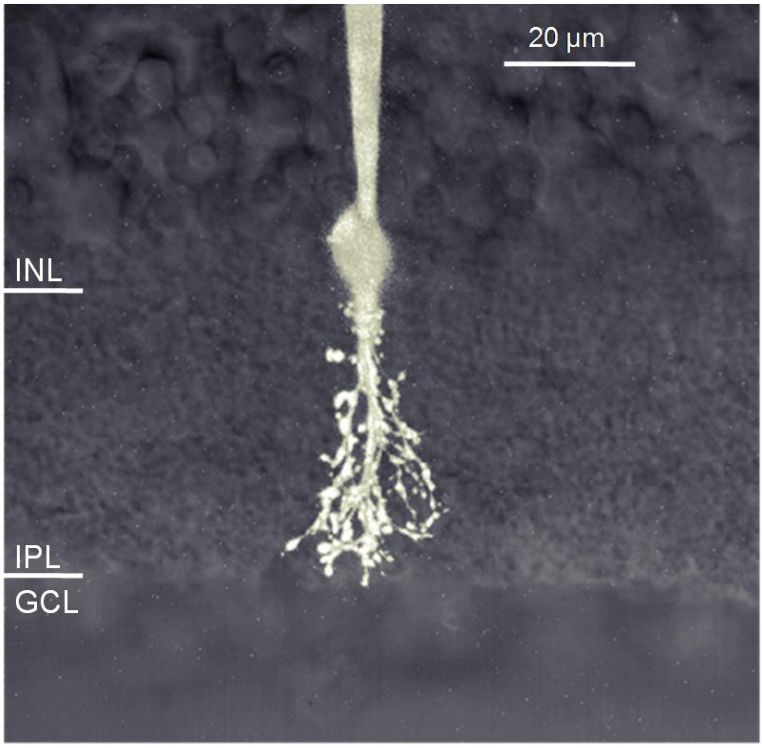

Figure 3. AII amacrine cell.

3D spatial reconstruction using two-photon microscopy (800nm) of Alexa594 (40µM; loaded through the recording pipette) and superimposed on a single IR differential interference contrast image of the retinal slice.

A17 amacrine cell

Although the A17 is one of two amacrine cells receiving the majority of the RBC input, only a handful of reports have made significant progress elucidating its functional characteristics. The first light-evoked responses recorded in A17 had spectral properties matching AII recordings and were abolished in photopic light conditions, suggesting that A17s are predominately driven by the rod pathway (Nelson and Kolb, 1985). The dome-like cell body of A17 sits on the INL border, directly adjacent to the IPL. From the soma many fine dendrites extend into the distal most parts of the IPL, producing a dendritic tree that is >300μm in diameter. These dendrites infrequently branch but typically form swellings (or varicosities) in ~10-20μm intervals along their lengths (Figure 4 and Table 3).

The first electron microscopy studies in the cat retina revealed that A17 varicosities receive excitatory input from RBC ribbon synapses and provide reciprocal inhibitory (negative) feedback to the same RBC terminals (Kolb and Famiglietti, 1974; Nelson and Kolb, 1985). A functional reciprocal inhibitory connection proved difficult to observe and was not reported until 1999 in rat (Hartveit, 1999). The report demonstrated that evoked inhibitory feedback to the RBC was blocked independently by both antagonists of excitatory transmission (presumably acting on the A17) and antagonists of inhibitory transmission (presumably acting on the RBC terminal). More recent reports have further investigated this reciprocal feedback in rat and found it to be dependent on calcium influx through CP-AMPARs (Chavez *et al.*, 2006). This novel form of synaptic

transmission could prove capable of producing highly localized inhibition, possibly on the level of a single synapse. Some evidence supports this idea. Immunocytochemistry studies (a molecular biology technique used to test tissue for specific protein expression) in rabbit provided evidence that each individual A17 varicosity contacts a distinct RBC terminal (Zhang *et al.*, 2002). Serial electron micrograph reconstructions of a varicose amacrine cell in cat concluded that each varicosity contained one synaptic input and one synaptic output. Furthermore, a simplified passive steady state electrical model suggested that varicose swellings could act to maximize local depolarizations and minimize distant ones (Ellias and Stevens, 1980). Just as in the AII, active conductances can greatly contribute to attenuation or amplification of propagating changes in membrane potential and can have profound effects on output. Reports on A17 spiking are inconsistent. Intracellular A17 recordings from cat failed to detect spiking patterns (Nelson and Kolb, 1985) while recordings from rabbits detected spikes in one but not both of the two homologous cells (Bloomfield, 1996). Current-clamp recordings from A17 cells in rat retinal slices are unable to detect spikes in response to somatic current injections or synaptic stimulation (Figure 9). However, voltage-clamp recordings revealed the presence of fast-activating, fast-inactivating, TTX-sensitive currents, indicative of voltage-gated sodium channels (Figure 7). While not sufficient for spike production, these sodium channels might be involved in spreading synaptically evoked depolarizations to neighboring varicosities. These topics are further addressed in Chapter 3. In addition to sodium channels, simultaneous two-photon calcium imaging and intracellular voltage-clamp recordings in rat retinal slice have

revealed the presence of L-type calcium channels in the varicosities and soma of A17 (Figure 14). Determining whether or not these channels help drive synaptic transmission in A17s is important for understanding the cell's physiology and network effects and is to be discussed in Chapter 4.

Very few studies have focused on A17 contributions to network behavior. A report from 2003 demonstrated that ablation of A17s in rabbit by the toxic serotonin analog 5,7-DHT enhanced the time course of the b-wave component in ERGs (reflecting bipolar cell activity) suggesting that A17s act to shorten the time course of the RBC signal *in vivo* (Dong and Hare, 2003). However, in rat, reciprocal feedback to the RBC is predominately mediated by $GABA_A$Rs (Singer and Diamond, 2003; Chavez *et al.*, 2006). In mouse retina, $GABA_C$Rs on the terminals of RBCs act to truncate glutamate release, making responses in postsynaptic cells more transient. In contrast, $GABA_A$Rs and glycine receptors affect the initial release of glutamate and therefore reduce the amplitude of the EPSC (Eggers and Lukasiewicz, 2006a). These facts taken together might suggest that reciprocal feedback in rat modulates the gain of RBC synaptic transmission, but not its temporal aspects. Considering the wide dendritic (and receptive) field of the A17, one might expect that it could spatially and temporally integrate input and provide a proportional output to RBCs. Careful experiments using two-photon uncaging of glutamate on single varicosities while recording calcium fluorescence responses (as an indication of output) in varicosities along a dendrite could address some of these questions.

Figure 4

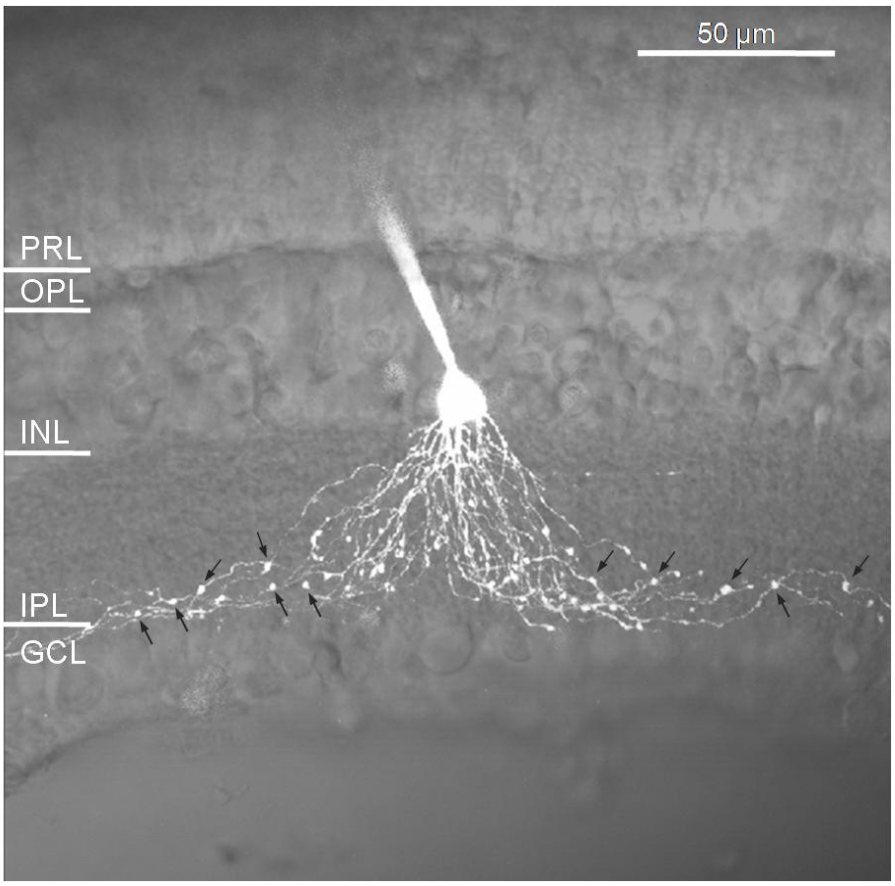

Figure 4. A17 amacrine cell.

3D spatial reconstruction using two-photon microscopy (λ_{exc} = 800nm) of Alexa594 (40µM; loaded through the recording pipette) and superimposed on a single IR differential interference contrast image of the retinal slice. Black arrows indicate examples of synaptic feedback varicosities.

Rod Pathway Amacrine Cells Other Than AII and A17

It is likely that other amacrine cells are involved in the rod pathway. In 1983, Kolb and Nelson observed rod-level light responses in three other amacrine cells, the A6, A8, and A13. These cells had similar morphology to the AII but produced hyperpolarizing responses to light onset (Kolb and Nelson, 1983). Electron microscopy studies using antibodies (with undetermined molecular targets) identified a subset of putative amacrine cells making reciprocal synapses with RBCs. These cells also made apparent synaptic contacts with 'on' CBCs and both 'on' and 'off' alpha ganglion cells (Sterling and Lampson, 1986). The functional importance of these additional amacrine cells has not yet been demonstrated.

Aims

Relatively little is known about the nearly 30 amacrine cell types with the exception of the starburst amacrine cell and the AII amacrine cell. It is clear that without a more typical neuronal morphology, consisting of distinct input and output regions (dendrites and axons, respectively), that this class of neurons uses very atypical approaches to signaling. Therefore to make significant progress in understanding the physiology of these poorly understood interneurons it is important to first thoroughly characterize the subcellular components which include ligand and voltage-gated ion channels, intracellular calcium stores and synaptic mechanisms as well as the unique morphological features. Once obtained, this information can be used to build a working model of cell physiology and to design experiments to test the input/output functions. Where technical limitations exist that limit the questions

that can be asked experimentally, computational models, based on experimental evidence, can be utilized to extend our understanding of signaling characteristics and to make predictions for future experimental tests.

This body of work focuses on one particular amacrine cell in the scotopic pathway, the A17 amacrine cell. The aim of Chapter 3 is to understand the extent to which A17 amacrine membranes are excitable and how these membrane properties and the average anatomical structure influence the cellular input/output function. Specific experimental questions to be addressed include: 1) Do A17 amacrine cells express the functional Na_v channels that would be necessary for action potential signaling, and if so, what are their biophysical characteristics? 2) Do A17 amacrine cells express K_v channels and what are their biophysical properties? 3) Are A17 amacrine cells capable of firing action potentials? 4) If A17 amacrine cells express Na_v channels, how do they impact dendritic signaling? The answers to these scientific questions led to new questions which were impossible to address with currently available experimental techniques. Therefore quantitative analysis of 3-dimensional A17 reconstructions and electrophysiology measurements were incorporated into an electrotonic model of the A17 amacrine cell. Questions to be addressed with this model include: 1) How do varicose structures influence signaling along a dendrite? 2) How are synaptic response amplitudes influenced by location on the dendrite and how is this affected by dendritic diameter? 3) How do synaptic potentials spread within the thin non-branching dendrites of A17? 4) To what extent are A17 dendrites electrically isolated? The answers to these questions provide a new

framework for understanding the input/output function of A17 and will then be interpreted in the context of reciprocal and lateral inhibition.

As previously mentioned, a recent report from our lab has provided evidence for a novel mechanism for triggering the reciprocal release of GABA transmitter back onto the RBC terminal which can occur independently of canonical voltage-dependent mechanisms (i.e. Ca_v channels) . In Chapter 4 we expand on these original finding and describe several additional levels of complexity which regulate reciprocal GABA release. 2-photon calcium imaging, electrophysiology, neuropharmacology, immunohistochemistry and computational modeling approaches are used to answer question regarding calcium dynamics in individual varicosities and the pre- and postsynaptic electrical signaling which underlie reciprocal inhibition. Specific questions to be addressed include: 1) Are Ca_v channels expressed in A17 synaptic feedback varicosities and, if so, what are their biophysical characteristics? 2) If Ca_v channels are colocalized with synaptic feedback machinery, is this source of calcium biochemically isolated from sources known to trigger release, such as intracellular calcium stores? 3) What inhibitory conductances are present in synaptic feedback varicosities, and what are their biophysical characteristics? 4) How do inhibitory conductances influence excitatory synaptic transmission to A17s? 5) How do inhibitory conductances modulate reciprocal GABA release and under what conditions? The experiments expand on our current understanding of the mechanisms of reciprocal inhibition from A17 amacrine cells as well as providing insight into novel interactions that influence dendritic signaling.

Recent evidence suggests that gain control under dim light conditions occurs independently at individual RBCs (Dunn and Rieke, 2008). With this in mind I intend to use the questions aforementioned to test two particular hypotheses. First, under dim light conditions A17 amacrine cells provide reciprocal inhibition in a synapse-specific manner, thus maintaining the independence of RBC gain controls. This highly compartmentalized form of reciprocal synaptic signaling is made possible by colocalization of the excitatory input machinery and the inhibitory output machinery to individual varicosities (Nelson and Kolb, 1985; Zhang *et al.*, 2002), minimal contributions from Na_v channels to membrane exitability, high axial resistance between feedback varicosities, attributable to thin dendritic diameters, and intravaricosity inhibitory conductances that shunt synaptic depolarizations. Second, multiple biochemical and biophysical mechanisms including Ca_v channels, large conductance calcium-activated potassium channels (BK), and two types of postsynaptic inhibitory receptors with distinct affinities for GABA and dramatically different response kinetics work in concert to provide RBCs with an appropriate range of inhibitory responses for signaling between neurons which respond with analog responses. All-in-all, I aim to elucidate the physiology of the A17 amacrine cell by studying its abilities to integrate excitatory synaptic inputs, compartmentalize electrical and biochemical signals and respond with the correct inhibitory release of inhibitory neurotransmitter.

Chapter 2: Methods

Electrophysiology

Solutions and Dissection

Retinal slices were prepared from juvenile (P17-21) Albino rats (Sprague-Dawley). Rats were euthanized by decapitation following isoflurane (Baxter, Illinois, USA) anesthesia. Immediately after enucleating, the cornea, lens, vitreous and sclera (in order) were removed while submerged in artificial cerebrospinal fluid (ASCF) that contained (in mM): 119 NaCl, 26 NaHCO3, 1.25 Na2HPO4, 2.5 KCl, 2.5 CaCl2, 1.5 $MgSO_4$, 10 glucose, 2 Na-Pyruvate, 0.5 Ascorbic acid, 4 Na-lactate bubbled continuously with carbogen (95% O_2/5% CO_2). The final osmolarity of the ACSF was checked with a vapor pressure osmometer (Wescor, Utah, USA) and adjusted to 290 mOsm if necessary. Using a scalpel, the retina was halved and a rectangular peripheral piece (~2x3 mm) was cut and placed on a clean slide. After removing excess solution, was embedded in a heated (39-41º C) agarose type VII solution (3% in ASCF with HEPES substituted for NaHCO3) and immeadiately cooled. The embedded retina was then glued to a small agar block and mounted in a Vibratome slcicing chamber (Vibratome Corporation, St. Louis, MO) where 200-210 μM slices were cut perpendicular to the retinal surface. Retinal slices were collected and stored at room temperature. Retinal slices could be maintained for up to 6 hours in ASCF

bubbled continuously with carbogen and under normal operating laboratory light conditions (light-adapted).

For patch electrode recordings, retinal slices were placed in a microscope recording chamber that was continuously superfused with room temperature ACSF. The associated gravity-driven drip system allowed the carbogen-equilibrated ACSF to flow at a rate of 1-2 ml/min. Visualization of the retinal slice was achieved by infrared differential interference contrast (IR-DIC) using an upright Zeiss microscope (40x objective) with attached camera which aided in guiding the patch electrode to the cell type of interest. Whole-cell voltage-clamp recordings were made from RBCs using pipettes (~7-9 MΩ) containing (in mM): 100 Cs methanesulfonate, 20 TEA-Cl, 10 HEPES, 1.5 BAPTA, 10 Na phosphocreatine, 4 Mg-ATP, 0.4 Na-GTP, 10 L-glutamic acid and 0.02 Alexa-488 hydrazide (pH 7.35). RBC access resistance was 25-50 MΩ and was left uncompensated. Unless otherwise noted, whole-cell voltage-clamp recordings were made from A17s using pipettes (~5-6 MΩ) containing (in mM): 100 Cs methanesulfonate, 20 TEA-Cl, 10 HEPES, 10 EGTA, 10 Na phosphocreatine, 4Mg-ATP, 0.4 Na-GTP and 0.04 Alexa-594 hydrzide (pH 7.35). Potassium-based internal for A17s contained (in mM): 100 K methanesulfonate, 20 TEA-Cl, 10 HEPES, 2 EGTA, 10 Na phosphocreatine, 4Mg-ATP, 0.4 Na-GTP and 0.04 Alexa-594 hydrzide (pH 7.35). A17 access resistance was ≤30 MΩ (see Table 2 for examples) and was left uncompensated. Patch solutions were stored on ice and passed through a 4-mm nylon syringe filter (Nalgene, NY, USA) prior to filling of the patch pipettes. All neuropharmacology reagents were purchased from Tocris or Sigma, with the exception of TTX (Alabone Labs, Israel). These drugs were prepared

as stock solutions at millimolar concentration and stored at –20°C. Each day aliquots of stock solutions were freshly dissolved in ACSF solution just prior to the experiment. On the basis of solubility drugs were dissolved in DMSO, water or NAOH. Most pharmacological agents were applied via the superfuse solution. In general, to assure equilibrated binding, recordings were monitored online while drugs were applied. Positive effects correlated with an observed sigmoidal change in the response amplitude as a function of time. Typically, test solutions were perfused for no less than 6 minutes before acquiring test data.

Setup & data acquisition

Voltage- or current-clamp recordings were made using an Axopatch 1D amplifier (Axon Instruments, Foster City, CA) which was interfaced with an Instrutech ITC-18 analog-to-digital board and controlled by custom software written for Igor Pro (Wavemetrics). Synaptic responses recorded in A17 were elicited by electrical stimulation of bipolar cells in the OPL (~10-30 µA for 200-300 µs; Getting Instruments, Iowa City, IA). Synaptic responses recorded in RBCs were elicited by focal puff application of glutamate (50 or 500 µM for 25 ms) onto A17 dendrites in sublamina 5 of the IPL using a Picospritzer (General Valve, Fairfield, NJ). For synaptic experiments, unless otherwise noted, ACSF was supplemented with the group III mGluR agonist L-AP4 (10 µM) and strychnine (1 µM) and tetrodotoxin (TTX, 1 µM) to block glycine receptors and voltage-gated sodium channels, respectively. For all non-synaptic experiments (ie. voltage-dependent responses), ACSF was supplemented with TTX (1 µM) and the AMPAR antagonist, NBQX (10

μM). For clearer observation of voltage-step activated BK currents, 4-AP (4 mM) was included in the bath solution to block A-type potassium channels. All current responses were collected at 12, 20 or 25 s intervals, low-pass filtered at 5 kHz and digitized at 10 kHz to obey Nyquist's theorem.

Analysis

Voltage steps were leak-subtracted using the p/4 subtraction protocol. Step-evoked currents and the raw fluorescence example in Figures 9,15,16, and 17 were smoothed using the built-in Igor binomial smoothing function to emphasize kinetics of the responses. Step-evoked IPSC amplitudes were measured by fitting the last 30-50 ms of the current response to the voltage step to a straight line, extrapolating the line to the time point of the IPSC peak and measuring the difference. Glutamate-evoked IPSC amplitudes were measured as the difference between the average peak response amplitude and the baseline current before stimulation. Data analysis and graphical data presentation were performed using Igor Pro. Unless indicated otherwise, statistical comparisons were made with a paired, two-tailed Student's t test (Igor Pro) and significance was determined as $p < 0.05$ (*), $p < 0.01$ (**), or $p < 0.001$ (***). The number of cells used for a particular experiment (n) is indicated in parentheses. Data are presented as mean ± SD, and illustrated traces are averages of 5-10 responses.

2-photon Ca^{2+} imaging

Setup & data acquisition

Intracellular Ca^{2+} dynamics were observed by replacing the standard intracellular Ca^{2+} chelator, EGTA, with a fluorescent chelator (either Fluo-5F (200 μM) or Fluo-4 (200 μM)), whose emissions dramatically increase upon binding Ca^{2+}ions (Grynkiewicz *et al.*, 1985). Whole-cell recordings were allowed to dialyze for ~30 min. before imaging to allow for equilibration of the dye. Fluorescence was acquired from individual compartments of A17s using a modified Zeiss LSM 510 2-photon microscope with Multi-Time acquisition software. Several advantages make 2-photon microscopy superior to confocal microscopy for the imaging of live retinal tissue. Longer wavelength, lower energy infrared light is less toxic to neuronal tissue than visible wavelengths. Lower wavelength light has the additional benefit of increased transmission attributed to reduced scattering, thus providing better focus of the light at greater tissue (up to ~1 mm). The probability of the nonlinear 2-photon excitation goes as the intensity squared producing in a probability of excitation that falls of quickly in the z direction and results in minimal out of focus light (Zipfel *et al.*, 2003). Phototransduction in the photoreceptors can occur in the infrared spectrum (Euler *et al.*, 2002) though it is dramatically less than for visible wavelengths. For these experiments the excitation source consisted of a computer-controlled Chameleon infrared laser (λ = 810 nm; Coherent) and was modulated by an acoustic optical modulator (Zeiss). For time-dependent imaging of varicosities, a 40x objective (0.8 NA, Zeiss) and digitized zoom were used to collect 1-2 s of the

individual responses in frame scan mode (~16^2 -24^2 pixels) at 33-50 Hz. Emissions from the dyes were separated into green and red channels by the combination of a 565 nm dichroic mirror and 500-550 nm and 570- 640 nm bandpass filters, respectively. The photons from each channel were collected with Hamamatsu PMTs (Figure 5).

Figure 5

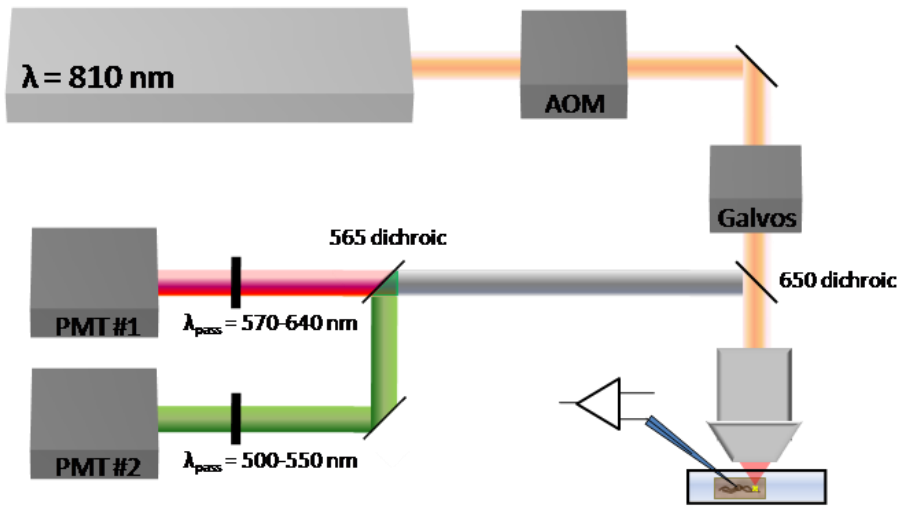

Figure 5. Experimental setup for imaging experiments.

An infrared laser source (810 nm) provided ~1.5 W of pulsed power. The acoustic optical modulator controls beam power to the galvanometer-driven steering mirrors in the microscope. After exciting the sample, fluorescence is collected by the objective and directed towards the detectors with a 650 nm dichroic. A second dichroic (565 nm) splits the emissions, sending the longer wavelength light through a sputter oxide coated red bandpass filter (570-640 nm) and the shorter wavelength light through a coated green bandpass filter (500-550 nm) to their respective photomultiplier tubes.

Ca^{2+} measurements and analysis

The relationship between free calcium concentration and bound fluorophore can be derived from the law of mass action,

$$[FCa] = \frac{[F]_T[Ca^{2+}]}{K_D + [Ca^{2+}]}, \quad (1)$$

where K_D is the dissociation constant for the process. From this, free calcium concentration, $[Ca^{2+}]$, is related to fluorescence as follows:

$$\frac{[Ca^{2+}]}{K_D} = \frac{f - f_{min}}{f_{max} - f}. \quad (2)$$

Although impractical for most measurements because f_{min} is difficult to measure *in situ*, this expression can be reformulated to provide resting calcium measurements, $[Ca^{2+}]_o$, in terms of the intrinsic range of the indicator ($R_f = F_{max}/F_{min}$) and saturating measurements within cells ($\delta f_{max} = (f_{max} - f_o)/f_o$; Maravall *et al.*, 2000).

$$\frac{[Ca^{2+}]_o}{K_D} = \frac{(1 - R_f^{-1})}{\delta f_{max}} - R_f^{-1} \quad (3)$$

This equation is particularly useful for making single-wavelength measurements of resting calcium because it means that values can obtained that are independent of the typically confounding factors of dye loading and dye concentration. Error associated with the experimental measurements of R_f can be reduced in the equation (R_f^{-1}) by choosing an indicator with a large dynamic range, such as those indicators from the Fluo family (R_f ~100). An example of a dye saturation experiment from an A17 amacrine call varicosity using Fluo-4 (200µM) is displayed in Figure 6. On average A17 varicosities had a resting calcium value of 79.7 ± 8.8 nM (n = 7; range: 69.3-90.9

nM), which is within the range (20-250 nM) of measurements from other neurons in the central nervous system (Nakajima *et al.*, 1993; Woodruff *et al.*, 2002).

For most of the scientific questions posed in this dissertation we are interested in transient changes in intracellular calcium such as that resulting from the influx of calcium through voltage-gated calcium channels. One consequence of introducing calcium-binding dyes to the intracellular compartment is that they also act as mobile buffers which perturb the endogenous calcium dynamics. Under these conditions the change in free calcium is expressed as

$$\Delta[Ca^{2+}] = \frac{\Delta[Ca^{2+}]_T}{1 + \kappa_B + \kappa_F} \qquad (4)$$

where $\Delta[Ca^{2+}]_T$ is the total calcium influx (i.e. integral of the VGCC-mediated current), κ_B is the endogenous buffering capacity and κ_F is the buffering capacity of the added dye. Determining the correct indicator for a particular scientific question is critical. If one wants to study the physiological calcium dynamics then it is important to choose the appropriate indicator and concentration to ensure that $\kappa_{F<<} \kappa_B$ ($\kappa_F \approx [F]/K_D$). If instead, one desires to observe a change in fluorescence which is proportional to calcium influx then the dye and concentration should be chosen such that the exogenous buffer dominates the endogenous buffers ($\kappa_{F>>} \kappa_B$). Other important considerations include choosing an indicator with a K_D which is greater than the dynamic range of interest (this avoids non-linearities in the response) and one with the largest dynamic range to maximize SNR. Table 1 provides published information on the relevant properties of some indicators used in these studies.

For most experiments Fluo-4 or Fluo-5F (200μM) were added to the patch solution in addition to a calcium-insensitive red dye (Alexa594; 40 μM). Background

fluorescence was corrected for the varicosity-containing regions-of-interest (ROIs) by measuring average red and green signals at regions near the dye-filled dendrite. When comparing responses between cells ΔG/G (ΔF/F) was calculated by subtracting the baseline from the fluorescence trace and dividing by the baseline value. However, if testing the effects of drugs *relative* to control fluorescence, the average red signal was used as the denominator (ΔG/R). This approach has the advantage of having a larger denominator (Alexas have a higher quantum yield than the Fluo family) which is insensitive to changes in intracellular calcium, therefore providing a more robust measurement of relative influx (Yasuda *et al.*, 2004). Imaging data was analyzed using custom Matlab scripts. In Figure 15 a correction factor of 1.05 was used to correct the ΔG/R for the differential transmission of red and green emissions in the presence of NBQX (10 μM; transmission spectra not shown).

Figure 6

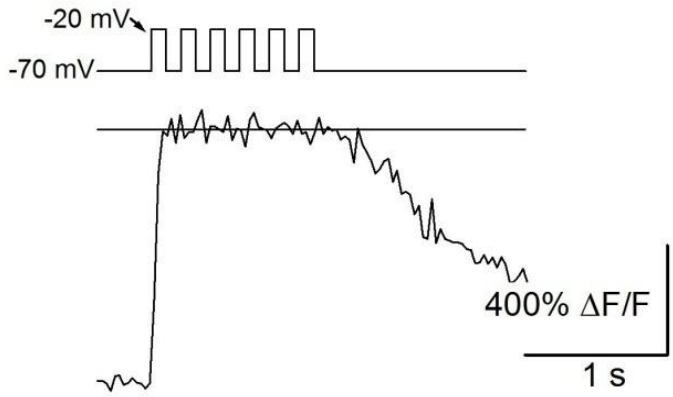

Figure 6. Example of saturating protocol and response from a single A17 varicosity. The resultant resting calcium measurement from this cell was 86 nM.

Table 1

Indicator	K_D *(μM)*	R_f *(F_{max}/F_{min})*	κ_{dye} *(100 μM)*
OGB-1	0.38	10	310
Fluo-4	0.8	~100	220
Fluo-5F	1.6	~100	70
Fluo-4FF	10.4	~100	10

Table 1. Properties of fluorescent Ca^{2+} indicators.

Adapted from Maravall *et al.*, 2000 and Yasuda *et al.*, 2004.

Immunocytochemistry

For tracer injections, 50 mM of Neurobiotin (Vector Laboratories, Burlingame, CA) was added to the pipette solution. Whole-cell voltage-clamp recordings were made from A17s. Recordings were held for 20 minutes to allow Neurobiotin to diffuse into the fine dendrites. Slices were fixed in 4% paraformaldehyde for 15~20 minutes, washed with a standard solution (0.1 M phosphate buffer with 0.5% Triton X–100 and 0.1% NaN_3, pH 7.4) and blocked overnight in the standard solution with 4% donkey serum. Slices were then incubated for two hours in the standard solution containing an antibody to PKC-α (mouse, Santa Cruz Biotechnology, Santa Cruz, CA; 1:100) and an antibody to BK_{Ca} or BK_{Ca} β2 subunit (rabbit, Alomone, Jerusalem, Israel; 1:100). After extensive washing, slices were incubated for one hour in 0.1 M phosphate buffer containing Alexa-488 conjugated streptavidin (Invitrogen, Carlsbad, CA; 1:200), donkey anti–rabbit Cy3 (Jackson ImmunoResearch Laboratories, West Grove, PA; 1:200), and donkey anti–mouse Cy5 (Jackson ImmunoResearch Laboratories, West Grove, PA; 1:200). Slices were imaged using a Leica SP2 confocal microscope (Leica, Germany) with a 63x (1.32 N.A.) oil immersion objective or a Zeiss LSM–510 META confocal microscope (Zeiss, Germany) with a 100x (1.45 N.A.) oil immersion objective. For whole-mount tissues, the process was the same except the incubation period was longer (five days for the primary antibody and overnight for the secondary antibody). For quantification purposes, varicosities were defined as obvious enlargements along the A17 dendrites that were greater than or equal to twice the diameter of the adjacent

dendrite. A second criterion was the close apposition of the varicose structure to a rod bipolar terminal.

Modeling

Electrotonic modeling with NEURON

An electrotonic compartmental model of the A17 amacrine cell was built and tested using the electrotonic compartmental modeling program, NEURON (Hines and Carnevale, 1997; Hines and Carnevale, 2001). This computational approach takes advantage of the well documented approximation of describing a neuron in terms electrical cables. The cable equation

$$\lambda^2 \frac{\delta^2 V}{\delta x^2} - V - \tau \frac{\delta V}{\delta t} = 0 \qquad (5)$$

describes potential changes along a cable where λ is the length constant of the core conductor and τ is the membrane time constant. NEURON uses the backward Euler method to solve the cable equations for complex cable arrangements (Hines and Carnevale, 1997). To address specific questions about A17, anatomical measurements taken from 3D reconstructions were used to constrain the model (example cell- Figure 4; results- Table 3). Several assumptions were made: 1) C_{mem} = 1 μF/cm^2, 2) all compartments have the same leak conductance and leak reversal (-65 mV) and 3) R_{axial} = 110 Ω*cm (Taylor *et al.*, 1996; Hallermann *et al.*, 2003; Engel and Jonas, 2005). An alpha synapse

$$g_{syn} = \frac{g_{max} * t}{\tau} * e^{-\frac{(t-\tau)}{\tau}} \qquad (6)$$

provided the synaptic conductance, where g_{max} is the maximum conductance and τ is the time to peak. The values of these parameters were chosen to create a synaptic conductance with a time course of decay of ~3 ms, which is similar to experimentally observed synaptic events recorded from A17s (Figure 19d). Electrotonic model parameters are indicated in Table 2 unless otherwise indicated in the text. Simulations were run using 25 μs time steps and all results were analyzed using IGOR pro.

Simulating Synaptic GABAR Activation with Channelab

To gain a more conceptual understanding of the results from RBC step-evoked feedback experiments (Chapter 4) a range of GABA waveforms were applied to $GABA_A$ and $GABA_CR$ state models using Channelab. Both $GABA_A$ (Lavoie *et al.*, 1997) and $GABA_C$ (Chang and Weiss, 1999) kinetic models were derived from similar room temperature heterologous systems. The solutions to the coupled differential equations for model and waveform were numerical integrated using the forth-order Runga Kutta method using 0.1 ms time steps.

Table 2

Properties	*Model Values*
R_{axial}	110 Ω*cm
R_{mem}	2,632, 11,905 or 18,519 Ω*cm^2
dendritic diameter	0.1, 0.3 or 0.5 µm
C_{mem}	1 µF/cm^2
g_{max}	200 pS
T	1.6 ms
τ_{decay} (fit)	~3 ms

Table 2. A17 electronic model parameters (unless otherwise noted).

Chapter 3: Dendritic integration in A17 amacrine cells

Introduction

Biophysical properties of excitable membranes and unique anatomical structures are fundamentally responsible for the spatial and temporal characteristics of electrical signaling in neurons. Each neuronal subclass in the central nervous system has a unique combination of ion channels and neuronal structure that enables these neurons to perform distinct, specialized tasks. For instance, voltage-gated sodium channels (Na_v channels) and voltage-gated potassium channels (K_v channels) work in concert to produce action potentials which allow for reliable all-or-none electrical signaling over great lengths (Hodgkin and Huxley, 1945; Hodgkin and Huxley, 1952c; Hodgkin and Huxley, 1952a; for review see Stuart *et al.*, 1997).

In the rod pathway of the mammalian retina, absorption of photons in rod photoreceptor outer segments leads to graded changes in membrane potential that regulate voltage-gated calcium channel (Ca_v channel) activation and excitatory transmitter release. The postsynaptic rod bipolar cells (RBCs) also respond to the imposed light signals with nonlinear, but yet graded potential changes (Euler and Masland, 2000; Field and Rieke, 2002). These analog signals can transmit more information about the stimulus than digital, action-potential dependent signaling by encoding information in the response amplitude in addition to the timing and patterns of membrane potential changes. Ultimately, the retina relies on action potential signaling to reliably transmit the visual signal over long distances to the brain via the

axons of ganglion cells which form the optic nerve. Before this analog-to-digital conversion takes place, the rod-driven visual signal is shaped both spatially and temporally by a class of inhibitory interneurons called amacrine cells.

Electron micrographs of the RBC axon terminal reveal the presence of two distinct postsynaptic amacrine cells at each ribbon-type synapse. While the AII amacrine cell is essential for transmitting the feed-forward signaling on towards the brain, the A17 amacrine cell makes a reciprocal inhibitory synapse back onto the RBC terminal. The proximity of this inhibitory feedback synapse to the RBC release machinery makes it ideally suited to locally regulate membrane potential near the active zones. *In vivo* experiments have indicated that reciprocal inhibition from A17 amacrine cells shapes the time course of the rod-driven response by regulating bipolar cell activity. Although much is known about the biophysical mechanisms that underlie the physiology of AII amacrine cells (Veruki and Hartveit, 2002b; Habermann *et al.*, 2003; Veruki *et al.*, 2003; Gill *et al.*, 2006; Tamalu and Watanabe, 2007), little is known about A17 amacrine cells. In addition to providing local reciprocal inhibition, A17 amacrine cells are thought to produce center surround inhibition (Volgyi *et al.*, 2002; Zhang *et al.*, 2002). The spatial extent of this reciprocal inhibition should be related to spatial extent of electrical signaling within A17 dendrites. Action potential signaling would greatly enhance the distance over which electrical signals could travel in A17s, however, it remains controversial as to whether or not these cells are capable of spiking (Nelson and Kolb, 1985; Menger and Wassle, 2000, but see Bloomfield, 1992; Bloomfield, 1996). To gain further insight into reciprocal signaling from A17 amacrine cells, combinations of

electrophysiology, neuropharmacology and theorectical modeling approaches were employed. The biophysical properties of Na_v and K_v channels in individual A17s from retinal slice were characterized and the impact of these channels on the cellular response was tested. The results from these experiments were then used in conjunction with anatomical measurements to construct an electrotonic model of the A17 amacrine cell. This model was extensively tested to address questions about the spatial extent of electrical signaling in the dendrites of these neurons that would be impractical to address experimentally due to the technical complexities. The results indicate that the unique anatomical structure and biophysical membrane properties of A17 give rise to highly compartmentalized signaling within dendrites that decreases the capacity for center surround inhibition and therefore increases the degree to which reciprocal inhibition is synapse specific.

Results

A17s express a small population of Na_v channels

Na_v channels have fast activating and fast inactivating kinetics and a large driving force with respect to the midpoint of voltage-dependent activation (~90-100 mV). It is well accepted that Na_v channels underlie critical aspects of neuronal signaling throughout the central nervous system. Specifically, these channels underlie the rising phase and propagation of action potentials (spikes) and the amplification of excitatory postsynaptic potentials (EPSPs; Araya *et al.*, 2007; Rotaru *et al.*, 2007; Hodgkin and Huxley, 1952c; Hodgkin and Huxley, 1952b; McCormick *et al.*, 2007). Mixed experimental evidence has argued for (Hartveit, 1999; Vigh and

von Gersdorff, 2005) and against (Chavez *et al.*, 2006) a role for Na_v channels in enhancing reciprocal inhibition to bipolar cells. To test for functional Na_v channel expression in A17, whole-cell voltage clamp recordings were made from rat retinal slices. A Cs^+-based intracellular solution was used to block potassium channels from within the recorded neuron and NBQX (10 µM) was included in the bath to block excitatory RBC inputs (Singer and Diamond, 2003; Chavez *et al.*, 2006). A17 identity was confirmed by post-recording three-dimensional reconstruction (see methods and Chapter 4). The somatic patch electrode delivered a family of depolarizing voltage steps (-70 to +30 mV in 20 mV increments; 100 ms) which were proceeded by a hyperpolarizing conditioning step (to -100 mV; 100 or 500 ms) to relieve the inactivation of Na_v channels. This protocol elicited fast, transient inward currents that were completely blocked by tetrodotoxin (TTX; 1 µM; Figure 7a), indicating the presence of Na_v channels. The TTX-sensitive current from a group of A17s was converted to conductance, via Ohm's law, and fit with a Boltzmann equation,

$$G_{Na} = \frac{1}{1 + e^{\frac{-qZ\delta(\Delta V - w)}{k_b T}}} \qquad (7)$$

to estimate the biophysical gating properties of A17 Na_v channels. The normalized gating charge, Zδ, was 3.1 and the activation energy barrier/midpoint of voltage-dependent activation, $V_{1/2}$, was -30 mV (n = 9, Figure 7c). To quantify the inactivation process of the TTX-sensitive Na_v channels, the patch electrode was used to deliver depolarizing test steps (to -10 mV; 100 ms) that were preceded by a series of conditioning steps (-140 to -30 mV, 10 mV increments; 100 ms, Figure 7b). Interestingly, the measured midpoint of inactivation was considerably more negative

($V_{1/2}$ = -98 mV) than the typical resting membrane potential of A17 (-62 ± 3mV; n = 10, Figure 7d). In fact, at resting membrane potentials only ~5% of A17 Na_v channels are available to contribute to membrane excitability. On average, the preceding conditioning step to -140 mV produced 179 ± 89 pA of TTX-sensitive current (p = 0.003; n = 6) which is substantially less than that previously reported for spiking neurons in the retina (~1000 pA; Henne *et al.*, 2000; Kim and Rieke, 2003).

Figure 7

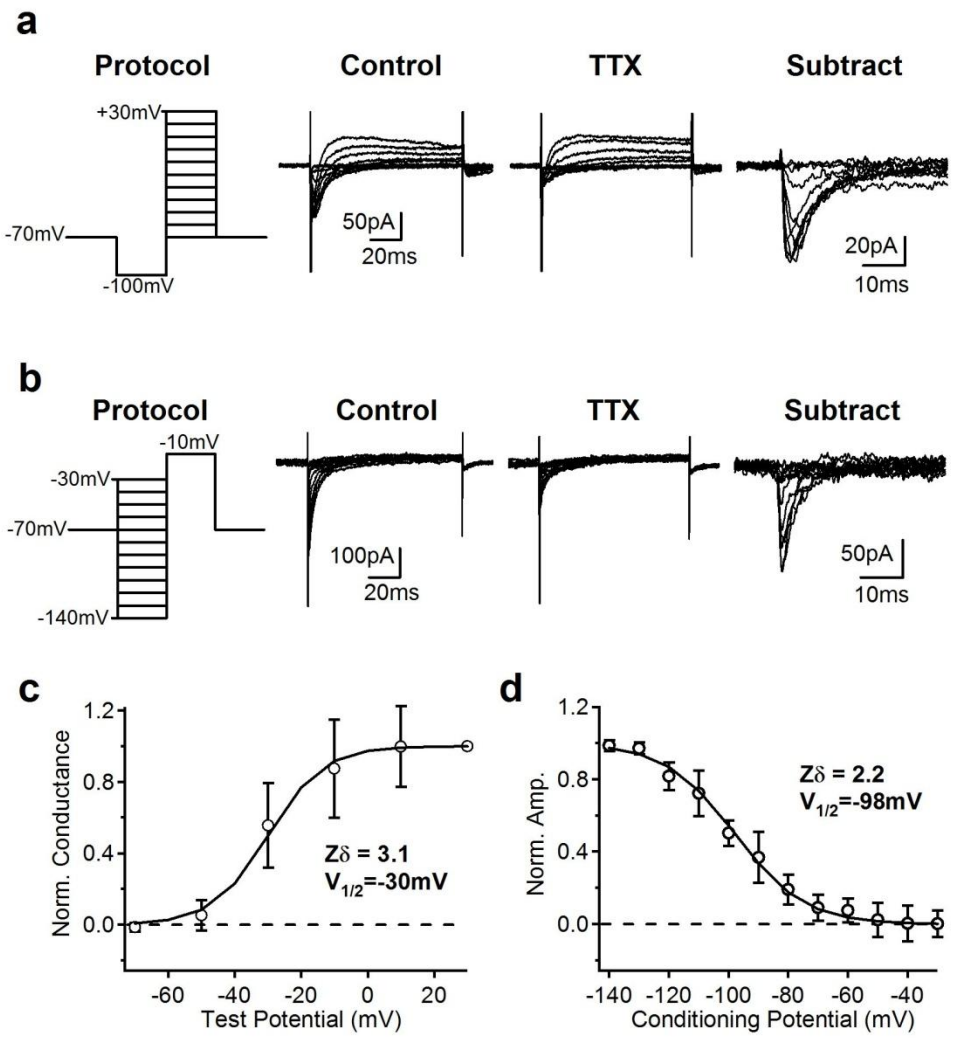
a
Protocol
Control
TTX
Subtract
+30mV
-70mV
-100mV
50pA
20ms
20pA
10ms
b
Protocol
Control
TTX
Subtract
-10mV
-30mV
-70mV
-140mV
100pA
20ms
50pA
10ms
c
Norm. Conductance
1.2
0.8
0.4
0.0
Zδ = 3.1
V1/2=-30mV
-60
-40
-20
0
20
Test Potential (mV)
d
Norm. Amp.
1.2
0.8
0.4
0.0
Zδ = 2.2
V1/2=-98mV
-140
-120
-100
-80
-60
-40
Conditioning Potential (mV)

Figure 7. A17 amacrine cells express functional Na_v channels.

(**a**) Activation protocol: When preceded by a hyperpolarizing voltage step (-100 mV; 100 ms), a series of depolarizing voltage steps (-70 to +30 mV in 10 mV increments; 100 ms) elicited fast and transient TTX (1 μM) -sensitive inward currents. (**c**) Pooled data can be fit with the Boltzman equation to derive the half maximal activation potential and Zδ (gating charge times distance traveled relative to membrane thickness). (**c**) Inactivation protocol: A series of conditioning steps (-140 to -30 mV in 10 mV increments; 100 ms) preceding a 100 ms step to -10 mV revealed rapidly-inactivating TTX-sensitive currents. (**d**) Fitting the normalized conductance indicates distinct mechanisms for activation and inactivation.

A17s express K_v channels

K_v channels are ubiquitous in the CNS, however this very general classification includes voltage-gated potassium channels with very diverse biophysical properties. For instance, delayed rectifier potassium channels provide persistent outward currents in response to sustained depolarizations whereas A-type potassium channels rapidly inactivate on the time scale of tens of milliseconds. These K_v channels, among others, participate in several key aspects of neuronal signaling which include the setting of resting potentials, the repolarization of the membrane during an action potential and the limiting of spike frequency (Hodgkin and Huxley, 1945; Hodgkin and Huxley, 1952a; McKay and Turner, 2004; Shevchenko *et al.*, 2004; Newell and Schlichter, 2005). Although previous experiments in rat retinas indicate that A17s express K_v channels (Menger and Wassle, 2000), the biophysical properties and functional classes of K_v channels remain undetermined. To record and characterize K_v channels expressed in A17, whole-cell voltage clamp recordings were made using potassium-based internal solution (to allow permeation of K_v channels). Additionally, synaptic transmission, Na_v channels and Ca_v channels were pharmacologically blocked with NBQX (10 µM), TTX (1 µM) and cadmium (200 µM), respectively. The patch electrode was used to deliver a series of depolarizing steps (-70 to +30 mV in 20 mV increments; 200 ms) which, after the p/4 subtraction method, revealed outward currents at potentials >-50 mV (Figure 8a). Subsequent application of the A-type potassium channel blocker, 4-AP (4 mM), significantly blocked outward currents at potentials ≥-30 mV for both the transient (3-8 ms from onset of step; to 15 ± 47% of control at -30 mV, $p = 0.016$; Figure 8a,b) and sustained

(150-170 ms from onset of step; to 9 ± 11% of control at -30 mV, p = 0.003, n = 6; Figure 8a,c) components of the response. The remaining current was sustained and activated at potentials ≥-10 mV, presumably mediated by delayed rectifiers. Comparison of the distinct shapes of the transient and sustained 4-AP-sensitive current indicates that it is mediated by inactivating A-type channels and other K_v channels which are non-specifically blocked by 4 mM 4-AP and respond with sustained opening. To isolate the inactivating A-type potassium current and to quantify the voltage-dependence of its inactivation, the patch electrode was used to deliver a maximum activation test step (to +30 mV for 200 ms) that was preceded by a 500 ms conditioning step to a range of potentials (-90 to +20 mV; Figure 8d). The maximally inactivated trace (conditioning step to +20 mV) was subtracted from all traces to reveal the inactivating A-type potassium current (Figure 8e). The peak amplitude of the A-type current was 717 ± 258 pA (n = 5) while the total 4-AP sensitive current was 1,457 ± 383 pA. The peak amplitude response of the subtracted trace for each conditioning potential was grouped across cells and fit to quantify the properties of inactivation (Figure 8f). The midpoint of inactivation was -13 mV, indicating that A-type K_v channels expressed in A17 are >99% available at typical resting potentials. These experiments demonstrate that together, the population of K_v channels expressed in A17 amacrine cells can conduct more than a nanoamp of current, thus capable of significantly impacting membrane excitability. Additionaly, this population of channels is heterogeneous, consisting of both inactivating and non-inactivating K_v channels implying the distinct biophysical properties have differential effects of signaling.

Figure 8

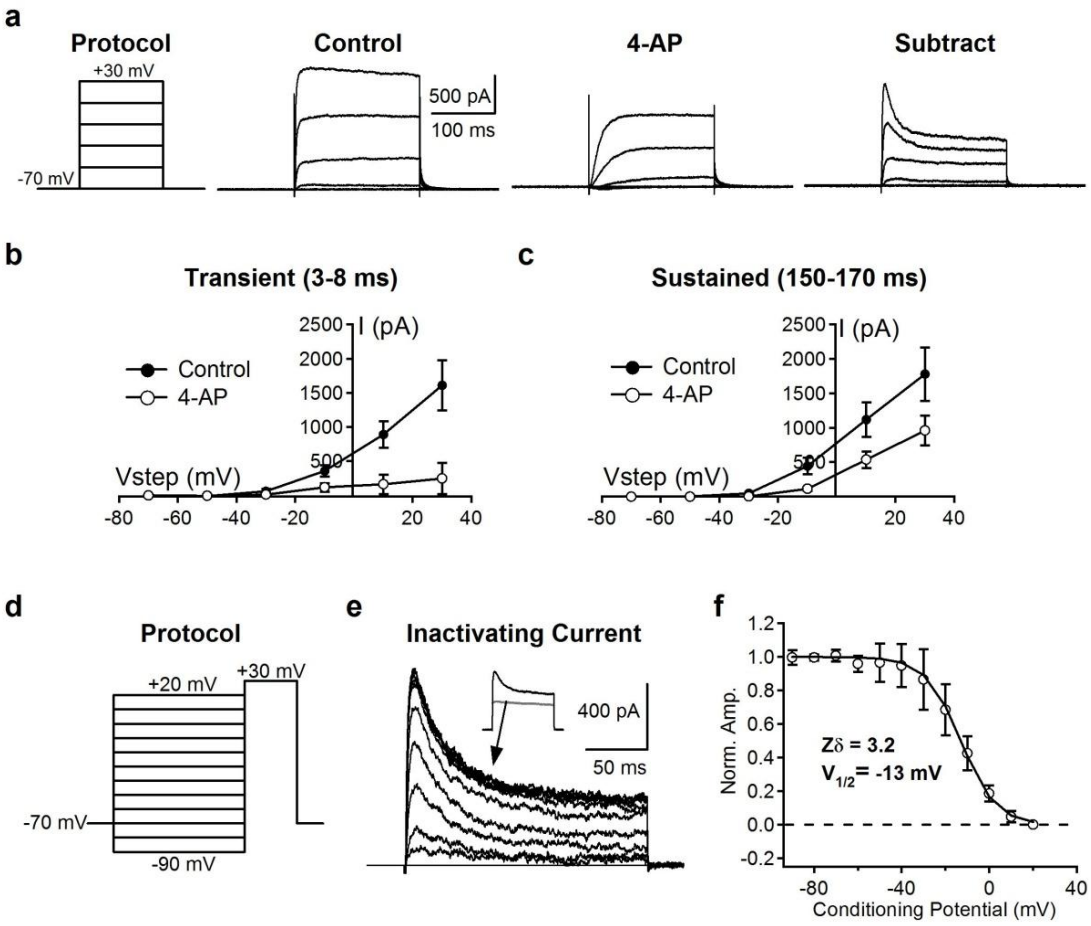
a
Protocol
Control
4-AP
Subtract
+30 mV
-70 mV
500 pA
100 ms
b
Transient (3-8 ms)
I (pA)
Control
4-AP
Vstep (mV)
c
Sustained (150-170 ms)
d
Protocol
+20 mV
+30 mV
-70 mV
-90 mV
e
Inactivating Current
400 pA
50 ms
f
Norm. Amp.
Zδ = 3.2
V1/2= -13 mV
Conditioning Potential (mV)

Figure 8. A17 amacrine cells express functional A-type K_v channels. (**a**) Activation protocol: A series of depolarizing voltage steps (-70 to +30 mV in 20 mV increments; 200 ms) elicited large outward currents that where partially sensitive to an A-type channel antagonist (4-AP; 4 mM). (**b-c**) Plotting the transient (**b**; 3-8 ms) or sustained current (**c**, right; 150- 170 ms) as a function of voltage for control and 4-AP conditions indicate a nonspecific action of 4-AP. (**d**) An inactivation protocol (conditioning steps: -90 to +20 mV in 10 mV increments; 500 ms; test pulse: +30 mV; 200 ms) revealed inactivating and non-inactivating components of the 4-AP-sensitive currents (panel **e** *inset*). (**f**) Pooled data can be fit with the Boltzman equation to derive the half maximal inactivation potential and Zδ of inactivation.

Impact of Na_v and K_v channels on A17 signaling

How do Na_v and K_v channels influence signaling within A17 amacrine cells? Together, these two channel types are required for action potential signaling but reports on A17 spiking are inconsistent. Intracellular A17 recordings from cat failed to detect spiking patterns (Nelson and Kolb, 1985) while recordings from rabbits detected spikes in one but not both of the two homologous cell types (Bloomfield, 1996). Observation of both Na_v and K_v channels in rat A17s suggests that this cell could be capable of firing action potentials. However, previous current clamp recordings from rat A17 amacrine cells, in which the somatic patch electrode was used to inject depolarizing currents steps, were unable to elicit traditional action potentials (Menger and Wassle, 2000). The measurements of A17 Na_v channel inactivation presented herein indicate that these channels are largely inactive at typical resting membrane potentials. Therefore, to maximize the probability of initiating A17 action potentials, a current clamp recording electrode was used to inject a hyperpolarizing current step (-200 pA for 200 ms) that preceded the test steps (-200 to +1000 pA in 200 pA increments, 200 ms; Figure 9a), and hence relieving the inactivation of Na_v channels. This experiment failed to elicit action potentials (0 out of 5 cells) and further bath inclusion of TTX (1 µM) had no obvious effects on the output (data not shown). In the current clamp recording examples from Menger and Wassle, 2000, some transient events appeared to superimpose upon the recording examples, but the mechanisms underlying these events were not explored. In those experiments, excitatory synaptic transmission was not blocked, therefore the occurrences could have resulted from spontaneous synaptic input. It is worth noting,

that these types of events were not observed under our conditions (with NBQX in the bath). Another possibility is that these events were dendritic spikes such as those observed in direction-selective ganglion cells (Oesch *et al.*, 2005). If so, then synaptic stimulation might be more efficacious than somatic current injection at eliciting dendritic spikes. To test this hypothesis, current clamp recordings were made from A17s (V_{hold} adjusted to -65 mV) and an electrical stimulating electrode, placed in the OPL, was used to depolarize RBC dendrites (10-20 µA for 300 µs) and elicit glutamate release onto A17. Additionally, glycine, $GABA_A$ and $GABA_C$Rs were pharmacologically blocked with strychnine (1 µM), GABAzine (25 µM) and TPMPA (50 µM), respectively. This form of stimulation evoked excitatory postsynaptic potentials (EPSPs) in A17 that were 3.1 ± 0.8 mV (n = 5) in amplitude, but regardless of the response amplitude from individual cells, spike-like potentials were not observed (Figure 9b). If A17 Na_v channels do not give rise to spiking behavior, what is the physiological role of these channels? Na_v channels might be localized to synaptic feedback varicosities, where they could amplify synaptic events such as that observed in the spines of pyramidal cells (Araya *et al.*, 2007) and facilitate the propagation of synaptic potentials, therefore enhancing communication between neighboring varicosities along a single dendrite. However, blocking Na_v channels with bath application of TTX (1 µM) had no significant affect on EPSPs (to 88 ± 17 % of control, p = 0.24, n = 5). This response was blocked completely by further inclusion of the AMPAR antagonist, NBQX (10 µM; to -3 ± 9% control; p = 0.0037; n= 5; Figure 9b). These experiments confirm that A17 amacrine cells of rat retinas are incapable of firing action potentials. Several of the results presented here

could provide plausible explanations for the lack of spikes and the minimal contributions of Na_v channels to dendritic integration. The absolute amplitude of TTX-sensitive sodium current indicates a low density of Na_v channels or small total sodium conductance and appears to be largely outbalanced by several types of K_v channels. In addition, the hyperpolarized midpoint of inactivation of the Na_v channels, with respect to resting potentials, reduces the number of channels that can contribute to cellular signaling. These factors, in addition to others (i.e. morphology), likely gives rise to electrical isolation of the dendrites and compartmentalization within individual dendrites.

Figure 9

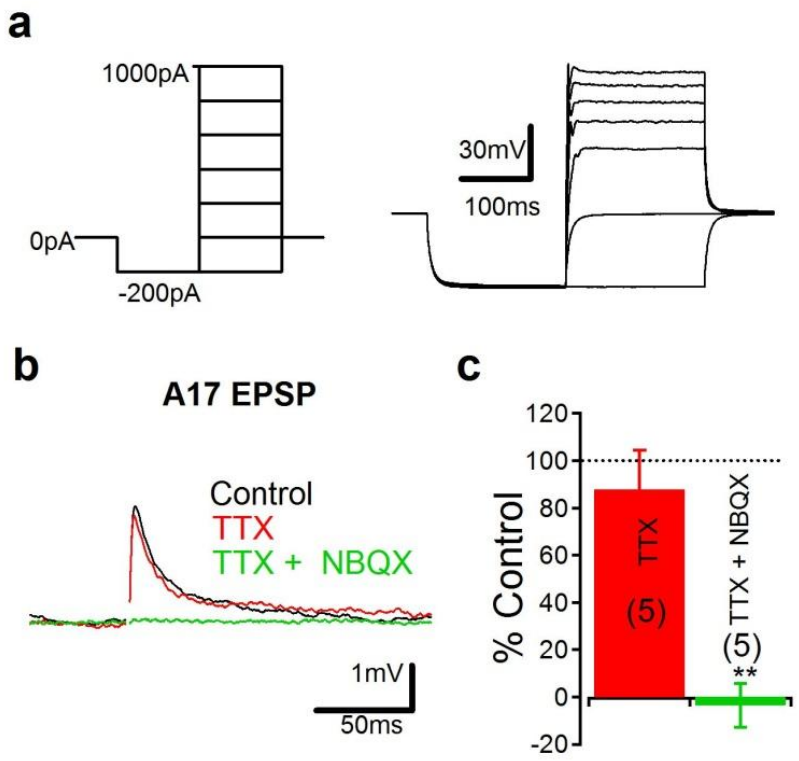

Figure 9. Na_v channels do not significantly enhance membrane excitability or dendritic integration. (**a**) Using the patch electrode to inject current steps (-200 to +1000 pA in 200 pA increments; 200 ms; following a hyperpolarizing conditioning step;-200 pA; 200 ms) into the soma failed to elicit spiking patterns in A17 (0 of 5 cells). (**b,c**) Excitatory postsynaptic potentials were insensitive to application of TTX (1 µM; red) but were completely blocked by further inclusion of NBQX (10 µM; green).

Electrotonic A17 model

Many aspects of synaptic and neuronal signaling are difficult to test experimentally due to technical limitations such as spatial and temporal resolution and sensitivity. Therefore, modeling approaches derived from first principles are often utilized to gain theoretical insights into complex phenomena on the neuronal level. Cable theory has provided a solid framework for understanding the excitable membranes and signaling characteristics of individual neurons (Jackson, 1993; Smith and Vardi, 1995; Engel and Jonas, 2005; Angelo *et al.*, 2007; Takashima and Takahata, 2008; Sikora *et al.*, 2005). Previous attempts, based on quantitative morphological results, have been made to model putative lateral antagonistic surround inhibition from the analogous A17 cell type (S2) in rabbit retinas (Zhang *et al.*, 2002). In that study, two scenarios were evaluated to provide a quantification of the falloff of lateral inhibition as a function of distance from the stimulating RBC. The first scenario, in which input to single A17 varicosities gave rise to uniform output from all varicosities (global response), suggested that the population of A17s provide surround inhibition which extends for ~200 μm. The second scenario, in which input from a single RBC triggered an inhibitory response from A17s that was limited to, but uniformly distributed throughout the varicosities of the stimulated dendrite (dendritic isolation), suggested a surround response that decayed over ~100 μm. It has also been postulated that A17s respond with a high degree of synapse

specificity, and that reciprocal inhibition could possibly be compartmentalized to individual varicosities (Chavez *et al.*, 2006).

In the present study, we have demonstrated that A17s from rat retinas are incapable of firing action potentials, thus strongly arguing against the possibility of a global response. However, several specific questions regarding A17 signaling and a putative surround inhibitory response remain unanswered. 1) Are dendrites completely electrically isolated from one another? 2) To what extent do signals spread within individual dendrites? 3) How do anatomical structures and ion channels influence signals within dendrites? Here we use anatomical measurements from 3D reconstructions and electrophysiology measurements to build an electrotonic model that captures the average characteristics of the A17 amacrine cell in an attempt to gain a conceptual understanding the average signaling properties and the factors that influence this signaling.

The impact of varicose structures

How do varicose structures influence signaling along a typically non-branching A17 dendrite? To test this question independently of additional complexities, a simple infinite cable of either 0.1, 0.3 or 0.5 µm dendritic diameter was created and tested using the descretized electrotonic modeling program, NEURON. The solution to the cable equation for these conditions indicates that the voltage along a smooth, infinite dendrite decays exponentially,

$$V(x) = V_o e^{-x/\lambda}, \qquad (8)$$

where V_o is the voltage at the origin and λ is the space constant of the cable. The space constant of the infinite cable is dependent on the specific cytoplasmic resistivity (R_i), specific membrane resistivity (R_{mem}) and cable (dendrite) diameter (D) as follows:

$$\lambda = \sqrt{\frac{D * R_m}{4 * R_i}} \qquad (9)$$

For these initial simulations, the specific cytoplasmic resistivity (R_i) and the specific membrane resistivity (R_{mem}) were fixed at 110 Ω*cm and 15,000 Ω*cm^2, respectively. A steady state current was applied at the origin and the voltage was monitored at 20 µm increments for each cable diameter (normalized to origin voltage; Figure 10a). The effective space constants were ascertained by fitting the results from each case with a single exponential. The measured space constants, when plot versus dendritic diameter, accurately matched cable theory (Figure 10c), therefore validating the models. Varicose swellings (diameter = 2 µm) were incorporated into the dendrite at 20 µm intervals and the simulations were repeated for each of the intervaricosity dendritic diameters (0.1, 0.3 or 0.5 µm; Figure 10b). The addition of dendritic varicosities decreased the effective space constants of the cables by 40%, 23% and 15% for each of the respective cable diameters (0.1, 0.3 or 0.5 µm) when compared to the non-varicose cables (Figure 10c). Consistent with previous models (Ellias and Stevens, 1980), these results indicate that varicose dendrites have a reduced capacity to signal over long ranges compared to smooth dendrites of the same diameter.

Figure 10

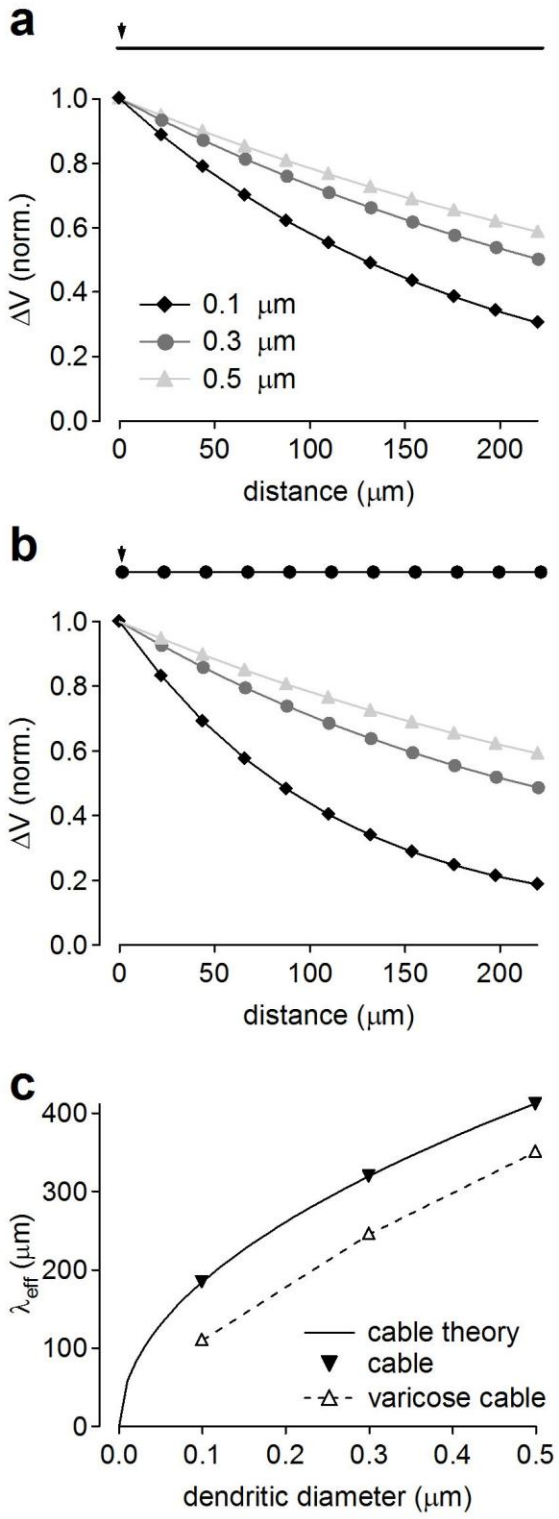
a
1.0
0.8
0.6
0.4
0.2
0.0
ΔV (norm.)
0.1 μm
0.3 μm
0.5 μm
0
50
100
150
200
distance (μm)
b
1.0
0.8
0.6
0.4
0.2
0.0
ΔV (norm.)
0
50
100
150
200
distance (μm)
c
400
300
200
100
0
λeff (μm)
cable theory
cable
varicose cable
0.0
0.1
0.2
0.3
0.4
0.5
dendritic diameter (μm)

Figure 10. Varicose structures on a simple cable decrease steady state length constant. (**a**) Potential response as a function of distance for an infinite cable of diameters: 0.1 µm (black), 0.3 µm (grey) and 0.5 µm (light grey). A constant current electrode supplies a 200 ms current step to the cable origin. (**b**) Potential measurements from varicosity-studded cables (2 µm varicosities at 20 µm intervals). (**c**) Length constant measurements plotted as a function of dendritic diameter for the varicose and non-varicose cable simulations. Solid black line indicates the space constant of the cable, as derived from the solution to the cable equation for an infinite cable, as a function of dendritic diameter (Equation 9).

A17 anatomical measurements

The colocalization of synaptic input and output machinery within individual varicosities along typically non-branching dendrites (Ellias and Stevens, 1980; Nelson and Kolb, 1985) make A17 a particularly intriguing model for studying neuronal input/output. To construct an electrotonic compartmental model that correctly represents the average anatomical features of A17 amacrine cells, quantitative measurements were taken from five 3-dimensionally reconstructed A17s (Figure 4). These measurements included (in µm) the cell body height and width, the number of dendrites, varicosity diameter and the intervaricosity dendritic length (Table 3). Because some dendrites were likely sheared off during the slicing process care was taken to count processes proximally to the soma, however we wish to convey that the reported value could be an underestimate. Additionally, we were unable to resolve the diameter of intervaricosity dendritic sections because they were either at or below the spatial resolution of our technique (~600 nm), but previous electron microscopy studies indicate that these sections are approximately 100 nm in diameter (Ellias and Stevens, 1980; Nelson and Kolb, 1985). The dendritic tree was estimated to be ~400 µm in diameter. The anatomically-constrained computational model therefore had 10 varicosities per each of the 22 dendrites at uniform spacings to produce a 2-dimensional dendritic field of 429 µm in diameter.

Table 3

Property	*Across cells (n)*	*All structures (#)*
Soma width (µm)	12.3 ± 0.3 (5)	
Soma height (µm)	11.9 ± 1.7 (5)	
# of dendrites	22 ± 4.6 (5)	
Varicosity diameter (µm)	1.9 ± 0.2 (5)	1.8 ± 0.4 (47)
Intervaricosity dendritic length (µm)	19.2 ± 1.6 (5)	19.3 ± 7.0 (31)
Input Resistance (MΩ)	212 ± 72 (150)	

Table 3. Anatomical measurements from A17 3D 2-photon reconstructions.

Measurements are presented as mean ± SD.

Determination of model parameters and effective space clamp

The discrete element electrotonic A17 model was constructed using morphological measurements, but should also be constrained by experimental electrophysiology measurements. Because A17 dendritic diameter was at or below the diffraction limit of our imaging approach, it was used as a variable parameter, ranging from the approximate diffraction limit (0.5 µm), to the previously reported value (0.1 µm) in 0.2 µm intervals. To further improve the viability of each of the three models, effective input resistance (R_{in}) was measured and adjusted to match experiment. This was accomplished by using a simulated somatic voltage clamp electrode to elicit a test pulse (5 mV for 100 ms) that was used to derive the input resistance of the simulated neuron. Specific membrane resistivities were adjusted for each of the amacrine cell models to match the average experimentally measured A17 input resistance (212 ± 72, n = 150; Figure 11a). The resultant specific membrane resistivities for the models with dendritic diameters of 0.l, 0.3 and 0.5 µm were 2,632, 11,905, and 18,519 Ω*cm^2, respectively. These values fall within the range of specific membrane resistivities used for previous amacrine cell (2,000 Ω*cm^2, Ellias and Stevens, 1980; 25,000 Ω*cm^2, Smith and Vardi, 1995) and ganglion cell (60,000 Ω*cm^2; Taylor *et al.*, 1996) electronic models. For all further simulations presented here, these values were used in conjunction with the associated dendritic diameter. Because the true dendritic diameter must be within the range tested, we asked what the effective space clamp of the recording electrode would be for each of the three cases. As expected, dendritic diameter (and therefore specific membrane resistivity)

strongly influenced the voltage imposed to subsequent varicosities along dendrites when a steady state voltage step was applied to the soma. The thinnest dendritic diameter produced the highest axial resistance and therefore the largest voltage drops between varicosities. The results from this simulation indicate that while dendritic diameters of 0.3 and 0.5 µm allowed the most distal varicosities (~200 µm from soma) to experience depolarizations that were attenuated by <30% of those observed in the soma, the thinnest dendritic diameter, 0.1 µm, reduced the relative depolarization in the most distal varicosities by >95% (Figure 11b). In fact, the response for this model decayed to 1/e within 56 µm suggesting that only the first two varicosities along a dendrite see >37% of the somatic potential and that the most distal varicosities are negligibly influenced by somatic voltage clamp.

Figure 11

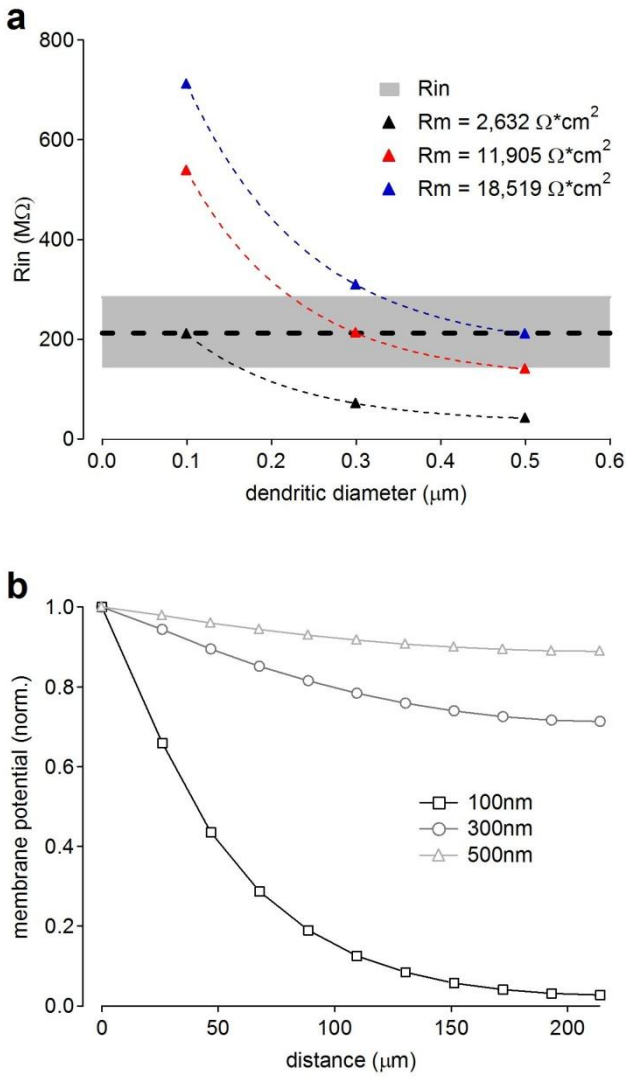

Figure 11. Determination of membrane resistivity and effective space clamp for A17 model. (**a**) Membrane resistivity was varied to match experimentally measured average input resistance for each dendritic diameter tested. This approach assures that both unknowns are restricted by real physiological parameters even though they are non-independent variables. (**b**) Applying a depolarizing step (200 ms) with a somatic voltage-clamp electrode gives rise an estimate of the respective space clamp.

Dendritic isolation and local dendritic signaling

Experimental evidence indicates that feedback inhibition mediated by $GABA_A$ and $GABA_C$Rs in the inner retina, presumably located on RBC terminals, modulates the spatial extent of feed forward signaling in the rod pathway (Volgyi *et al.*, 2002). This effect of RBC inhibition is further supported by studies showing that light-evoked inhibition modulates the amplitude and time course of glutamate release from RBCs via $GABA_A$ and $GABA_C$R activation (Eggers and Lukasiewicz, 2006a). Center-surround inhibition has been shown to be sensitive to TTX, indicating that Na_v channels and/or action potentials underlie signaling in the interneurons that are responsible for this form of inhibition. Although at least one of the homologous A17 cells from rabbit fires action potentials (Bloomfield, 1996), it is now clear that A17 amacrine cells in rat retinas do not (Figure 9). Are A17s in rat capable of providing center surround inhibition in addition to local reciprocal inhibition? This type of signaling would likely require a synaptic depolarization within a single dendritic varicosity to propagate or spread into additional varicosities along the stimulated dendrite. Traditionally, because vesicular neurotransmitter release is a calcium-dependent process, the intermediate between membrane depolarization and neurotransmitter release from most neurons in the CNS is Ca_v channels. In Chapter 4, we demonstrate that voltage-dependent calcium-permeable ion channels, specifically L-type Ca_v channels, are expressed in the synaptic feedback varicosities of A17, thus providing the standard link. To examine signal processing within passive A17 dendrites, a synaptic conductance (see methods), similar to that observed

experimentally (Figure 19b,d), was introduced to a single dendritic varicosity while membrane potential was observed in all varicosities along the stimulated dendrite. This was repeated for all varicosities along the dendrite to determine how position, relative to the capped end and the soma, would influence signaling (Figure 12a). Figure 12 shows the raw responses to synaptic stimulations for each of the passive A17 models (dendritic diameters of 0.l, 0.3 and 0.5 µm). Synaptically stimulated varicosities centrally located on the thinnest dendrites (0.1 µm diameter) responded with larger depolarizations than on thicker dendrites (Figure 12b,c,d). For all three models, the response amplitude within the stimulated varicosity was a function of location on the dendrite. Responses increased with increasing distance from the soma. This effect is related to differences in the total axial resistance for a particular direction, with the capped-end dendrite acting as an infinite resistor. For the model with the largest dendritic diameter (0.5 µm diameter), the stimulated varicosity response amplitude was linear, but as dendritic diameter decreased (and therefore R_m) the responses became increasingly nonlinear (Figure 12e). This emerging non-linearity gives rise to a central region of the dendrite in which synaptic responses vary minimally between neighboring varicosities, indicating that varicosities within this region are electrically isolated from the capped end of the dendrite, cell body, neighboring dendrites, etc. The dendritic responses to the stimulation of individual varicosities were normalized to the stimulated varicosity response for a clearer indication of how signals spread within dendrites independently of absolute amplitudes (Figure 13a,c,e). Responses within the central regions of the 0.1 µm dendrites decayed to 1/e within ~50 µm, and therefore, within approximately two

neighboring varicosities. The spatial response from stimulation of the central most varicosity (5^{th} from the soma) was highly symmetric as indicated by a dendritic symmetry factor (DSF = $\Delta V_{Distal\_neighbor} / \Delta V_{Proximal\_neighbor}$) of 1.007. Responses from the most proximal and distal varicosities were also plotted as a function of stimulus location to better indicate the full extent of centrifugal and centripetal spread within entire dendrites (Figure 13b,d,f). As indicated in Figure 13b, the centrifugal and centripetal spread of synaptic signals were almost identical for the thinnest dendrite model (0.1 µm). Propagation of synaptically-evoked depolarization within the dendrites of the models with thicker dendrites (0.3 and 0.5 µm) was increasingly asymmetric as indicated by the DSFs of 1.173 and 1.209 for the respective central varicosities. The results also indicate that thicker dendrites and higher specific membrane resistivities give rise to enhanced centrifugal propagation of synaptic depolarization (Figure 13d,f).

Nonlinear signaling in the A17 model with the thinnest dendrites (0.1 µm) and preferential centrifugal propagation of signals in the thicker dendrite models (0.3 and 0.5 µm) suggests a high degree of dendritic isolation in all three of the tested amacrine cell models. To properly assess signaling between dendrites, potentials were observed in varicosities of an unstimulated dendrite in response to stimulation (as in Figure 12a) of individual varicosities of an adjacent dendrite. The responses in the unstimulated dendrite were normalized to the response amplitude of the stimulated varicosity to determine a transmission percentage for each of the models (Figure 14a,b,c). Anatomical data indicates that the most proximal A17 varicosities on the descending portions of the dendrites can exist in layers other than sublamina 5

and that these varicosities are often adjacent to $GABA_C$Rs on RBC terminals (Zhang *et al.*, 2002). However, previous electron microscopy data revealed that these high varicosities rarely make output synapses but that these regions of A17 dendrites receive input from other amacrine cells (Nelson and Kolb, 1985). The thickness of the rat IPL was measured to be 44 ± 3 μm (n = 5), indicating that the most proximal varicosity on each modeled dendrite (19.3 ± 7.0 n = 31intervaricosity spacings) was not located in sublamina 5. To our knowledge, these proximal varicosities have not been shown functionally or anatomically to receive an excitatory synaptic input. The membrane potential responses to excitatory synaptic stimulation of the proximal varicosity are indicated in gray and it should only be considered putative sites of excitatory input. For all tested models, potential responses in unstimulated dendrites decreased as a function of both observation distance and stimulus distance from the soma. For the model with 0.1 μm dendrites, transmission into the first varicosity of any unstimulated dendrite was <4% if excitation to the proximal varicosity on the stimulated dendrite was considered and <2% if not (Figure 14d). The models with 0.3 and 0.5 μm dendrites transmitted ~18% and <31%, respectively, when excitation of the proximal varicosity was considered and <11% and <19% when excluded. These results indicate that under all tested conditions unstimulated dendrites responded by less than 1/e to that of the stimulated dendrite. We conclude, therefore, that A17 dendrites are highly electrically isolated from one another.

Figure 12

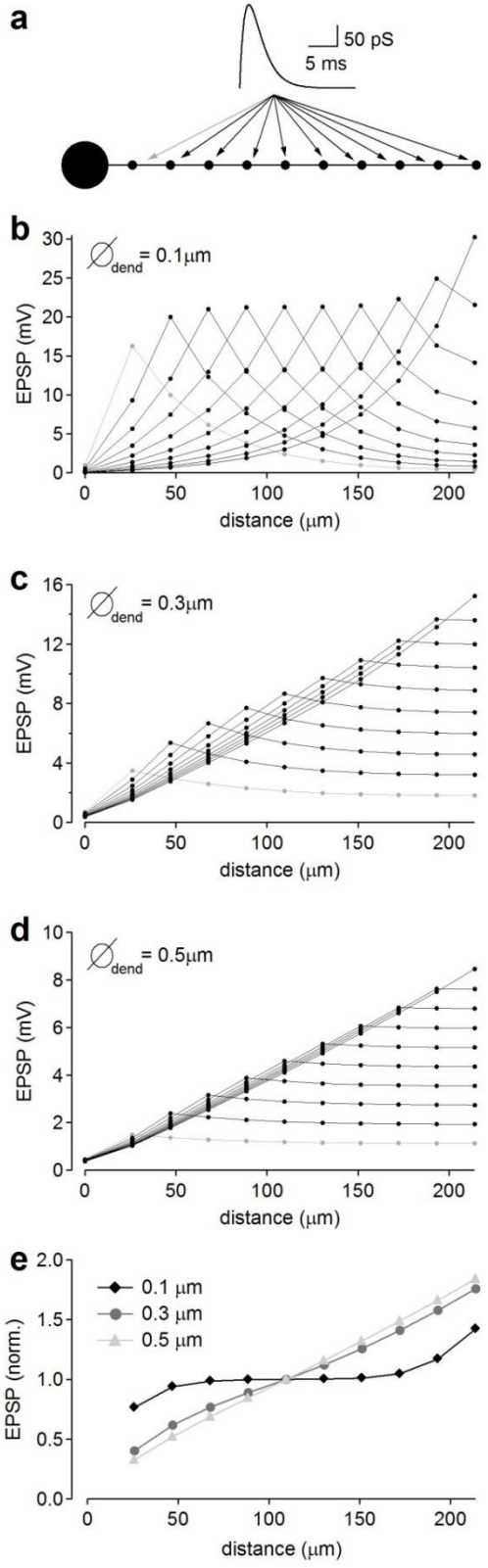
a
50 pS
5 ms
b
∅dend = 0.1µm
EPSP (mV)
distance (µm)
c
∅dend = 0.3µm
EPSP (mV)
distance (µm)
d
∅dend = 0.5µm
EPSP (mV)
distance (µm)
e
0.1 µm
0.3 µm
0.5 µm
EPSP (norm.)
distance (µm)

Figure 12. Propagation of synaptically-evoked depolarizations in passive A17 dendrites. (**a**) The simulated synaptic conductance was imposed on individual varicosities while simultaneously monitoring membrane potential at all varicosities on the stimulated dendrite. (**b**) 100 nm dendrites give rise to a high degree of synapse-specific varicosity depolarization and have an effective length constant that is shorter than the total dendritic length. (**c-d**) Larger dendritic diameters (300 and 500 nm) with correspondingly larger membrane resistivities enhance the spread of synaptic depolarizations and produce graded amplitude responses which increase with distance from the soma. Previous electron microscopy measurements indicate that A17 dendritic diameter is ~100 nm (Ellias and Stevens, 1980; Nelson and Kolb, 1985). (**e**) Normalized response amplitudes (normalized to response from the 5^{th} varicosity) for each stimulated varicosity indicates a linear increase as a function of distance from the soma for the 0.5 µm dendrite model. For the thinner dendritic diameters the responses become increasingly non-linear which produces a plateau of response amplitudes around the center of the dendrite.

Figure 13

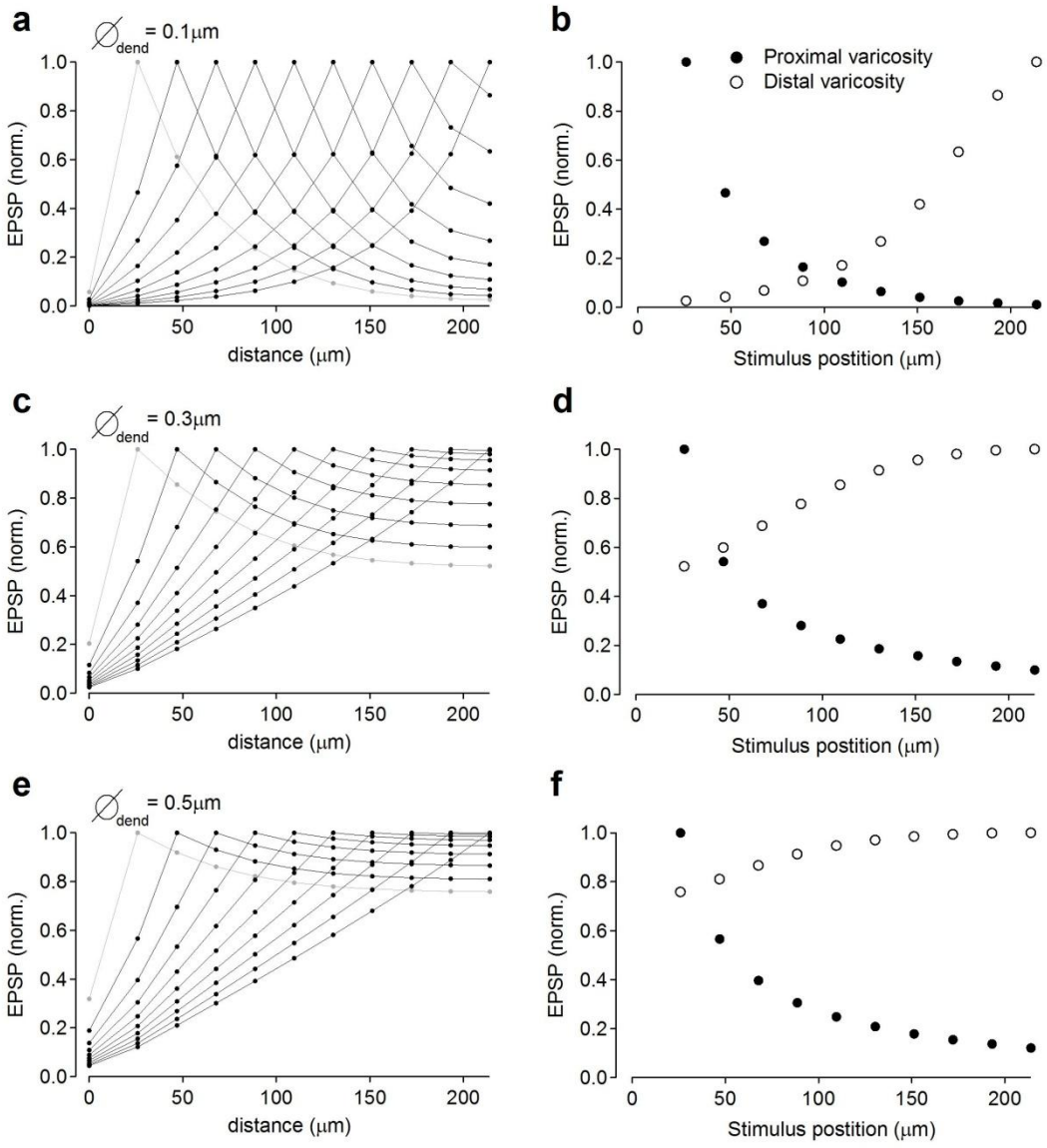
a
∅dend = 0.1μm
EPSP (norm.)
distance (μm)
b
Proximal varicosity
Distal varicosity
EPSP (norm.)
Stimulus postition (μm)
c
∅dend = 0.3μm
EPSP (norm.)
distance (μm)
d
EPSP (norm.)
Stimulus postition (μm)
e
∅dend = 0.5μm
EPSP (norm.)
distance (μm)
f
EPSP (norm.)
Stimulus postition (μm)

Figure 13. The impact of A17 morphology and dendritic diameter on the spreading of synaptically-evoked depolarizations. (**a,c,e**) Normalized potential changes observed in all varicosities in response to synaptic stimulation of a single varicosity (stimulating a different varicosity in each of the ten trials). (**b,d,f**) Response amplitudes in the most proximal and most distal varicosities to synaptic stimulation of individual dendritic varicosities. Thinner dendrites (such as 0.1 µm) minimize the spread of synaptic depolarizations into neighboring varicosities. The synaptically-evoked depolarizations propagate more symmetrically in the thinnest dendrites (0.1 µm; b) whereas the models with larger dendritic diameters (0.3 µm (**d**) and 0.5 µm (**f**)) dendrites respond with a more asymmetric, centrifugal propagation.

Figure 14

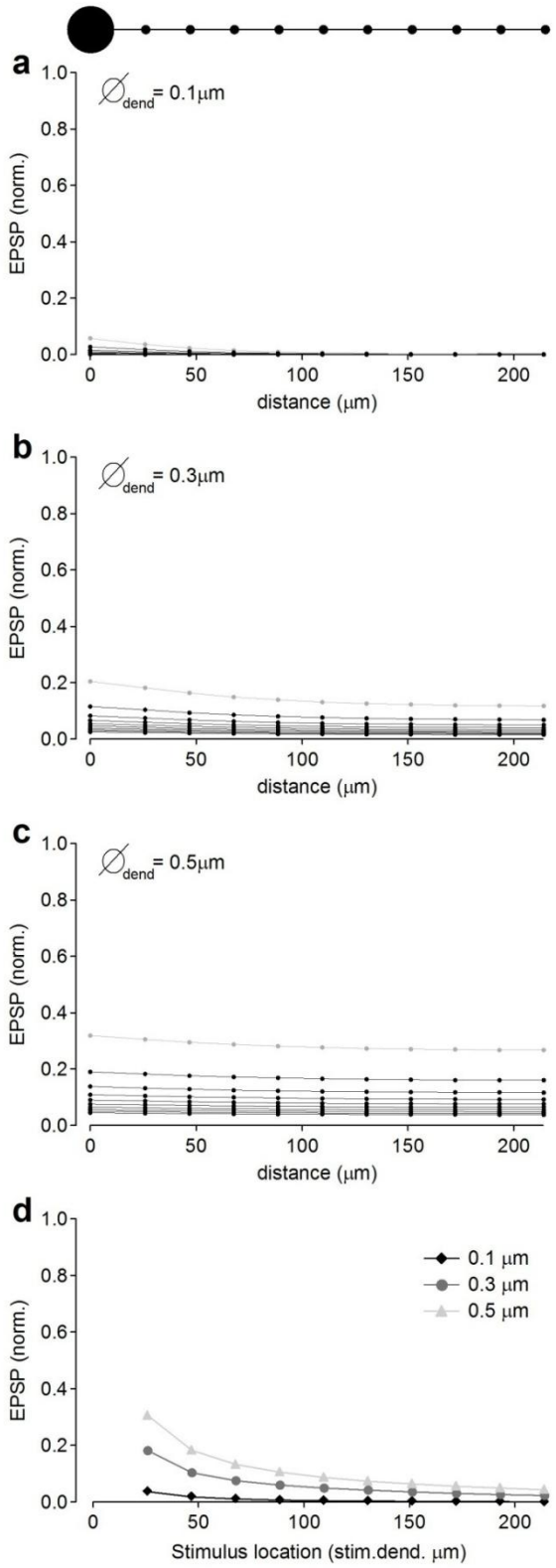
a
∅dend= 0.1μm
EPSP (norm.)
distance (μm)
b
∅dend= 0.3μm
EPSP (norm.)
distance (μm)
c
∅dend= 0.5μm
EPSP (norm.)
distance (μm)
d
0.1 μm
0.3 μm
0.5 μm
EPSP (norm.)
Stimulus location (stim.dend. μm)

Figure 14. A17 morphology limits the spread of synaptically-evoked depolarizations into neighboring dendrites. (**a-c**) Normalized potential responses to the stimulation of individual varicosities (See Figure 12a) observed in a unstimulated, neighboring dendrite. The grey traces in a-c correspond to synaptic stimulation of the most proximal varicosity on the stimulated dendrite which is located in the off layer of the IPL and has not yet been shown to receive excitatory synaptic input. (**a**) Thin dendrites (0.1 µm) minimize the spread of synaptic depolarizations between dendrites. The neighboring dendrite in the 0.1 µm dendritic diameter model is isolated from the stimulate dendrite by >96%. (**b**) The dendrites of the 0.3 µm dendritic diameter A17 model are isolated by >81% from the stimulated dendrite. (**c**) The dendrites of the 0.5 µm dendritic diameter A17 model are isolated by >69% from the stimulated dendrite. (**d**) Normalized potential responses observed in the most proximal varicosity of the unstimulated dendrite to subsequent synaptic stimulation of varicosities on an adjacent dendrite (stimulating a different varicosity in each of the ten trials).

Discussion

Graded A17 signaling

The first two neurons in the rod pathway, rod photoreceptors and RBCs, encode analog signals via action potential-independent, graded membrane potential changes. These excitatory neurons make specialized, ribbon type synapses onto postsynaptic neurons that are capable of releasing glutamate proportionally to membrane depolarization (Singer and Diamond, 2003). In the rod pathway, amacrine cells are critical for transmitting the rod-driven visual signals to the binary-signaling ganglion cells (Freeman *et al.*, 2008; Gollisch and Meister, 2008; Trong and Rieke, 2008), whose axons conduct the retinal output to the brain via the optic nerve. However, it remains unclear, and even controversial, as to which, if any, amacrine cells are capable of firing action potentials. Ultimately, this digital-to-analog conversion that takes place in the retina is still a poorly understood process and appears to rely on multiple synaptic mechanisms that extend the range of inputs to ganglion cells (Chen and Diamond, 2002). Although experimental results from rabbit retinas suggest that at least one of the two homologous A17 amacrine cells fire action potentials, the data presented here clearly indicate that rat A17 amacrine cells do not. Lack of action potential signaling indicates that A17 amacrine cells respond with graded membrane potential changes, and has several physiological implications.

Intuitively, graded signaling should underlie feedback. Similar analog-type signaling mechanisms between RBCs and A17 would enhance the range of information that can be encoded in the feed forward pathway. It also does not seem

logical for A17s to receive a more complex graded signal and then reduce the information into a simplified binary signal to feedback in an all or none response. Graded signaling has the additional advantage of enhancing the spatial acuity of reciprocal inhibition. A global response from A17 amacrine cells would likely eliminate the independence of gain control that occurs at individual RBC under extremely dim conditions (Dunn and Rieke, 2008). Global signaling from large dendritic field (~0.5 mm) of A17 would extend the gain modulation over distances that would be inappropriate for distinguishing contrasting objects in space. Therefore by balancing sensitivity and the risk of saturation over shorter lengths, graded signaling can increase the acuity of visual signaling while maintaining sensitivity to dim portions of the visual scene.

Compartmentalized signaling: local reciprocal inhibition versus lateral inhibition

A17 amacrine certainly provide local reciprocal inhibition to the stimulated RBC as indicated by step evoked feedback recordings from individual RBCs (Figure 22, Hartveit, 1999; Singer and Diamond, 2003; Chavez *et al.*, 2006). Because A17s were unable to elicit action potentials an electrontonic model of the A17 was used to determine the spatial extent of electrical signaling in dendrites and estimate the extent of lateral inhibition. This study indicates that the biophysical membrane properties and anatomical features of the A17 amacrine cell combine to compartmentalize electrical signaling within and between dendrites. In addition to creating high axial resistance between varicosities, thin dendrites are also likely to limit the diffusion of calcium between reciprocal release sites in neighboring varicosities. We suggest that

these forms of subcellular compartmentalization could allow these reciprocal synapses to act as independent neural circuits. However, without additional mechanisms to further attenuate electrical signaling between neighboring varicosities communication clearly can occur within ~50 µm of the stimulus point (Figure 13a), indicating that reciprocal inhibition in not necessarily entirely synapse specific.

Signaling asymmetries in dendrites

For most neurons, electrical signals need to propagate through the cell body for a chance to trigger an output response. Wide-field amacrine cells, such as starburst and A17, contain both synaptic inputs and release machinery within individual dendrites eliminating the need for signaling through the cell body as an intermediate. The passive models presented here argue, that in the absence of active conductances such as Na_v channels, general amacrine cell morphology alone produces a preferential centrifugal spread of synaptically evoked depolarizations. The DSFs and Figure 13 indicate that as dendritic diameter and specific membrane resistivity increase signals travel over longer distances and are more significantly affected by the differential axial resistance at either end of the dendrite leading to more efficient charging of the more distal membranes. This finding could, in part, explain why starburst amacrine cells respond with preferred centrifugal signaling, and, unlike other starburst models, does not rely on a tonic potential gradient (Hausselt *et al.*, 2007).

Concluding remarks

This study provides direct evidence that A17 amacrine cells do not fire action potentials and that Na_v channels minimally contribute to membrane excitability. Electrotonic modeling the A17 amacrine cell indicates that biophysical membrane properties and anatomical characteristics reduce the spatial extent of signaling. However, it should be clearly noted that passive membrane properties were used as a first approximation and might not accurately reflect the true properties of A17 membranes. For example, uniformly expressed voltage gated potassium channels would likely act to further attenuate electrical signals within dendrites and reduce interactions between varicosities and should be tested in future simulations. Although these models provide a framework for understanding amacrine signaling, experimental evidence is required to validate the findings. Future experiments to address these issues will likely rely on the improving imaging technologies for monitoring membrane potentials in neurons.

Chapter 4: BK channels modulate reciprocal feedback inhibition

Introduction

In the mammalian retina, the rod bipolar cell (RBC)/ AII amacrine cell/ A17 amacrine cell dyad limits the gain of the rod pathway (Dunn *et al.*, 2006). The RBC makes an excitatory ribbon-type synapse onto AII and A17 amacrine cell processes and, in return, the A17 makes a reciprocal inhibitory synapse back onto the RBC terminal (Nelson and Kolb, 1985; Hartveit, 1999; Singer and Diamond, 2003) that sharpens the time course of the rod-driven visual signal *in vivo* (Dong and Hare, 2003) . Reciprocal GABA release from A17s can be triggered directly by Ca^{2+} influx through Ca^{2+}-permeable AMPA receptors (CP-AMPARs) and subsequent calcium-induced Ca^{2+} release (CICR) from intracellular stores, resulting in the activation of $GABA_A$- and/or $GABA_C$Rs on RBC terminals (Chavez *et al.*, 2006). Those experiments in rat retina suggested that feedback from A17s can occur independently of voltage-gated calcium (Ca_v) channels. Although indirect evidence for Ca_v channels in A17s has been reported (Menger and Wassle, 2000; Chavez *et al.*, 2006), the type and location of these channels is unknown. Even if Ca_v channels were localized to the bouton-like synaptic varicosities where GABA feedback occurs, it is possible that their contribution to GABA release could be prevented either by

biochemical compartmentalization, or perhaps another conductance that could counteract synaptic depolarization and limit Ca_v channel activation.

Recent studies have elucidated important roles for Ca^{2+}-activated potassium (K_{Ca}) channels in regulating fundamental components of neuronal signaling in the CNS such as synaptic transmission and spike frequency (Hu *et al.*, 2001; Skinner *et al.*, 2003; Womack and Khodakhah, 2003; Raffaelli *et al.*, 2004; Faber *et al.*, 2005; Maher and Westbrook, 2005; Ngo-Anh *et al.*, 2005; Xu and Slaughter, 2005; Liu and Shipley, 2008; Lin *et al.*, 2008). K_{Ca} channel nomenclature refers specifically to the size of the single channel conductance (γ), but other biophysical properties also differ substantially. Small-conductance K_{Ca} (SK) channels (γ = 9-10 pS) are activated solely by intracellular Ca^{2+} levels, whereas large (big)-conductance K_{Ca} (BK) channels (γ = 100-270 pS) are activated both by voltage and Ca^{2+} and can inactivate rapidly if additional auxiliary β subunits are present (Hicks and Marrion, 1998; Wallner *et al.*, 1999; Orio *et al.*, 2002). SK channels can be activated by rises in intracellular Ca^{2+} attributed to influx through Ca_v channels, release from intracellular stores or synaptic activation of NMDARs. This coupling has direct consequences for synaptic plasticity, calcium spikes and action potential shape and firing frequency in several areas of the CNS (Ngo-Anh *et al.*, 2005; Faber *et al.*, 2005). The effects of BK channel activation on network signaling in the CNS are less well understood, but it is clear that the voltage-dependence of these channels shifts towards negative potentials when intracellular Ca^{2+} levels increase (Berkefeld *et al.*, 2006; Marty, 1981) and that BK activation can significantly affect action potential repolarization and spontaneous firing (Sun *et al.*, 2003; Meredith *et al.*, 2006).

Here we show that rapidly-inactivating BK channels modulate both excitatory and inhibitory synaptic transmission at the RBC-A17 reciprocal feedback synapse in rat retina. Experiments employing a combination of electrophysiology, pharmacology, two-photon Ca^{2+} imaging and immunohistochemistry approaches indicate that BK channels are colocalized with L-type Ca_v channels, intracellular calcium stores and AMPAR-mediated synaptic inputs within individual synaptic varicosities along A17 dendrites. Blocking BK channels in A17s enhances EPSPs and inhibitory feedback, recruiting an additional, kinetically distinct population of GABA receptors. Together these interconnected mechanisms regulate and extend the input/output characteristics of this reciprocal feedback synapse.

Results

L-type Ca_V channels and intracellular Ca^{2+} stores are colocalized with synaptic inputs at A17 varicosities

Although previous work suggests that A17 membranes exhibit voltage-activated Ca^{2+}-permeability (Menger and Wassle, 2000), GABA release from A17s can occur independently of Ca_v channels (Chavez *et al.*, 2006). One possible explanation for this apparent paradox is that Ca_v channels may not be located in the A17 varicosities where GABA feedback occurs. To test this idea, we made Ca^{2+} fluorescence measurements from the specialized synaptic compartments along A17 dendrites that have been shown to be reciprocally connected to RBC ribbon synapses (Nelson and Kolb, 1985; Zhang *et al.*, 2002). Whole cell recordings were made from

amacrine cells with relatively large somas (diameter ~ 10 μm) adjacent to the inner plexiform layer (IPL). Fluo-5F (200 μM) and Alexa 594 (40 μM) were included in the patch pipette to monitor intracellular Ca^{2+} and cell morphology, respectively. A17 amacrine cells (Figure 15a and 17a) were identified by the combination of several features: 1) multiple non-branching appendages extending from the soma into sublamina 5 of the IPL, where A17s receive synaptic input from RBCs; 2) small varicosities along the length of the dendrites (at ~15-20 μm intervals; Zhang *et al.*, 2002); and 3) input resistance in the range of 150-350 MΩ (244.5 ± 74.5 MΩ, n = 159). After an approximately 30-minute dialysis period, we electrically stimulated bipolar cells in the outer plexiform layer (OPL) and searched for time-locked fluorescence transients in individual A17 varicosities. Synaptically-evoked Ca^{2+} responses under voltage-clamp were difficult to locate due to the small size and low density of varicosities. Cyclothiazide (50 μM) was included in the bath solution to enhance AMPAR affinity for glutamate and remove desensitization (Partin *et al.*, 1993). Under these conditions, synaptically-evoked fluorescence transients could be observed in a small subset of varicosities (Figure 15b *middle*). Varicosities adjacent to the responding varicosity along a single dendrite were typically unresponsive to synaptic stimulation (not shown), suggesting that the Ca^{2+} response was predominantly a result of synaptic activation of the responding varicosity. If a synaptically evoked Ca^{2+} signal was observed, we then tested the varicosity for a voltage-activated Ca^{2+} response by applying a depolarizing voltage step through the somatic recording electrode (-70 mV to -10 mV, 100 ms; Figure 15b *right*). In general, varicosities which responded to synaptic stimulation also responded to

voltage steps (35 of 36 varicosities, n = 23 different cells; Figure 15f) indicating that Ca_v channels are colocalized with synaptic inputs at individual feedback varicosities and that Ca^{2+} compartmentalization does not occur on scales ≥ 600 nm, the spatial resolution of the imaging system. These signals arose via distinct mechanisms: application of the AMPAR antagonist NBQX (10 μM) blocked synaptically evoked currents (to 0.4 ± 0.8% of control, n = 5; P = 0.0052; Figure 15d *left*) and fluorescence (to 0.5 ± 6.9% of control, n = 5, P = 0.0097; Figure 15b *middle*) but not step evoked currents (100.5 ± 14.2% of control, n = 5, P = 0.616; Figure 15d *right*) or fluorescence (98.9 ± 44.0% of control, n = 5, P = 0.2912; Figure 15b *right*).

To identify the subtypes and location of Ca_v channels in A17s, we examined the voltage-dependence and pharmacology of Ca_v signals with electrophysiological and imaging techniques. Families of 100 ms voltage steps (-70 mV to +30 mV, 20 mV increments) revealed sustained inward currents that were sensitive to isradipine (-37.7 ± 15.9 pA block at -10 mV, n = 17, P < 0.0001; Figure 16a), indicating the presence of L-type Ca_v channels. Consistent with blockade of inward Ca^{2+} current, isradipine strongly reduced voltage-step evoked fluorescence transients in the cell bodies (to 33.6 ± 10.8% of control, n = 6, P = 0.004) and varicosities (to 22.6 ± 12.7% of control, n = 5, P = 0.006) of A17 (Figure 16c). Voltage-activated fluorescence transients were observed in all varicosities tested within 150 μm of the soma as well as in all somata.

Both CP-AMPARs and CICR have been shown to trigger neurotransmitter release from A17s (Chavez *et al.*, 2006). To examine the contributions of CICR to voltage-activated Ca^{2+} signaling in A17 varicosities, excitatory and inhibitory

synaptic transmission was pharmacologically blocked and voltage-activated (-70 mV to -20 mV, 100 ms) single varicosity fluorescence (Figure 17b, white box in Figure 17a) was observed under control conditions and in the presence of thapsigargin (1 µM), which depletes internal Ca^{2+} stores by blocking SERCA pumps (Treiman *et al.*, 1998). Depletion of intracellular stores did not reduce the recorded Ca^{2+} current (99.7 ± 15.7% of control at -20 mV, n = 5, P = 0.57; Figure 17d,e) but did significantly reduce the observed fluorescence (to 58.7 ± 18.7% of control at -20 mV, n = 5, P = 0.0091; Figure 17c,d), indicating that Ca^{2+} influx through Ca_v channels triggers CICR within varicosities.

Figure 15

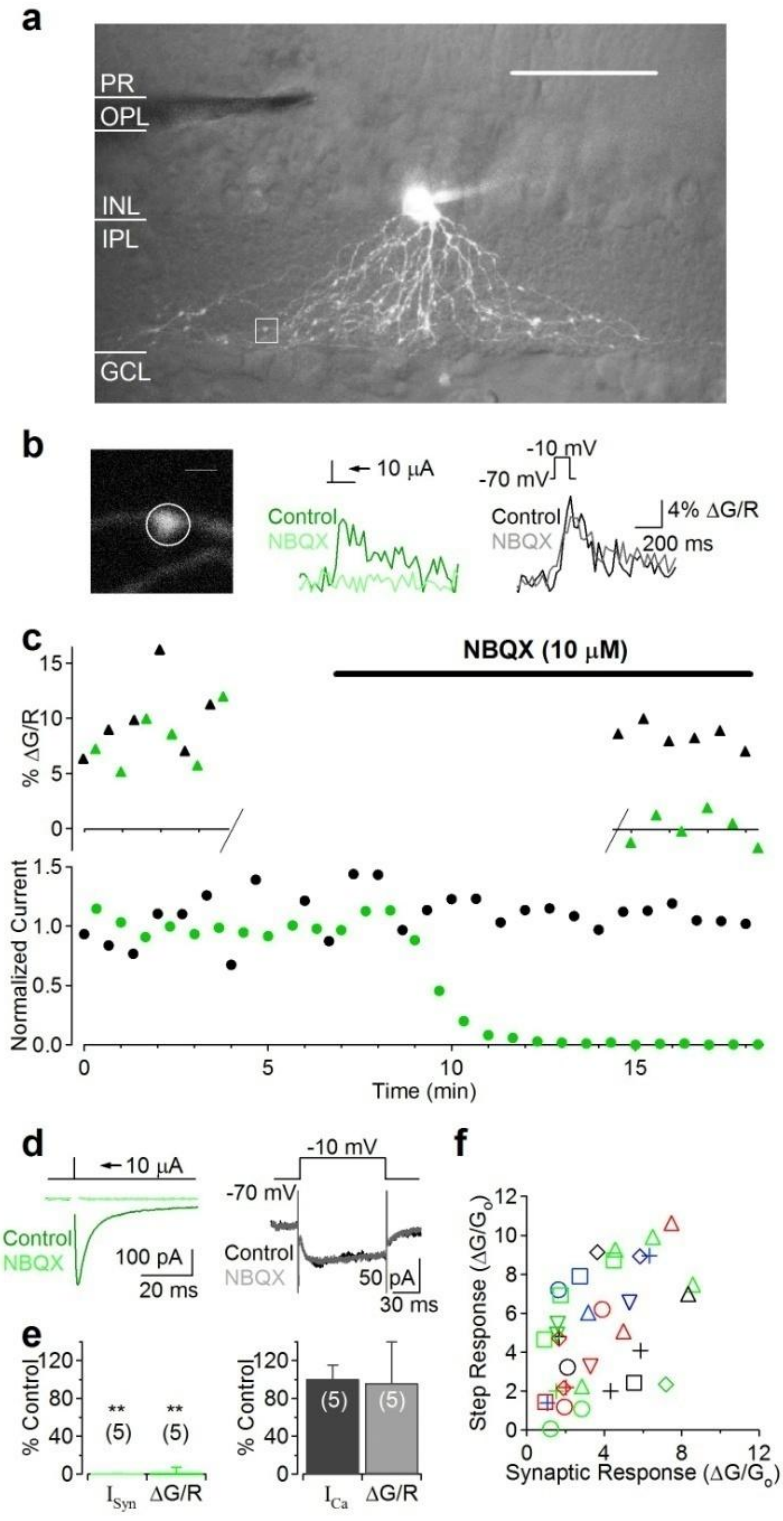
a
PR
OPL
INL
IPL
GCL
b
10 μA
-10 mV
-70 mV
Control
NBQX
4% ΔG/R
200 ms
c
NBQX (10 μM)
% ΔG/R
Normalized Current
Time (min)
d
10 μA
Control
NBQX
100 pA
20 ms
-10 mV
-70 mV
50 pA
30 ms
e
% Control
(5)
I_Syn
ΔG/R
I_Ca
f
Step Response (ΔG/G_o)
Synaptic Response (ΔG/G_o)

Figure 15. Voltage-gated calcium channels are colocalized with synaptic inputs at individual A17 varicosities. (**a-d)** Single cell experiment. (**a**) 3D 2-photon reconstruction of an A17 amacrine cell superimposed on a single IR-DIC image of the retinal slice. Scale bar = 50 μm. (**b**) Single varicosity (left) calcium transients were observed in response to synaptic stimulation (center; green) or voltage step (right; black; -70 mV to -10 mV; 100 ms). Scale bar = 2 μm. (**c**) Fluorescence (top) and current (bottom) amplitudes plotted over time in response to interleaved stimulation (green: synaptic, black: voltage step). Application of NBQX (10 μM) completely blocked synaptic currents and fluorescence. Single varicosity calcium fluorescence was observed for the first 12 responses (control) and for a subsequent 12 responses (NBQX) approximately 8 minutes after the onset of NBQX application to minimize photodamage. (**d**) Synaptic and voltage-dependent currents. (**e**) Summary of pharmacological effects on synaptically evoked (left) and step evoked (right) currents and fluorescence (n = 5 cells). (**f**) Varicosities that fluorescently responded to synaptic stimulation also responded to a single voltage step (35 of 36 varicosities; n = 23 cells).

Figure 16

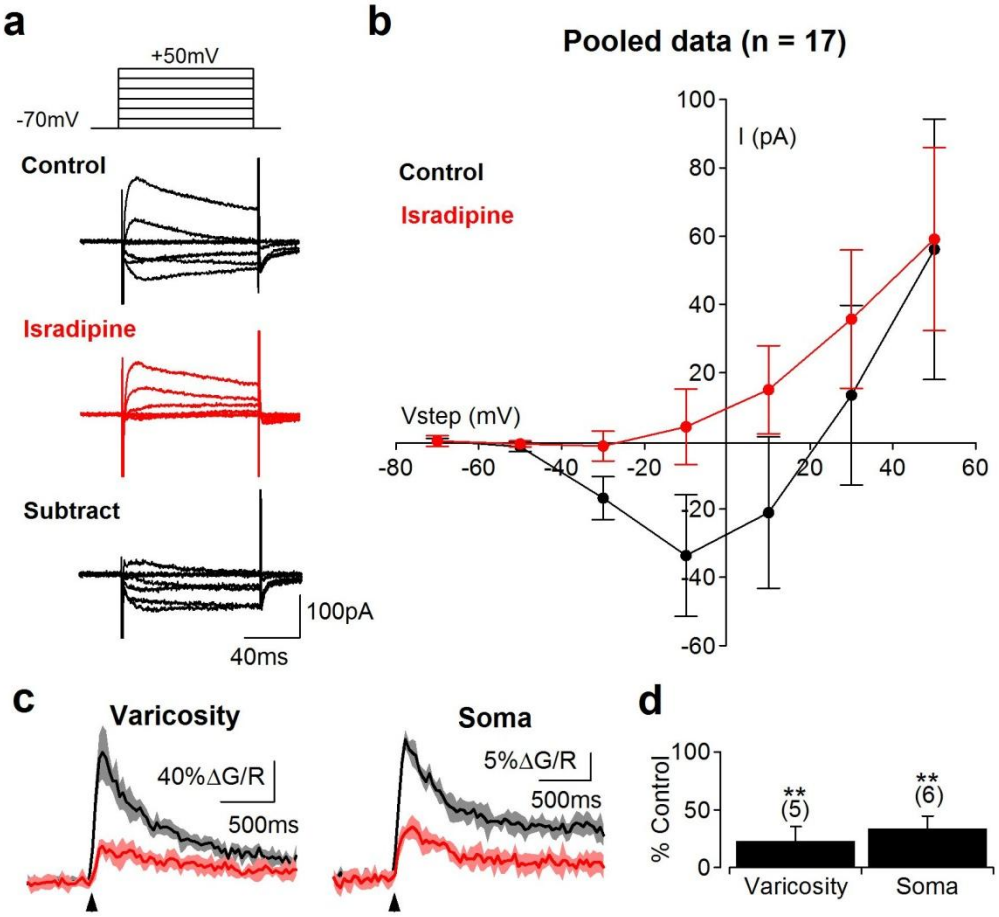
a
+50mV
-70mV
Control
Isradipine
Subtract
100pA
40ms
b
Pooled data (n = 17)
Control
Isradipine
I (pA)
Vstep (mV)
c
Varicosity
40%ΔG/R
500ms
Soma
5%ΔG/R
500ms
d
% Control
(5)
(6)
Varicosity
Soma

Figure 16. Functional L-type VGCCs are expressed at A17 synaptic varicosities and somata. (**a**) A series of depolarizing voltage steps (-70 to +50 mV in 20 mV increments; 100 ms) elicited an isradipine- (10 μM) sensitive inward current. (**b**) Summary of the current-voltage relationship in control and in the presence of isradipine (10 μM; n = 17 cells). (**c**) Depolarizing voltage steps (100 ms to -10 mV) also elicited isradipine-sensitive fluorescence transients in the varicosities (top) and somas (bottom) of A17 amacrine cells. Fluorescence from a single varicosity (typically a 16x16 frame) was acquired at ~50 Hz and a small region of interest (as in figure **1b**) was drawn around the varicosity to produce an average pixel value. Traces are the average of eight responses to 100 ms voltage steps before and after isradipine application (arrow indicated onset of step). Shaded regions indicate ± SD. (**d**) Summary of the effects of isradipine on voltage-dependent fluorescence at individual varicosities (n = 5 cells) and somas (n = 6 cells).

Figure 17

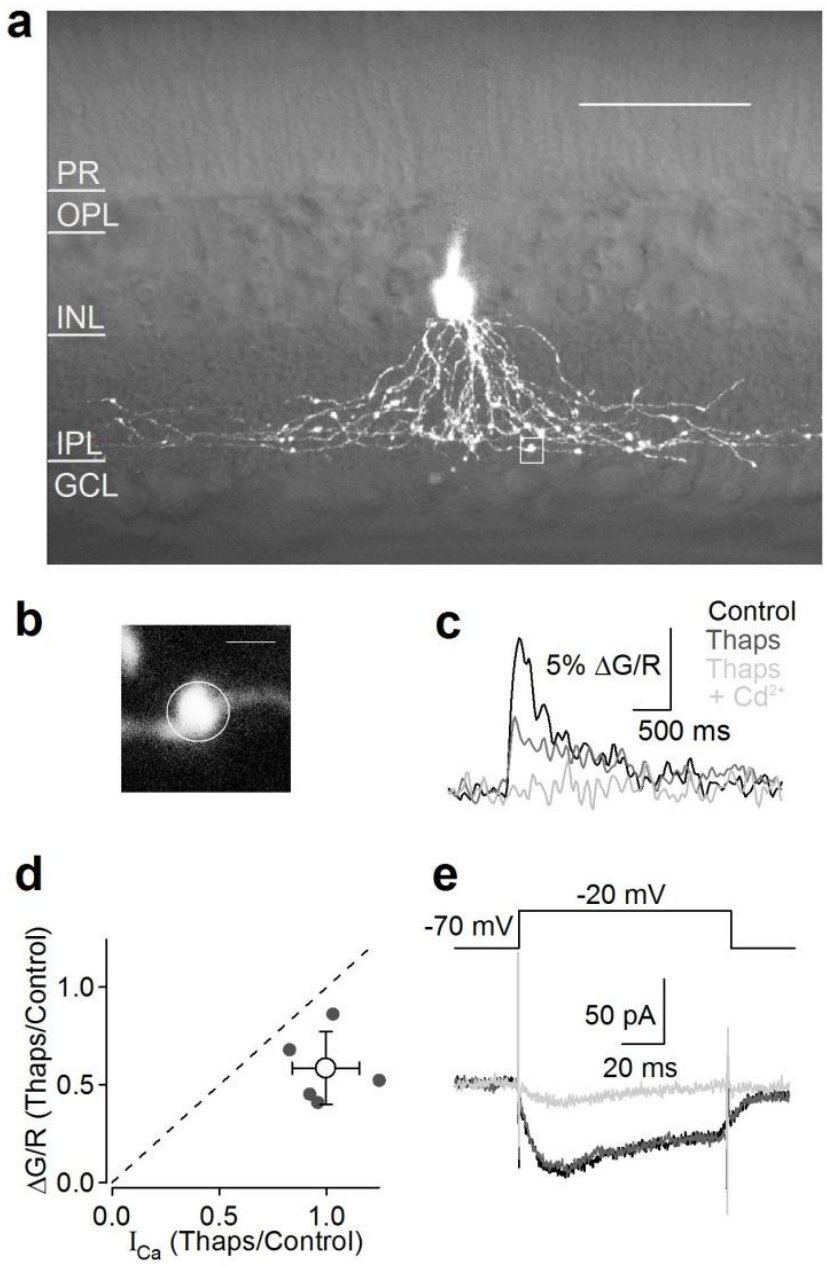
a
PR
OPL
INL
IPL
GCL
b
c
Control
Thaps
Thaps
+ Cd2+
5% ΔG/R
500 ms
d
ΔG/R (Thaps/Control)
1.0
0.5
0.0
0.0
0.5
1.0
ICa (Thaps/Control)
e
-20 mV
-70 mV
50 pA
20 ms

Figure 17. Intracellular stores amplify voltage-dependent calcium responses in varicosities. (**a-c, e**) Single cell experiment. (**a**) 3D 2-photon reconstruction of an A17 amacrine cell superimposed on a single IR-DIC image of the retinal slice. Scale bar = 50 μm. (**c**) Fluorescence trace was derived from the indicated ROI (**b**, white box in **a**) in control (black), thapsigargin (1 μM; gray), and thapsigargin plus Cd^{2+} (200 μM; light gray). Scale bar = 2 μm. (**e**) Ca^{2+} current in control (black), thapsigargin (gray), and thapsigargin plus Cd^{2+} (light gray). Imposed electrode potential (-70 to -20 mV; 100 ms). (**d**) Summary of the effects of thapsigargin on current and fluorescence amplitudes for 5 cells.

Rapidly-inactivating BK channels are localized to feedback varicosities and are coupled to activation of L-type Ca_v channels

If Ca_v channels are located in synaptic varicosities, why don't they contribute to GABAergic feedback? One possibility is that some other mechanism limits synaptic depolarization and, therefore, Ca_v channel activation. Spontaneous potassium currents have previously been observed in acutely dissociated amacrine cells from tiger salamander (Mitra and Slaughter, 2002). These transient currents were sensitive to iberiotoxin, a component of scorpion venom that selective antagonizes BK channels. A synaptic event causing a coincident local depolarization and increased cytosolic Ca^{2+}, via Ca^{2+} influx through CP-AMPARs, Ca_v channels and/or subsequent CICR, could activate a hyperpolarizing BK current to counteract AMPAR-mediated depolarization and quickly suppress Ca_v channel activation. To test for functional BK channels in A17s, voltage clamp recordings were made from A17 amacrine cells in slice with K^+-based internal solutions. To resolve BK-mediated currents more clearly, A-type K_v channels were blocked with 4-AP (4 mM). Depolarizing voltage steps (from -90 mV to -30 mV for 200 ms) elicited a sustained, inward Ca_v channel-mediated current and a transient outward current that was completely blocked by iberiotoxin (100 nM, to 2.3 ± 8.5% of control, P = 0.0105, n = 5; Figure 18a), indicating the presence of BK channels in A17s. Although L-type Ca_v channel inactivation and the observed (highly buffered) voltage-dependent calcium signals decayed on the order of hundreds of milliseconds (see Figure 16), the transient BK currents decayed much more quickly (τ = 4.39 ± 1.31 ms, n = 5), suggesting that BK channels in A17s inactivate rapidly. Pairs of steps (-90 mV to -30

mV, 40 ms) with incremental interstep intervals indicated that the Ca_v channel-coupled BK pathway recovers from inactivation with a time constant of 23.62 ± 4.74 ms (n = 5; Figure 18b).

We next tested whether BK channels were activated by Ca^{2+} influx through L-type Ca_v channels. Application of isradipine (10 μM) strongly reduced the transient outward current (to 13.1 ± 10.6% of control, n = 5, P = 0.0347; Figure 18c) indicating that L-type Ca_v channel activation could trigger BK currents. CICR makes little contribution to BK channel activation, as depleting intracellular stores with thapsigargin (1 μM) only slightly reduced BK currents elicited by voltage steps to -30 mV (to 92 ± 10.9% of control, n = 5, P = 0.0633; not shown).

As a further test for BK expression, A17s were filled through the patch pipette with neurobiotin (50 mM) and slices were incubated in antibodies to streptavidin (green, binds neurobiotin), PKCα (blue, labels RBCs), and BK channels (red) or the auxillary subunit responsible for BK inactivation, β2 (red). BK immunoreactivity was evident throughout the IPL and was strongest in sublamina 5, which contains the RBC terminals and A17 varicosities (Figure 18d). Higher magnification of sublamina 5 revealed clusters of fluorescent puncta surrounding RBC terminals (slice: Figure 18e; whole-mount: Figure 18g). In 89 A17 varicosities opposed to RBC terminals imaged in 5 different slices, 72 (81%) contained BK puncta (Figure 18e). Consistent with the physiological observation that A17 BK channels inactivate rapidly (Figure 18a, b), β2 subunit immunoreactivity displayed a similar pattern to that of BK antibodies, with individual puncta colocalized with A17 varicosities (Figure 18f) and surrounding RBC terminals (whole mount: Figure 18h).

Figure 18

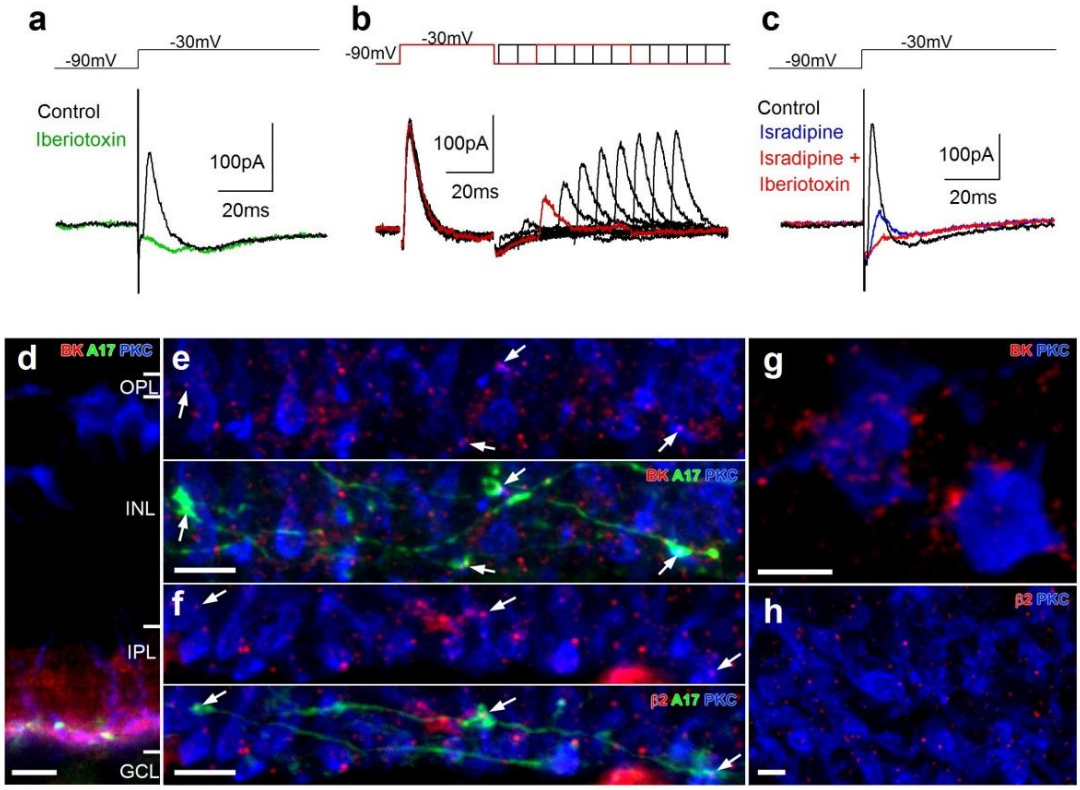
a
-90mV
-30mV
Control
Iberiotoxin
100pA
20ms
b
-90mV
-30mV
100pA
20ms
c
-90mV
-30mV
Control
Isradipine
Isradipine +
Iberiotoxin
100pA
20ms
d
BK A17 PKC
OPL
INL
IPL
GCL
e
BK A17 PKC
f
β2 A17 PKC
g
BK PKC
h
β2 PKC

Figure 18. A17s varicosities express rapidly inactivating BK channels that are functionally coupled to L-type VGCCs. (**a**) Depolarizing voltage steps (from -90 to -30mV; 100ms) in an A17 elicited a rapidly inactivating outward current (in potassium-based internal) that was blocked by iberiotoxin (100 nM) (**b**) Paired depolarizing steps delivered at varying intervals revealed the time course of recovery from inactivation. (**c**) The transient outward current also was blocked by the L-type VGCC blocker, isradipine (10μM). (**d**) Immunohistochemistry techniques reveal BK (red) channel expression throughout the inner plexiform layer of slice. Anti-PKCα was used to label RBCs (blue) and the dendrites of a single A17 were filled with neurobiotin (green) through the patch pipette. Scale bar = 10 μm. (**e**) A higher-magnification view of sublamina 5 in the IPL indicates that BK (top half) and β2 subunit (bottom half) puncta are localized to A17 varicosities that are adjacent to RBC terminals. Scale bars = 5 μm. (**f**) Antibody staining for PKC (blue) and BK (red, top) or β2 (red, bottom) in whole-mount retina illustrates the clustering of channels antibody around RBC terminals. Scale bars = 2 μm.

BK channels suppress synaptic depolarization

If BK channels were activated during synaptic transmission, they perhaps could counteract AMPAR-induced depolarization and reduce EPSPs in A17s. To test this hypothesis, we recorded from A17s in the current-clamp configuration (K^+-base internal) with inhibition blocked and elicited EPSPs by electrical stimulation of afferent bipolar cells in the outer plexiform layer (OPL). Blocking BK channels with iberiotoxin potentiated EPSPs (141.22 ± 30.21% of control, n = 6, P = 0.0496; Figure 19a), suggesting that synaptically-activated BK channels limit synaptic depolarization. Iberiotoxin did not affect EPSCs (with Cs-based internal solution, 97.2 ± 8.1% of control; n = 5; P = 0.184; Figure 19b) indicating that the drug does not affect transmitter release from RBCs or AMPARs on A17s. These results indicate that BK currents counterbalance synaptic AMPAR-mediated EPSCs in A17 synaptic varicosities, an interaction that may be optimized by the kinetic similarities between the two currents (EPSC τ_{decay} = 3.2 ± 1.6 ms, n = 5; BK current $\tau_{inactivation}$ = 4.4 ± 1.3 ms, n = 5; Figure 19d).

Figure 19

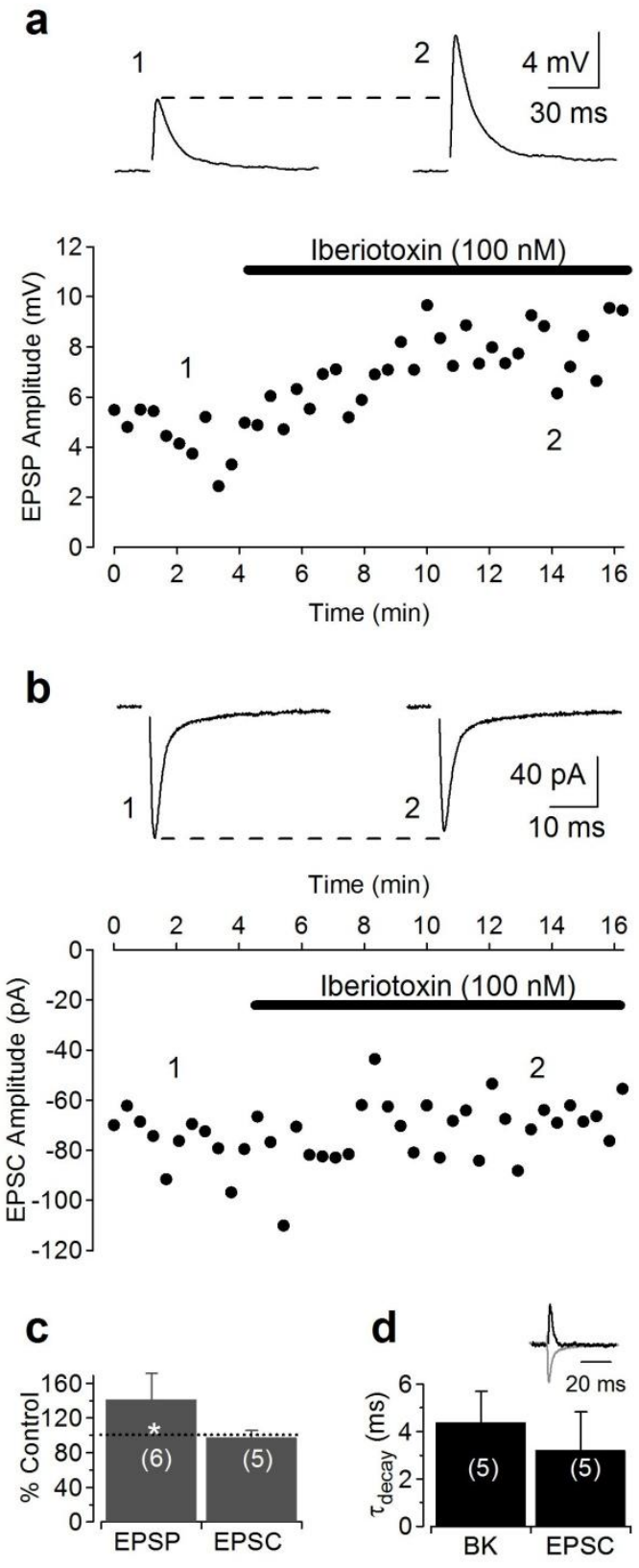
a
1
2
4 mV
30 ms
Iberiotoxin (100 nM)
EPSP Amplitude (mV)
Time (min)
b
40 pA
10 ms
Time (min)
Iberiotoxin (100 nM)
EPSC Amplitude (pA)
c
% Control
(6)
(5)
EPSP
EPSC
d
20 ms
τdecay (ms)
(5)
(5)
BK
EPSC

Figure 19. BK channels suppress synaptic transmission.

(**a**) Synaptic stimulation of current-clamped A17 elicited EPSPs which were potentiated by application of iberiotoxin (black bar, 100 nM). (**b**) EPSCs (in Cs-based internal) were recorded from A17 in control and iberiotoxin to test for possible presynaptic effects of the BK channel antagonist. (**c**) Pooled data from experiments in **a** and **b**. (**d**) The time course of BK inactivation and EPSC decay were similar across cells. (*inset*) AMPAR-mediated EPSC and voltage-activated BK current (normalized) from the same cell superimposed to demonstrate the similarity in kinetics and opposite polarity (at -70 mV).

BK channels limit GABA release from A17amacrine cells

To what extent do Ca_v channels and BK channels contribute to feedback inhibition onto RBC terminals? GABA release from A17s can be measured in RBCs by puffing glutamate onto A17 dendrites and recording IPSCs in voltage-clamped RBCs (Chavez *et al.*, 2006). Here we elicited IPSCs in RBCs (V_{hold} = 0 mV) with brief glutamate puffs (50 and 500 μM, 25 ms) in the presence of TTX (1μM) and strychnine (1 μM) to isolate A17-mediated feedback. In agreement with Chavez *et al.* (2006), application of Cd^{2+} (200 μM), a Ca_v channel pore blocker (Hobai *et al.*, 1997; Shen *et al.*, 2000), only slightly reduced the IPSCs evoked by 50 μM glutamate (90.87 ± 4.99% of control, n = 6, P = 0.0124; Figure 20a). Application of iberiotoxin (100 nM) significantly enhanced IPSCs evoked by 50 μM glutamate evoked IPSCs (116.69 ± 11.26% of control, n = 6, P = 0.022), indicating that BK channels limit GABA release from A17s. The enhancement caused by iberiotoxin was essentially removed by Cd^{2+} (97.23 ± 12.29% of control, n = 6, P = 0.328; Figure 20b), suggesting that BK channels prevent Ca_v channel contribution to GABA release elicited by 50 μM glutamate. Apamin (100 nM), an SK channel antagonist, had no significant affect on IPSCs (96.9 ± 10.4% of control, n = 6, P = 0.397). If blocking BK channels reveals a Ca_v channel dependent enhancement of reciprocal inhibition, one might predict that stronger activation of dendritic AMPARs could overwhelm BK channels and recruit Ca_v channels to trigger GABA release under basal conditions, thus exposing a voltage-dependent component of GABA release. Accordingly, puffing a higher concentration of glutamate (500 μM) onto A17 dendrites elicited larger IPSCs (500 μM puff: 27.86 ± 11.43 pA, n = 14 and 50 μM puff: 13.7 ± 3.87

pA, n = 12, p = 0.0005) in RBCs which were significantly reduced by Cd^{2+} (48.28 ± 19.15% of control, n = 9, P = 0.0029; Figure 20c). Application of iberiotoxin enhanced these IPSCs (118.17 ± 6.17% of control, n = 5, P = 0.0038) and, again, Cd^{2+} blocked a significant proportion of the response (to 42.55 ± 10.44% of iberiotoxin, n = 5, P = 0.0122; Figure 20d), suggesting that BK channels continue to suppress Ca_v channel activation even under stronger stimulus conditions. These results demonstrate that BK channels limit GABAergic transmission from A17s by reducing Ca^{2+} influx through Ca_v channels and thus suppressing neurotransmitter release.

The experiments presented thus far show that multiple mechanisms can trigger and modulate reciprocal GABA release from A17s and that these mechanisms are activated differentially depending on the strength of stimulation. To test this model further, cyclothiazide (50 μM) was applied to enhance the AMPAR's affinity for glutamate and to remove desensitization. Cyclothiazide strongly increased EPSPs in A17s (amplitude: 309 ± 52% of control, n = 5, P = 0.00036; Figure 21a,b), demonstrating that enhancing AMPAR receptor efficacy strongly potentiates the post-synaptic response. Application of cyclothiazide should increase IPSCs elicited by weak presynaptic activation (50 μM glutamate puff; 25 ms) by increasing the total inward charge transfer to overwhelm the rapidly inactivating inhibitory BK conductance. Consistent with this prediction, cylcothiazide increased IPSC amplitude (153 ± 44% of control, n = 15, P = 0.00099); the enhanced IPSCs were significantly blocked by Cd^{2+} (71.76 ± 14% of cyclothiazide, n = 7, P = 0.0113; Figure 21c,d), suggesting that increasing the responsivity of AMPARs enables access to Ca_v channel-dependent feedback mechanisms. 5,7-DHT (50 μM), a toxic serotonin

analog that ablates indoleamine-accumulating cells such as A17s (Dong and Hare, 2003; Chavez *et al.*, 2006; Vaney, 1986), abolished the cyclothiazide-enhanced IPSCs (2.32 ± 2.03% of cyclothiazide, n = 4, P = 0.0026; Figure 21d), indicating that the enhanced inhibition was entirely attributed to A17s.

Figure 20

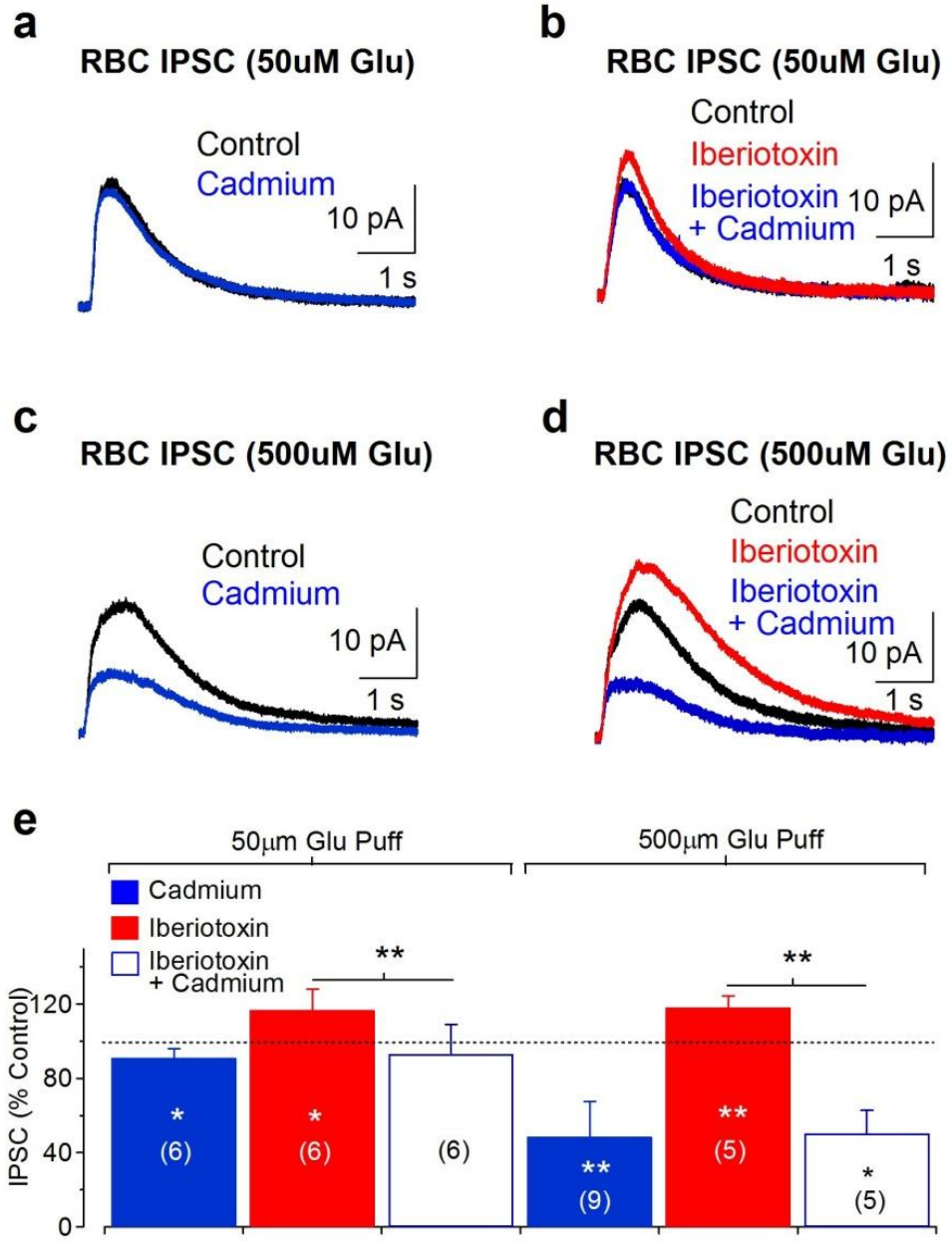
a
RBC IPSC (50uM Glu)
Control
Cadmium
10 pA
1 s
b
RBC IPSC (50uM Glu)
Control
Iberiotoxin
Iberiotoxin
+ Cadmium
10 pA
1 s
c
RBC IPSC (500uM Glu)
Control
Cadmium
10 pA
1 s
d
RBC IPSC (500uM Glu)
Control
Iberiotoxin
Iberiotoxin
+ Cadmium
10 pA
1 s
e
50μm Glu Puff
500μm Glu Puff
Cadmium
Iberiotoxin
Iberiotoxin
+ Cadmium
IPSC (% Control)
120
80
40
0
**
**
*
(6)
*
(6)
(6)
**
(9)
**
(5)
*
(5)

Figure 20. BK channel-modulated Ca_v channels enhance GABA release from A17s. (**a**) Puffing 50 μM glutamate (25 ms) onto A17 dendrites elicited IPSCs in RBCs that were only minimally sensitive to the divalent Ca_v channel blocker Cd^{2+} (200 μM). (**b**) Blocking BK channels with iberiotoxin (100 nM) enhanced IPSCs (50 μM puff) and increased Cd^{2+} sensitivity. (**c**) Increasing the glutamate puff concentration (500 μM) elicited RBC IPSCs that were sensitive to Cd^{2+}, providing evidence that Ca_v channels contribute to GABA release. (**d**) Application of iberiotoxin enhanced the IPSCs (500 μM puff) and increased the Cd^{2+} sensitivity of the response. (**e**) Summary of the results from experiments in **a**-**d**.

Figure 21

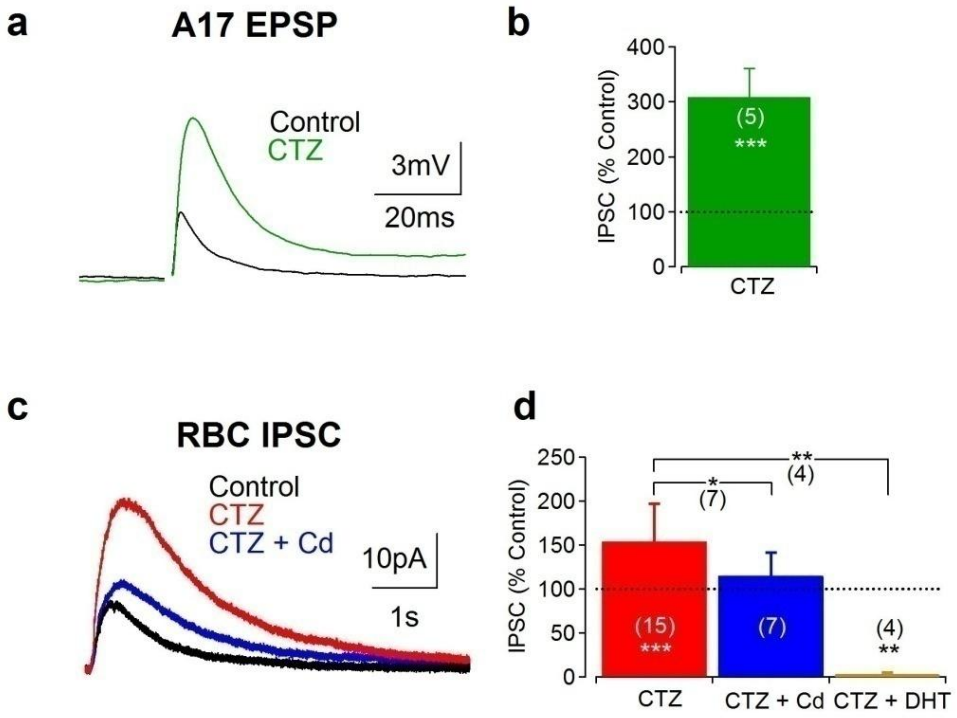

Figure 21. Modification of AMPAR kinetics with cyclothiazide recruits Ca_v channel-dependent enhancement of GABA release. (**a**) Electrically-evoked A17 EPSPs were strongly potentiated by cyclothiazide. (**b**) Summary of results from experiments described in **a**. (**c**) RBC IPSCs evoked by 50 μM glutamate puff were strongly enhanced by cyclothiazide application (50 μM). Cylcothiazide-enhanced IPSCs were reduced by Cd^{2+} (200 μM) application or abolished by the toxic serotonin analog DHT (50 μM; example trace not shown). (**d**) Summary of results from the experiment described in **c**.

BK channels permit preferential activation of specific GABAR subtype

Previous reports in rat have indicated that reciprocal inhibitory feedback elicited by excitatory input from a single RBC is mediated primarily by $GABA_A$Rs (Singer and Diamond, 2003; Chavez *et al.*, 2006, but see Hartveit, 1999). However, light evoked IPSCs recorded in RBCs exhibit both $GABA_A$R and $GABA_C$R-mediated components (Eggers and Lukasiewicz, 2006b; Eggers and Lukasiewicz, 2006a). Application of cyclothiazide recruits a $GABA_C$R-mediated component to the single RBC feedback response (Singer and Diamond, 2003), suggesting that the recruitment of $GABA_C$Rs depends on the strength of A17 activation. One possibility is that BK channels, by limiting postsynaptic depolarization, Ca_v channel activation and GABA release, restricts activation of $GABA_C$Rs . To test this idea, we elicited single RBC-evoked feedback by stepping the RBC membrane potential from -60 to -10 mV (100 ms) to evoke a reciprocal GABAR-mediated IPSC superimposed upon the sustained RBC Ca^{2+} current (vIPSC; Singer and Diamond, 2003; Chavez *et al.*, 2006). Consistent with previous reports, application of the $GABA_C$R antagonist TPMPA (50 μM) did not affect the vIPSC amplitude (94.61 ± 7.31% of control, n = 5, P = 0.2221) or decay (101.3 ± 51.6% of control, n = 5, P = 0.6045; Figure 22a). vIPSCs evoked in the presence of iberiotoxin exhibited slower kinetics (156.5 ± 37.5% of control, n = 5, P = 0.0339) and larger amplitudes (169.56 ± 27.33% of control, n = 5, P = 0.0033; Figure 22b), indicating that BK channels modulate reciprocal feedback in response to activation/depolarization of a single RBC. The vIPSCs evoked in the presence of iberiotoxin were sensitive to TPMPA (amplitude: 84.49 ± 9.87% of iberiotoxin, n = 6,

P = 0.0409; decay: 63.6 ± 20.8 % iberiotoxin, n = 6, P = 0.0453; Figure 21c), indicating the emergence of $GABA_C$R activation when BK channels are inactive. These results suggest that BK channels preferentially limit the activation of slower, $GABA_C$R-mediated reciprocal inhibition.

Why are reciprocally-triggered $GABA_C$Rs only activated under enhanced excitatory stimulus conditions? At least two possible explanations exist: 1) Putative extrasynaptic location (Eggers and Lukasiewicz, 2006b) of $GABA_C$R requires that multiple synapses in the vicinity must concurrently release GABA-filled vesicles in order to expose the $GABA_C$Rs to GABA waveforms with sufficiently long decays. 2) Multi-vesicular release of GABA at individual reciprocal synapses could occur, leading to enhanced transmitter concentrations within the cleft and therefore synaptic $GABA_C$R activation. We tested how a range of GABA waveform amplitudes (1, 5 and 10 mM peak amplitudes) and decay times (0.5, 1, 5 and 10 ms) would differentially activate $GABA_A$ versus $GABA_C$Rs using Channelab (see methods; Markovian models adapted from Lavoie *et al.*, 1997 and Chang and Weiss, 1999, respectively). By a rough estimate, the lowest concentration GABA waveforms tested, 1mM, with the shortest decay time, 0.5 ms (experimentally observed as ~0.5 ms; Bruns and Jahn, 1995), should approximately correspond to the synaptic waveform response to the release of a single vesicle (Figure 23a). Although ~55% of $GABA_A$Rs (unitary conductance ~30 pS) open in response to this stimulus, the open probability for $GABA_C$Rs (unitary conductance ~1 pS) is only ~0.1 %, indicating that the release of a single vesicle would be unlikely to trigger an observable response from synaptically located $GABA_C$Rs. For this quasi-physiological GABA waveform,

the low open probability and relatively small single channel conductance would require a total $GABA_C$ to $GABA_AR$ ratio of ~16,500:1 for these channel populations to provide a similar total conductance, which seems unlikely. Thus if reciprocal signaling results from the release of only one vesicle per synapse and these synapses act completely independent of one another, then a $GABA_CR$-mediated component would not be expected to emerge in the step-evoked IPSCs, which is consistent with experimental observation (Chavez *et al.*, 2006; Singer and Diamond, 2003). When the time course of the 1mM waveform is increased to 10 ms, $GABA_CRs$ responded with a P_o of ~10 % but $GABA_AR$-mediated responses developed a 'shoulder', indicative of receptor saturation, which is not observed experimentally. In fact, decay times ≥5 ms produced saturating $GABA_AR$ responses for all concentrations tested. Therefore, arguing that although temporally longer transmitter waveforms result in $GABA_CR$ activation it is unlikely that they occur within the synapse and also argues that reciprocal synapses do not work with a high degree of cooperativity. Simulated responses to higher concentrations of GABA (5 and 10 mM) with short decay times (0.5 ms) recruited $GABA_CR$ components (1.3 and 5.0%, respectively; Figure 23b,c). These results indicate that multi-vesicular release, if correlated with enhanced excitatory signaling, could trigger the activation of synaptic $GABA_CRs$. Although not conclusive, together the modeling results argue for enhanced release from individual synapses over pure extrasynaptic activation of $GABA_CRs$.

Figure 22

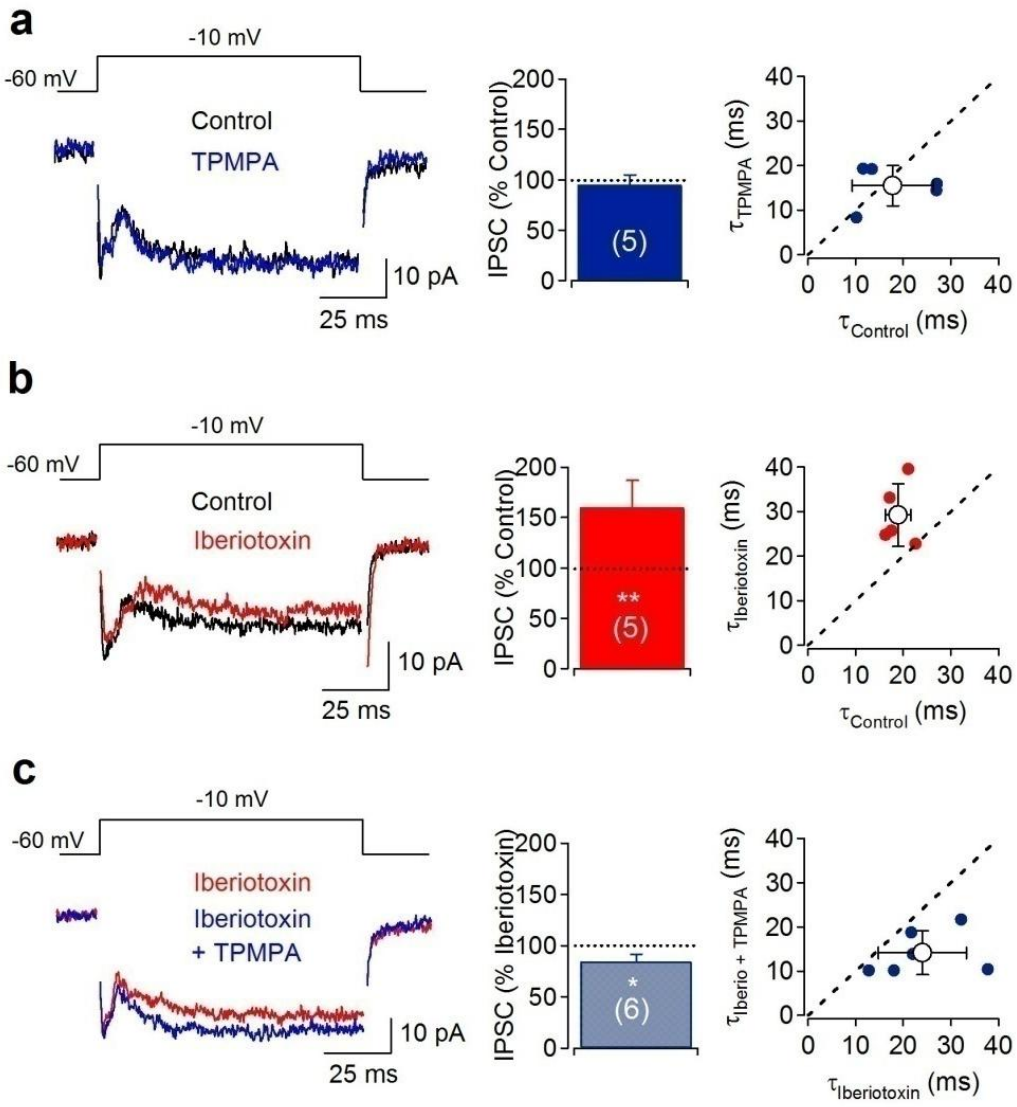
a
-10 mV
-60 mV
Control
TPMPA
10 pA
25 ms
IPSC (% Control)
200
150
100
50
0
(5)
τTPMPA (ms)
40
30
20
10
0
0 10 20 30 40
τControl (ms)
b
-10 mV
-60 mV
Control
Iberiotoxin
10 pA
25 ms
IPSC (% Control)
200
150
100
50
0
**
(5)
τIberiotoxin (ms)
40
30
20
10
0
0 10 20 30 40
τControl (ms)
c
-10 mV
-60 mV
Iberiotoxin
Iberiotoxin
+ TPMPA
10 pA
25 ms
IPSC (% Iberiotoxin)
200
150
100
50
0
*
(6)
τIberio + TPMPA (ms)
40
30
20
10
0
0 10 20 30 40
τIberiotoxin (ms)

Figure 22. BK channels suppress reciprocal feedback and $GABA_CR$ activation. Depolarizing RBCs (from -60 mV to -10 mV; 100 ms) produced a sustained inward calcium current with a superimposed reciprocal GABAergic IPSC (Singer and Diamond, 2003; Chavez *et al.*, 2006). (**a**) TPMPA (50 μM), a $GABA_CR$ antagonist, did not reduce reciprocal inhibition under control conditions. (**b**) Blocking BK channels with iberiotoxin (100 nM) enhanced reciprocal feedback inhibition. (**c**) When BK channels were blocked, TPMPA significantly reduced reciprocal feedback.

Figure 23

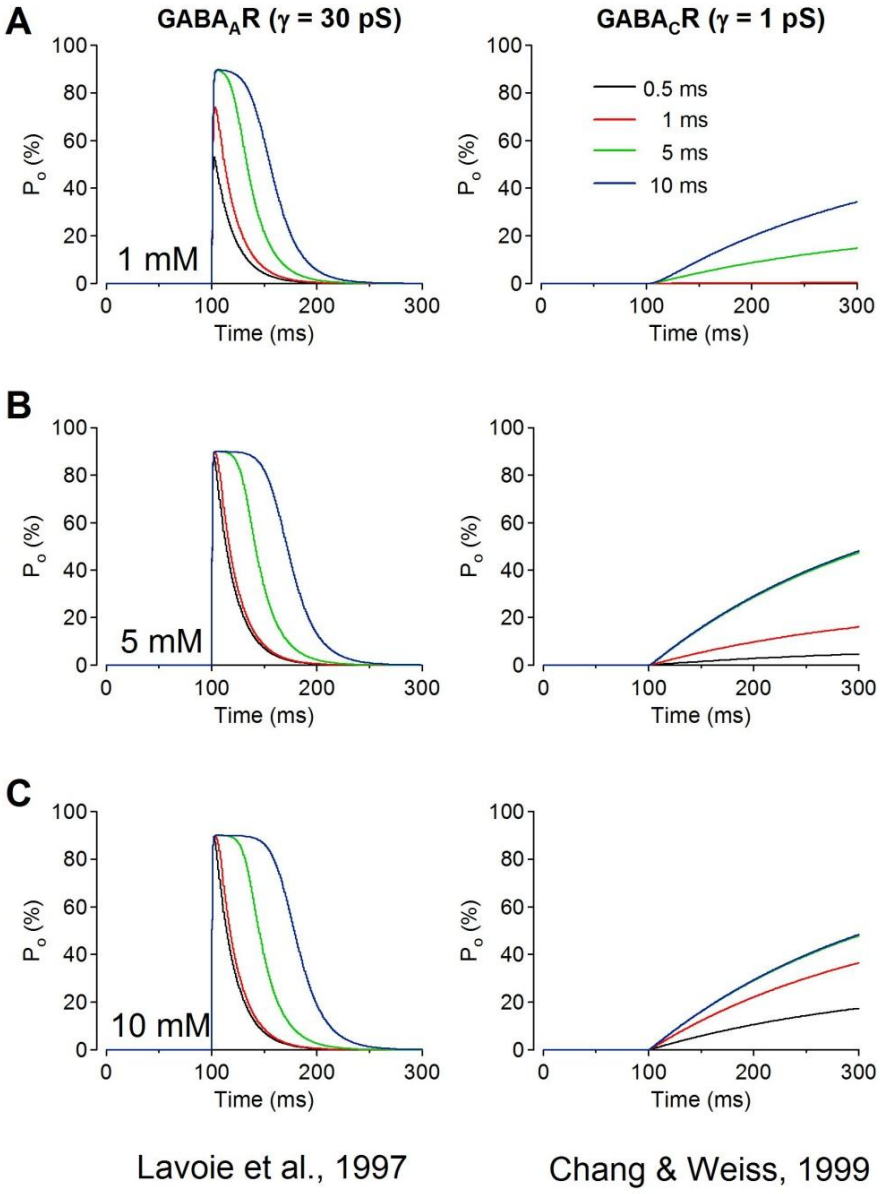

Figure 23. Simulating $GABA_A$ and $GABA_CR$ activation in response to a range of synaptic-like glutamate waveforms with Channelab. (**a**) Glutamate waveforms of 1mM in amplitude and 0.5, 1, 5 or 10 ms decay times were applied to Markovian $GABA_AR$ (left) and $GABA_CR$ (right) models while monitoring the open probability of the channels (P_o). An extended range of GABA concentrations were tested to account for the possibility of multivesicular release (5 (**b**) and 10 (**c**) mM).

Discussion

BK channels extend the range of inhibitory signaling by regulating the excitatory synaptic response

In this study we have demonstrated that BK channels can modulate both excitatory and inhibitory synaptic transmission via suppression of glutamatergic synaptic depolarizations and the consequential decrease in Ca_v channel activation. Functionally analogous to interactions between NMDARs and SK channels in the hippocampus and lateral amygdale (Faber *et al.*, 2005; Ngo-Anh *et al.*, 2005), our data suggest that BK channels in A17 dendritic varicosities are tightly coupled to AMPAR-mediated synaptic responses. BK channels also form macromolecular complexes with L-, N- and P/Q-type Ca_v channels (Berkefeld *et al.*, 2006; Berkefeld and Fakler, 2008); in our system, BK conductances not only can be triggered directly by L-type Ca_v channel activation but also can feed back to reduce Ca_v channel contributions to driving GABA release. Glutamate puff-evoked IPSC experiments demonstrate that Ca_v channels enhance GABA release only when A17 dendrites are strongly activated and that BK channels regulate the extent of this voltage-dependent signaling. Vesicular glutamate release from RBC ribbon synapses is proportional to membrane depolarization (Singer and Diamond, 2003), thereby providing a discrete but extended range of inputs to A17 varicosities. Taken together with previous results from our laboratory, we argue that L-type Ca_v channel, BK channels, CP-AMPARs and CICR within single varicosities work in concert to provide an extended range of reciprocal feedback inhibition that is membrane potential dependent or independent,

depending on the strength of feedforward signaling. Further experiments are required to determine whether BK channels can be activated directly by CP-AMPARs independently of Ca_v channels.

Biophysical properties of BK suggest a dynamic role in regulating reciprocal inhibition

Non-inactivating SK channels provide an inhibitory conductance that is well suited to suppress a long lasting NMDAR mediated response (Faber *et al.*, 2005; Maher and Westbrook, 2005; Ngo-Anh *et al.*, 2005). The similarity between the inactivation kinetics of A17 BK channels (~4 ms) and the decay time of AMPAR-mediated EPSCs (~3 ms) suggests that rapidly inactivating BK channels constitute a temporally precise mechanism to suppress AMPAR-mediated inputs. Our immunohistochemisty results and inactivation/recovery measurements suggest that fast BK inactivation in A17s is attributable to the presence of β2 auxiliary subunits. Each β2 subunit has a charged N-terminus that inactivates BK channels by blocking the pore (Hicks and Marrion, 1998). The presence of β2 subunits also shifts the midpoint of voltage-dependent BK activation at a particular intracellular Ca^{2+} concentration towards more negative, physiological potentials in a stoichiometry-dependent (β:α) manner (Wang *et al.*, 2002). Reducing the energy barrier to BK activation may facilitate a reduction in the spatial spread of synaptic depolarization, thus increasing synapse specificity in the dendrites of A17s. The inactivation properties of β2-BK channels in A17s may enable them to modulate feedback

inhibition in a dynamic manner that depends on the temporal coincidence of synaptic events.

BK channels limit $GABA_CR$ activation during feedback triggered by a single RBC

Reciprocal inhibition from A17 amacrine cells has been shown to truncate the time course of the rod-driven response *in vivo* via $GABA_CR$ activation (Dong and Hare, 2003). Numerous reports have identified both $GABA_A$- and $GABA_CRs$ at the terminals of bipolar cells (Qian and Dowling, 1995; Singer and Diamond, 2003; Eggers and Lukasiewicz, 2006a; Palmer, 2006a) and light-evoked signaling from RBCs is modulated in both amplitude and time course by $GABA_A$- and $GABA_CRs$, respectively (Eggers and Lukasiewicz, 2006a;). Under normal conditions, however, reciprocal inhibition in response to glutamate release from a single RBC is mediated primarily by $GABA_ARs$ (Singer and Diamond, 2003; Chavez *et al.*, 2006). When feedback is enhanced via presynaptic (Hartveit, 1999) or postsynaptic (Singer and Diamond, 2003) modifications, a $GABA_CR$ component emerges in the feedback IPSC triggered by a single RBC. The results here indicate that $GABA_CRs$ are recruited in the single RBC feedback response when BK channels are blocked (Figure 22c), suggesting that BK channels may constitute a postsynaptic mechanism that limits GABA release and consequent $GABA_CR$ activation in response to weaker feed-forward synaptic input. The recruitment of $GABA_CR$ activation in response to stronger stimulation likely extends the dynamic range of reciprocal signaling at this synapse.

Chapter 5: Discussion/Conclusions

Dendritic integration in A17 amacrine cells

The A17 amacrine cell provides a unique system for studying dendritic integration and its role in shaping the neuronal input/output function. Careful confocal analysis and electron microscopy studies provide evidence that excitatory inputs and inhibitory outputs are colocalized within individual varicosities (Ellias and Stevens, 1980; Nelson and Kolb, 1985; Zhang *et al.*, 2002), eliminating the requirement that signals pass through the cell body as an intermediate. This configuration indicates that electrical responses recorded with somatically placed electrodes, although providing valuable information regarding membrane properties and synaptic signaling, does not address relevant questions regarding the spatial extent of the local dendritic signaling and output. To address questions about the spatial characteristics of dendritic signaling, optical approaches, such as monitoring membrane potential with second harmonic generation (SHG), have been used to observe membrane potentials in dendrites (Millard *et al.*, 2003a; Millard *et al.*, 2003b; Nemet *et al.*, 2004; Jiang *et al.*, 2007), however, sections of the ultra thin (at or below the diffraction limit) A17 dendrites rarely lie within a single focal plane making it impossible to observe voltage changes over relevant distances. These and other technical limitations preclude our ability to experimentally probe the spatial

dimensions of dendritic signaling in A17 but modeling approaches can be used to conceptualize these processes and make predictions for future experiments.

Electrotonic models that utilize the well-established theory of electrical signaling in cables and are constrained by the unique, experimentally measured anatomical and electrophysiological characteristics of a particular neuron have often been used to examine features of neuronal signaling which are inaccessible by currently available experimental techniques. This approach has been applied to addressing questions about neuronal signaling in various areas of the central nervous system including the cortex, hippocampus, cerebellum and the retina (Smith and Vardi, 1995; Taylor *et al.*, 1996; Trevelyan and Jack, 2002; Tukker *et al.*, 2004; Hausselt *et al.*, 2007; Desjardins *et al.*, 2003; Williams and Stuart, 2003). The electrotonic modeling presented here, has revealed various aspects of dendritic signaling that are unique to the A17 amacrine cell and has made predictions for its role in a physiological context. First, varicose structures reduce the membrane resistance of a particular section of dendrite and thus decrease the axial current to locations which are more distal to the site of input (Figure 10). This effective shunt results in a decrease in the length over which synaptic potentials propagate and therefore enhances the spatial confinement of postsynaptic signaling. Second, identical synaptic conductances differentially depolarize varicosities depending on their dendritic location. Distal varicosities respond with larger synaptic depolarizations than proximal ones, this results from differences in lateral axial resistance at either end (capped end versus connection to cell body) of the stimulated dendrite. Larger responses in distal varicosities suggest that tonic excitation of the

dendrite would create a gradient of membrane potential along the dendrite and could explain the experimental observation of the dendritic potential gradients in the thicker dendrites of starburst amacrine cells (Hausselt *et al.*, 2007). Interestingly, those dendrites also gave rise to asymmetrical spreading of synaptically evoked potential changes with preferential, centrifugally-directed signaling (Indicated by a DSF of 1.209 and Figure 13b,d,f) . This result indicates that an amacrine cell model with passive membrane properties alone is sufficient to explain the centrifugal spread of signals observed in starburst amacrine cells (Euler *et al.*, 2002). In contrast thinner dendrites and lower specific membrane resistivities respond to the subsequent synaptic stimulation of individual varicosities along dendrites with an increasing non-linearity (Figure 12). This non-linearity give rise to a dendritic section (~100 µm), containing multiple varicosities, that only minimally differs in response amplitude and suggests an effective space constant that is shorter than the dendritic length. A DSF of 1.007 indicates that the propagation of synaptic signals is within this dendritic region is nearly symmetrical. Together, these results indicate that signal propagation within the central dendritic regions of this A17 model is not biased by the differential axial resistance at the two ends of the dendrite, hence supporting the idea of electrical isolation. Quantification of normalized signaling in varicosities that are adjacent to the stimulus location reveals that, without the influence of active conductances, interactions do occur within approximately 50 µm or two varicosities in either direction from the stimulated varicosity (Figure 13). Therefore, if center surround inhibition depends on voltage signaling within A17 dendrites, these results predict an ~100 µm diameter ring of lateral inhibition. This estimate is comparable to that

experimentally measured (Volgyi *et al.*, 2002) and theoretically modeled (Zhang *et al.*, 2002) in rabbit retinas. In fact, Zhang et al., 2002 proposed two models of reciprocal surround inhibition from indolamine accumulating amacrine cells. In those models the reciprocal release of GABA and therefore surround inhibition was directly and solely dependent on post-synaptic electrical signaling in A17 dendrites. In one model, it was assumed that A17 amacrine cells respond with a global, isopotential response, therefore resulting in transmitter release from all varicosities of all stimulated A17s. For this type of response to occur physiologically, action potential signaling would likely be required. This is clearly not the case for A17 amacrine cells of the rat retina, since they are unable to fire action potentials (Figure 9; Menger and Wassle, 2000). The second model proposed in that paper assumes that dendrites are electrically isolated, limiting the postsynaptic isopotential response to within individual dendrites and thus reducing the spatial extent of surround inhibition to ~100 µm. In our model, observation of potential changes elicited in the unstimulated dendrites of the A17 model indicate a high degree of dendritic isolation, this is especially true for the thinnest dendrite model; those dendrites were isolated from each other by greater than 96% (Figure 14). I therefore propose that the physiological response of A17 amacrine cells in rat retinas is more similar to the isolated dendrite model than the global response model. In addition to providing evidence against a particular, previously published model of reciprocal inhibition, our results expand on previous interpretations by determining that feedback/surround inhibtion occurs over distances shorter than the total dendritic length. This deviation from the isopotential dendritic results from a combination of a small population of

largely inactivated Na_v channels, thin dendrites that create high axial resistance and a low specific membrane resistance that allows more current to flow out of the dendrite rather than down the axial resistor.

Synaptic mechanisms of reciprocal inhibition

The rod pathway is a very specialized, highly sensitive system for converting very low photon absorption rates into signals the brain can detect and process. Adaptation occurs at light levels too low to cause cellular adaptation of the rods. Recent reports have indicated that adaptation at these levels occurs at the RBC dyad syanpse (Dunn *et al.*, 2006), and is partially accounted for by synaptic depression of this synapse (Singer and Diamond, 2006) which can be triggered by single photon responses (Dunn and Rieke, 2008). However, additional gain controls and clearly correlated regulatory mechanisms remain to be discovered. Modulation of AII to AII electrical coupling would seem a likely candidate to maximize the signal transfer of small signals under the lowest light conditions and to improve signal to noise by increased averaging for slightly brighter background conditions. Interestingly, Dunn *et al*. did not observe changes in gain at the RBC to AII synapse when using Connexin36 knockouts, but the authors did not make gain measurements from ganglion cells (in the knockout), where effects from modulation of AII networks would be expected to be observed. Another possibility is that plasticity in the A17 negative feedback to RBC could also play a role in gain control but to date has been reported only in goldfish (Vigh *et al.*, 2005). Could CP-AMPARs, VGCCs or other ion channels be involved in plasticity at the reciprocal synapse in rat? In chapter 4 I combined electrophysiology, 2-photon calcium imaging, immunohistochemistry,

neuropharmacology and modeling approaches to elucidate the mechanisms that underlie reciprocal feedback from A17 amacrine cells. First, glutamate puff-evoked IPSC experiments from Chavez *et al.*, 2006 were repeated to confirm that calcium influx through CP-AMPARs is sufficient for triggering reciprocal GABA release from A17s (Figure 20a,e), suggesting that voltage-dependent mechanisms for triggering transmitter release (i.e. Ca_v channels) might be absent from feedback varicosities. Calcium imaging experiments indicated that Ca_v channels were colocalized with synaptic machinery at individual feedback varicosities, which was surprising giving their apparent lack of contribution to triggering reciprocal feedback. The previously unstudied Ca_v channels expressed on A17 membranes displayed similar characteristics to channels expressed in RBCs (Protti and Llano, 1998) and AII amacrine cells (Habermann *et al.*, 2003) and were indicative of L-type Ca_v channels. In particular, these channels responded with sustained currents in response to 100 ms voltage steps to -10 mV (Figure 16a) and were abolished by application of the dihydropyridine Ca_v channel blocker, isradipine (10 μM). With minimal ability to inactivate, L-type Ca_v channels are capable of producing large charge transfers compared to rapidly desensitizing CP-AMPARs of the same total conductance. Unable to resolve this apparent contradiction with evidence from the body of retinal and A17 amacrine cell literature I continued to experimentally probe calcium interaction within feedback varicosities. Calcium release from intracellular stores has been shown to amplify inhibitory neurotransmitter release from amacrine cells in rat (Chavez *et al.*, 2006; Chavez and Diamond, 2008) and chick (Warrier *et al.*, 2005). Are the L-type Ca_v channels expressed in A17 varicosities biochemically isolated

from mechanisms which have been shown to enhance reciprocal GABA release such as calcium release from intracellular stores? One possible mechanism for this type of compartmentalization has been observed in acinar cells of the pancreas, where mitochondria form a physical and active barrier with respect to calcium (Dolman *et al.*, 2005). Voltage-dependent changes in intracellular calcium were found to be sensitive to a pharmacological depletion of intracellular calcium stores, indicating a direct coupling of the mechanisms (Figure 18). Although this does not rule out mitochondrial buffering (Medler and Gleason, 2002) within varicosities, it does provide direct evidence against complete isolation of Ca_v channels from mechanisms which have been shown to trigger reciprocal GABA release from A17s. I then began to investigate the possibility that the multiple sources of calcium within varicosities could trigger inhibitory conductances that suppress synaptic depolarization and therefore Ca_v channel activation. Multiple reports have indicated that calcium-activated potassium channels are expressed in a number of retinal neurons (Wang *et al.*, 1998; Henne and Jeserich, 2004; Xu and Slaughter, 2005; Palmer, 2006b; Bringmann *et al.*, 2007), including amacrine cells (Mitra and Slaughter, 2002), however, their physiological roles remain unclear. Voltage clamp recordings with potassium-based internal revealed rapidly-inactivating calcium-activated potassium currents that were mediated by BK channels, and furthermore, immunohistochemistry experiments indicated that these channels were localized to synaptic feedback varicosities. These experiments provided the first experimental evidence that A17 amacrine cells express calcium-activated potassium channels. Additional electrophysiology experiments revealed that these channels suppress synaptic

depolarization, Ca_v channel activation and reciprocal GABA release from A17s. To our knowledge this is the first direct observation of modulation of both excitatory and inhibitory signaling by BK channels within such a small compartmentalized space (~1.8 ± 0.4 µm; n = 47 varicosities; see Table 3). The observed rapid-inactivation of BK channels by auxiliary β2 subunits suggests a more dynamic role for these channels in regulating feedback inhibition. I propose two models in which BK channels could dynamically regulate A17 physiology. 1) When spontaneous release from RBCs is infrequent (under dim light conditions; Yang *et al.*, 2002; Dunn *et al.*, 2006), highly available BK channels suppress synaptic depolarizations (elicited by real signals) within stimulated varicosities and consequentially decrease depolarizations in neighboring varicosities on the same dendrite. Synapse-specific reciprocal inhibition is still triggered via calcium influx through CP-AMPARs (and possibly amplification of local calcium signals by CICR), however, BK channels, as a result of limiting the absolute amplitudes of depolarizations in neighboring varicosities, limit Ca_v channels and hence decrease the spatial extent of surround inhibition. As mean light levels increase, spontaneous synaptic input increases in frequency (noise), therefore increasing the probability that BK channels will be inactivated. When inactivated, coincident excitatory signals will provide stronger synaptic depolarizations within the stimulated varicosity and the neighboring varicosities, therefore increasing more distal Ca_v channel activation and increasing the spatial extent of surround inhibition. 2) The availability, or state of BK channels within the stimulated varicosity shape the time course of inhibition provided to the stimulating RBC. Under low noise conditions BK channels suppress Ca_v channel

activation therefore reducing the total number of GABA-filled vesicles that are released into the extracellular space (Figure 20). The decreased amplitude of extracellular GABA concentrations limits postsynaptic activation to only fast $GABA_A$Rs (Figures 22 and 23) therefore providing only brief inhibition to the RBC terminal. Under brighter conditions and therefore increased noise levels, tonically inactivated BK channels allow real excitatory signals to more efficaciously depolarize A17 varicosities. Unsuppressed depolarizations can then better activate Ca_v channels and maximize reciprocal release of GABA. The resulting higher concentrations of extracellular GABA activate both $GABA_A$ and $GABA_C$Rs on RBC terminals (Figures 22 and 23). The addition of slow $GABA_C$R currents extend the time course of inhibition to the RBC and has been shown to shorten the time course of glutamate release (Eggers and Lukasiewicz, 2006b). Although these models are constructed based on the newly observed biophysical mechanisms presented herein, it should be clearly noted that direct evidence supporting these models does not yet exist. Because BK channels have been observed to facilitate transmitter release from rod photoreceptors (Xu and Slaughter, 2005; personal observations-not shown), it is not feasible to specifically test the effects of BK channel antagonists on light evoked inhibition from A17 amacrine cells without confounding the results by influencing upstream signaling. Promising advancements in optical techniques could allow for direct testing of these models. In particular, channel-rhodopsin 2, a light activated ion channel expressed in green algae (Zhang *et al.*, 2006; Arenkiel *et al.*, 2007; Petreanu *et al.*, 2007; Huber *et al.*, 2008), has recently been genetically encoded into the *on* bipolar cells of the mouse retina (Lagali *et al.*, 2008). This genetic manipulation

could provide a powerful tool for directly addressing the models of dynamic reciprocal signaling from A17 amacrine cells that are presented here, as well as opening the door to uncover the functional roles of many other, previously unstudied, amacrine cells in the inner plexiform layer.

Concluding Remarks, Additional Points and Caveats

The results presented herein indicate that multiple structural and biophysical membrane properties combine to enhance the synapse specificity of reciprocal inhibition from A17 amacrine cells and that a concert of calcium sources and calcium dependent processes combine to allow for a larger dynamic range of reciprocal signaling to individual RBCs. This work expands on our current understandings of interactions between ion channels, mechanisms that modulate transmitter release and signaling from A17 amacrine cells, and GABAergic interneurons, in general. Although care has been taken to design experiments in a way that aims to provide clear answers, the experimental results can unexpectedly open up new questions and uncertainties. In particular, when taking into account recent related publications, one such question remains exceptionally puzzling: Can A17 membrane depolarization and the subsequent calcium influx through Ca_v channels trigger reciprocal GABA release from A17 amacrine cells? In Chavez *et al.*, 2006, high potassium evoked IPSC experiments and dual recordings from RBC-A17 pairs suggested that Ca_v channels were not sufficient to triggers release. In those experiments, 110 mM potassium was puffed onto A17 dendrites through a micropipette which elicited IPSC in the RBC. When excitatory synaptic transmission was blocked with NBQX (10 μM) the

observed IPSCs were nearly abolished, indicating that acute elevations in local extracellular potassium is insufficient to trigger the release of GABA from A17 when excitation is absent. Although it was expected that the large change in the potassium gradient (and hence the potassium reversal potential) would strongly depolarize A17 dendrites and activate Ca_v channels if localized to varicosities, control experiments indicated that potential changes observed in the A17 in response to the high potassium puff were on average less than 5 mV (4.69 mV ± 1.71 mV, n = 6). Furthermore, these responses were greatly reduced by application of NBQX (10 μM; to 32 ± 14% of control, p = 0.0016, n = 6, Figure 24), indicating that current mediated by AMPARs is responsible for the majority of the recorded potential changes. An extracellular potassium concentration of 110 mM results in a local potassium reversal potential that matches the non-specific AMPAR reversal (0 mV), therefore, efficient depolarization of A17 dendrites would eliminate the driving force for AMPARs. Because NBQX strongly reduced the A17 response to the high potassium puff, it is clear that this stimulus is does not efficiently depolarize A17 dendrite, and therefore implying that the results from the high potassium puff experiment in Chavez et al., 2006 are inconclusive. Paired recordings also support the idea that membrane depolarizations and therefore Ca_v channel activation in A17 are insufficient to trigger release. In those experiments the somatic RBC electrode was used to deliver a depolarizing step that activated Ca_v channels located in the axon terminal that provided the calcium influx necessary to trigger the release of glutamate onto the postsynaptic elements (AII and A17). If an excitatory synaptic response was recorded in the A17 amacrine cell then the cells were considered paired. Connected

pairs were then tested for a voltage dependent reciprocal response by delivering a depolarizing voltage step to the A17 amacrine cell and recording any inhibitory response in the RBC (V_{hold}= -10 mV). None of the pairs tested were able to produce bidirectional signaling (0 out of 7, Chavez *et al.*, 2006). The most likely and first explanation considered was that Ca_v channels were not localized to feedback varicosities, however, it is now clear that this is not the case (Figure 15). The newly available data provided here appears to conflict with previous findings and leads to the question, why are Ca_v channels in feedback varicosities unable to trigger transmitter release on their own? Although the experiments presented in Figure 20 demonstrate that Ca_v channels can enhance GABA release from A17 they do not provide any evidence that Ca_v channels are sufficient for triggering release. This question will need to be addressed in future experiments to determine if membrane potential changes experienced in varicosities adjacent to the stimulated varicosity can be correlated to GABA release.

Appendix

Figure 24

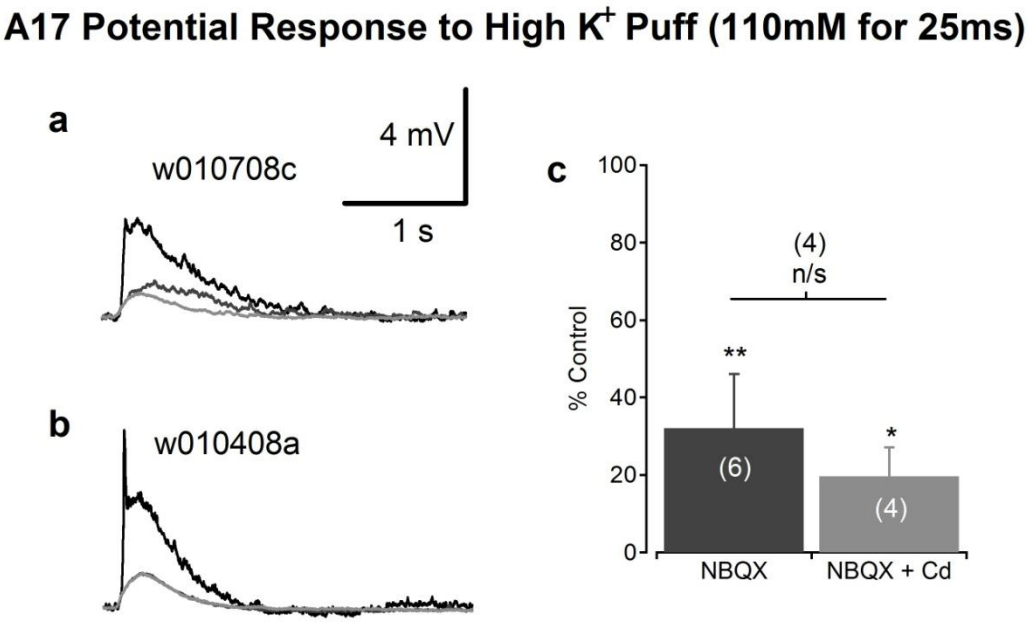

d

Condition	Average Response
Control	4.69+-1.71 mV
NBQX (10uM)	1.49+-0.96 mV
NBQX (10uM) + Cadmium (200uM)	0.82+-0.25 mV

Figure 24. A17 amacrine cells are inefficiently depolarized by high concentration extracellular potassium puffs. (**a-b**) Membrane potential recorded from an A17 amacrine cell in response to a 25 ms puff of 110 mM potassium in sublamina 5. Inclusion of the AMPAR antagonist NBQX (10 µM) strongly reduced the response in all cells indicating that the stimulus is efficiently triggering glutamate release from RBCs. Although additonal inclusion of cadmium (200 µM) occasionally reduced the remaining response (**a**), it often did not (**b**) , suggesting that Ca_v channels are minimally activated by high potassium puffs when excitatory inputs are blocked. (**c**) Bar graph indicating relative changes in the response amplitudes and significance of drug effects. (**d**) Raw response amplitudes across cells.

Glossary

5,7-DHT: *5,7-dihydroxytypamine*- toxic serotonin analog. Used to specifically ablate indolamine accumulating amacrine cells from retinal tissue.

AMPAR: *α-amino-3-hydroxy-5-methyl-4-isoxazole propionic acid receptor*- excitatory ion channel/receptor which is activated when bound with two glutamate molecules.

BK: *Large conductance calcium-activated potassium channel*- Intrinsically voltage-dependent potassium channel with intracellular calcium sensors. The binding of Ca^{2+}

CBC: *Cone bipolar cell*- second order neuron in the cone pathway. Receives direct input from cone photoreceptors.

CICR: *Calcium-induced calcium release*- SERCA pumps localized to endoplasmic reticulum in the intracellular compartment of neurons sequester calcium into the ER calcium stores where activation of ryanodine or IP_3 receptors by calcium can trigger its release. This results in an amplification of intracellular calcium levels.

CNS: *Central nervous system*- portion of the vertebrate nervous system containing the brain and spinal cord, this includes the retina.

CP-AMPAR: *Calcium permeable AMPAR*- AMPAR variant which is highly permeable to calcium when activated.

DSF: *Dendritic symmetry factor*- Defined as $DSF = \Delta V_{Distal\_neighbor} / \Delta V_{Proximal\_neighbor}$, this factory indicates how membrane potentials spread around a stimulus point along a dendrite. A DSF of >1 indicates a preferred centrifugal spreading (away from the cell body) of the electrical signals, and conversely, a DSF of <1 indicates a preferential spread in the centripetal direction (towards the cell body).

EPSC: *Excitatory postsynaptic current*- Synaptic activation of a cell's ligand-gated ion channels results in ion flux across the membrane. Ligand-gated channels are selective for particular ions whose charge and concentration gradients determine their effect on the cell's membrane potential. Glutamate and glutamate receptors are primarily responsible for excitation/depolarization in the central nervous system.

EPSP: *Excitatory postsynaptic potential*- The changes in membrane potential caused by an EPSC.

ERG: *Electroretinograph*-technique used to measure the retinal response to light in an intact eyeball.

GABA: *γ-amino-butyric acid*- an inhibitory neurotransmitter of the CNS which produces a hyperpolarizing response in the postsynaptic cell.

$GABA_AR$: *γ-amino-butyric acid-A receptor*- inhibitory ion channel/receptor which is activated by GABA and has fast kinetics and a large single channel conductance (γ~30 pS) compared to $GABA_C$Rs (Lavoie *et al.*, 1997)

$GABA_CR$: *γ-amino-butyric acid-C receptor*- inhibitory ion channel/receptor which is activated by GABA and has slower kinetics and a smaller single channel conductance (γ~1pS) compared to $GABA_A$Rs (Chang and Weiss, 1999)

INL: *Inner nuclear layer*- layer of the retina which contains the cells bodies of bipolar cells and amacrine cells.
ions to these intracellular sensors leads to a negative shift in the midpoint of voltage-dependent activation of the conductance.

IPL: *Inner plexiform layer*- one of two retinal regions/layers in which synaptic contacts are made between retinal neurons. In particular, this anterior layer contains synapses between bipolar cells, amacrine cells, and ganglion cells.

MVR: *Multi-vesicular release*- some synapses are capable of simultaneously releasing more than one neurotransmitter filled vesicle. This is known as multi-vesicular release.

NBQX: *2,3-dihydroxy-6-nitro-7-sulphamoyl-beno(f)quinoxaline*- specific antagonist for AMPARs.

OPL: *Outer plexiform layer*- Synaptic layer of the retina in which rod and cone photoreceptors make connections with both the feed-forward bipolar cells and feed-back horizontal cells.

PKA: *Protein kinase A*- Enzyme which phosphorylates certain proteins.

RBC: *Rod bipolar cell*- second order neuron in the rod pathway. Receives input directly from rod photoreceptors.

RRP: *Readily releasable pool*- most neurons have neurotransmitter filled vesicles which are docked to the membrane and ready for release. These 'primed' vesicles are most often referred as the readily releasable pool.

TTX: *Tetrodotoxin*- Specific antagonist for voltage-gated sodium channels. Derived from pufferfish.

VGCC: *Voltage-gated calcium channel*- ion channel which is highly permeable to calcium and its conductance is activated by a particular range of membrane voltages.

Bibliography

Angelo, K., M. London, S. R. Christensen and M. Hausser (2007). "Local and global effects of I(h) distribution in dendrites of mammalian neurons." J Neurosci **27**(32): 8643-53.

Araya, R., V. Nikolenko, K. B. Eisenthal and R. Yuste (2007). "Sodium channels amplify spine potentials." Proc Natl Acad Sci U S A **104**(30): 12347-52.

Arenkiel, B. R., J. Peca, I. G. Davison, C. Feliciano, K. Deisseroth, G. J. Augustine, M. D. Ehlers and G. Feng (2007). "In vivo light-induced activation of neural circuitry in transgenic mice expressing channelrhodopsin-2." Neuron **54**(2): 205-18.

Baylor, D. A., T. D. Lamb and K. W. Yau (1979). "Responses of retinal rods to single photons." J Physiol **288**: 613-34.

Baylor, D. A., B. J. Nunn and J. L. Schnapf (1984). "The photocurrent, noise and spectral sensitivity of rods of the monkey Macaca fascicularis." J Physiol **357**: 575-607.

Berkefeld, H. and B. Fakler (2008). "Repolarizing responses of BKCa-Cav complexes are distinctly shaped by their Cav subunits." J Neurosci **28**(33): 8238-45.

Berkefeld, H., C. A. Sailer, W. Bildl, V. Rohde, J. O. Thumfart, S. Eble, N. Klugbauer, E. Reisinger, J. Bischofberger, D. Oliver, H. G. Knaus, U. Schulte and B. Fakler (2006). "BKCa-Cav channel complexes mediate rapid and localized Ca2+-activated K+ signaling." Science **314**(5799): 615-20.

Bloomfield, S. A. (1992). "Relationship between receptive and dendritic field size of amacrine cells in the rabbit retina." J Neurophysiol **68**(3): 711-25.

Bloomfield, S. A. (1996). "Effect of spike blockade on the receptive-field size of amacrine and ganglion cells in the rabbit retina." J Neurophysiol **75**(5): 1878-93.

Bloomfield, S. A. and B. Volgyi (2004). "Function and plasticity of homologous coupling between AII amacrine cells." Vision Res **44**(28): 3297-306.

Bringmann, A., I. Iandiev, T. Pannicke, A. Wurm, E. Buhner, A. Reichenbach, P. Wiedemann and S. Uhlmann (2007). "Porcine Muller glial cells increase

expression of BKCa channels in retinal detachment." Curr Eye Res **32**(2): 143-51.

Bruns, D. and R. Jahn (1995). "Real-time measurement of transmitter release from single synaptic vesicles." Nature **377**(6544): 62-5.

Chang, Y. and D. S. Weiss (1999). "Allosteric activation mechanism of the alpha1beta2gamma2 gamma-aminobutyric acid type A receptor revealed by mutation of the conserved M2 leucine." Biophys J **77**(5): 2542-51.

Chavez, A. E. and J. S. Diamond (2008). "Diverse mechanisms underlie glycinergic feedback transmission onto rod bipolar cells in rat retina." J Neurosci **28**(31): 7919-28.

Chavez, A. E., J. H. Singer and J. S. Diamond (2006). "Fast neurotransmitter release triggered by Ca influx through AMPA-type glutamate receptors." Nature **443**(7112): 705-8.

Chen, S. and J. S. Diamond (2002). "Synaptically released glutamate activates extrasynaptic NMDA receptors on cells in the ganglion cell layer of rat retina." J Neurosci **22**(6): 2165-73.

Deans, M. R., B. Volgyi, D. A. Goodenough, S. A. Bloomfield and D. L. Paul (2002). "Connexin36 is essential for transmission of rod-mediated visual signals in the mammalian retina." Neuron **36**(4): 703-12.

Del Castillo, J. and B. Katz (1954). "Quantal components of the end-plate potential." J Physiol **124**(3): 560-73.

Desjardins, A. E., Y. X. Li, S. Reinker, R. M. Miura and R. S. Neuman (2003). "The influences of Ih on temporal summation in hippocampal CA1 pyramidal neurons: a modeling study." J Comput Neurosci **15**(2): 131-42.

Doan, T., A. Mendez, P. B. Detwiler, J. Chen and F. Rieke (2006). "Multiple phosphorylation sites confer reproducibility of the rod's single-photon responses." Science **313**(5786): 530-3.

Dolman, N. J., J. V. Gerasimenko, O. V. Gerasimenko, S. G. Voronina, O. H. Petersen and A. V. Tepikin (2005). "Stable Golgi-mitochondria complexes and formation of Golgi Ca(2+) gradients in pancreatic acinar cells." J Biol Chem **280**(16): 15794-9.

Dong, C. J. and W. A. Hare (2003). "Temporal modulation of scotopic visual signals by A17 amacrine cells in mammalian retina in vivo." J Neurophysiol **89**(4): 2159-66.

Dunn, F. A., T. Doan, A. P. Sampath and F. Rieke (2006). "Controlling the gain of rod-mediated signals in the Mammalian retina." J Neurosci **26**(15): 3959-70.

Dunn, F. A. and F. Rieke (2006). "The impact of photoreceptor noise on retinal gain controls." Curr Opin Neurobiol **16**(4): 363-70.

Dunn, F. A. and F. Rieke (2008). "Single-photon absorptions evoke synaptic depression in the retina to extend the operational range of rod vision." Neuron **57**(6): 894-904.

Eggers, E. D. and P. D. Lukasiewicz (2006a). "GABA(A), GABA(C) and glycine receptor-mediated inhibition differentially affects light-evoked signalling from mouse retinal rod bipolar cells." J Physiol **572**(Pt 1): 215-25.

Eggers, E. D. and P. D. Lukasiewicz (2006b). "Receptor and transmitter release properties set the time course of retinal inhibition." J Neurosci **26**(37): 9413-25.

Ellias, S. A. and J. K. Stevens (1980). "The dendritic varicosity: a mechanism for electrically isolating the dendrites of cat retinal amacrine cells?" Brain Res **196**(2): 365-72.

Engel, D. and P. Jonas (2005). "Presynaptic action potential amplification by voltage-gated Na+ channels in hippocampal mossy fiber boutons." Neuron **45**(3): 405-17.

Euler, T., P. B. Detwiler and W. Denk (2002). "Directionally selective calcium signals in dendrites of starburst amacrine cells." Nature **418**(6900): 845-52.

Euler, T. and R. H. Masland (2000). "Light-evoked responses of bipolar cells in a mammalian retina." J Neurophysiol **83**(4): 1817-29.

Faber, E. S., A. J. Delaney and P. Sah (2005). "SK channels regulate excitatory synaptic transmission and plasticity in the lateral amygdala." Nat Neurosci **8**(5): 635-41.

Famiglietti, E. V., Jr. and H. Kolb (1975). "A bistratified amacrine cell and synaptic cirucitry in the inner plexiform layer of the retina." Brain Res **84**(2): 293-300.

Field, G. D. and F. Rieke (2002). "Nonlinear signal transfer from mouse rods to bipolar cells and implications for visual sensitivity." Neuron **34**(5): 773-85.

Freeman, D. K., W. F. Heine and C. L. Passaglia (2008). "The maintained discharge of rat retinal ganglion cells." Vis Neurosci **25**(4): 535-48.

Gill, S. B., M. L. Veruki and E. Hartveit (2006). "Functional properties of spontaneous IPSCs and glycine receptors in rod amacrine (AII) cells in the rat retina." J Physiol **575**(Pt 3): 739-59.

Gollisch, T. and M. Meister (2008). "Rapid neural coding in the retina with relative spike latencies." Science **319**(5866): 1108-11.

Grynkiewicz, G., M. Poenie and R. Y. Tsien (1985). "A new generation of Ca2+ indicators with greatly improved fluorescence properties." J Biol Chem **260**(6): 3440-50.

Habermann, C. J., B. J. O'Brien, H. Wassle and D. A. Protti (2003). "AII amacrine cells express L-type calcium channels at their output synapses." J Neurosci **23**(17): 6904-13.

Hallermann, S., C. Pawlu, P. Jonas and M. Heckmann (2003). "A large pool of releasable vesicles in a cortical glutamatergic synapse." Proc Natl Acad Sci U S A **100**(15): 8975-80.

Hampson, E. C., D. I. Vaney and R. Weiler (1992). "Dopaminergic modulation of gap junction permeability between amacrine cells in mammalian retina." J Neurosci **12**(12): 4911-22.

Hartveit, E. (1999). "Reciprocal synaptic interactions between rod bipolar cells and amacrine cells in the rat retina." J Neurophysiol **81**(6): 2923-36.

Hausselt, S. E., T. Euler, P. B. Detwiler and W. Denk (2007). "A Dendrite-Autonomous Mechanism for Direction Selectivity in Retinal Starburst Amacrine Cells." PLoS Biol **5**(7): e185.

Hecht, S., Schlaer, S., Pirenne, M. H. (1942). "Energy, quanta and vision." J Gen Physiol **25**: 819-840.

Henne, J. and G. Jeserich (2004). "Maturation of spiking activity in trout retinal ganglion cells coincides with upregulation of Kv3.1- and BK-related potassium channels." J Neurosci Res **75**(1): 44-54.

Henne, J., S. Pottering and G. Jeserich (2000). "Voltage-gated potassium channels in retinal ganglion cells of trout: a combined biophysical, pharmacological, and single-cell RT-PCR approach." J Neurosci Res **62**(5): 629-37.

Hicks, G. A. and N. V. Marrion (1998). "Ca2+-dependent inactivation of large conductance Ca2+-activated K+ (BK) channels in rat hippocampal neurones produced by pore block from an associated particle." J Physiol **508 (Pt 3)**: 721-34.

Hines, M. L. and N. T. Carnevale (1997). "The NEURON simulation environment." Neural Comput **9**(6): 1179-209.

Hines, M. L. and N. T. Carnevale (2001). "NEURON: a tool for neuroscientists." Neuroscientist **7**(2): 123-35.

Hobai, I. A., J. A. Bates, F. C. Howarth and A. J. Levi (1997). "Inhibition by external Cd2+ of Na/Ca exchange and L-type Ca channel in rabbit ventricular myocytes." Am J Physiol **272**(5 Pt 2): H2164-72.

Hodgkin, A. L. and A. F. Huxley (1945). "Resting and action potentials in single nerve fibres." J Physiol **104**(2): 176-95.

Hodgkin, A. L. and A. F. Huxley (1952a). "Currents carried by sodium and potassium ions through the membrane of the giant axon of Loligo." J Physiol **116**(4): 449-72.

Hodgkin, A. L. and A. F. Huxley (1952b). "The dual effect of membrane potential on sodium conductance in the giant axon of Loligo." J Physiol **116**(4): 497-506.

Hodgkin, A. L. and A. F. Huxley (1952c). "Propagation of electrical signals along giant nerve fibers." Proc R Soc Lond B Biol Sci **140**(899): 177-83.

Hu, H., L. R. Shao, S. Chavoshy, N. Gu, M. Trieb, R. Behrens, P. Laake, O. Pongs, H. G. Knaus, O. P. Ottersen and J. F. Storm (2001). "Presynaptic Ca2+-activated K+ channels in glutamatergic hippocampal terminals and their role in spike repolarization and regulation of transmitter release." J Neurosci **21**(24): 9585-97.

Huber, D., L. Petreanu, N. Ghitani, S. Ranade, T. Hromadka, Z. Mainen and K. Svoboda (2008). "Sparse optical microstimulation in barrel cortex drives learned behaviour in freely moving mice." Nature **451**(7174): 61-4.

Isaac, J. T., M. Ashby and C. J. McBain (2007). "The role of the GluR2 subunit in AMPA receptor function and synaptic plasticity." Neuron **54**(6): 859-71.

Jackson, M. B. (1993). "Passive current flow and morphology in the terminal arborizations of the posterior pituitary." J Neurophysiol **69**(3): 692-702.

Jiang, J., K. B. Eisenthal and R. Yuste (2007). "Second harmonic generation in neurons: electro-optic mechanism of membrane potential sensitivity." Biophys J **93**(5): L26-8.

Kim, K. J. and F. Rieke (2003). "Slow Na+ inactivation and variance adaptation in salamander retinal ganglion cells." J Neurosci **23**(4): 1506-16.

Kolb, H. and E. V. Famiglietti (1974). "Rod and cone pathways in the inner plexiform layer of cat retina." Science **186**(4158): 47-9.

Kolb, H. and R. Nelson (1983). "Rod pathways in the retina of the cat." Vision Res **23**(4): 301-12.

Lagali, P. S., D. Balya, G. B. Awatramani, T. A. Munch, D. S. Kim, V. Busskamp, C. L. Cepko and B. Roska (2008). "Light-activated channels targeted to ON bipolar cells restore visual function in retinal degeneration." Nat Neurosci **11**(6): 667-75.

Lagnado, L. (2003). "Ribbon synapses." Curr Biol **13**(16): R631.

Lavoie, A. M., J. J. Tingey, N. L. Harrison, D. B. Pritchett and R. E. Twyman (1997). "Activation and deactivation rates of recombinant GABA(A) receptor channels are dependent on alpha-subunit isoform." Biophys J **73**(5): 2518-26.

Lin, M. T., R. Lujan, M. Watanabe, J. P. Adelman and J. Maylie (2008). "SK2 channel plasticity contributes to LTP at Schaffer collateral-CA1 synapses." Nat Neurosci **11**(2): 170-7.

Liu, S. and M. T. Shipley (2008). "Multiple conductances cooperatively regulate spontaneous bursting in mouse olfactory bulb external tufted cells." J Neurosci **28**(7): 1625-39.

Maher, B. J. and G. L. Westbrook (2005). "SK channel regulation of dendritic excitability and dendrodendritic inhibition in the olfactory bulb." J Neurophysiol **94**(6): 3743-50.

Manookin, M. B. and J. B. Demb (2006). "Presynaptic mechanism for slow contrast adaptation in mammalian retinal ganglion cells." Neuron **50**(3): 453-64.

Maravall, M., Z. F. Mainen, B. L. Sabatini and K. Svoboda (2000). "Estimating intracellular calcium concentrations and buffering without wavelength ratioing." Biophys J **78**(5): 2655-67.

Marty, A. (1981). "Ca-dependent K channels with large unitary conductance in chromaffin cell membranes." Nature **291**(5815): 497-500.

McCormick, D. A., Y. Shu and Y. Yu (2007). "Neurophysiology: Hodgkin and Huxley model--still standing?" Nature **445**(7123): E1-2; discussion E2-3.

McKay, B. E. and R. W. Turner (2004). "Kv3 K+ channels enable burst output in rat cerebellar Purkinje cells." Eur J Neurosci **20**(3): 729-39.

Medler, K. and E. L. Gleason (2002). "Mitochondrial Ca(2+) buffering regulates synaptic transmission between retinal amacrine cells." J Neurophysiol **87**(3): 1426-39.

Menger, N. and H. Wassle (2000). "Morphological and physiological properties of the A17 amacrine cell of the rat retina." Vis Neurosci **17**(5): 769-80.

Meredith, A. L., S. W. Wiler, B. H. Miller, J. S. Takahashi, A. A. Fodor, N. F. Ruby and R. W. Aldrich (2006). "BK calcium-activated potassium channels regulate circadian behavioral rhythms and pacemaker output." Nat Neurosci **9**(8): 1041-9.

Millard, A. C., P. J. Campagnola, W. Mohler, A. Lewis and L. M. Loew (2003a). "Second harmonic imaging microscopy." Methods Enzymol **361**: 47-69.

Millard, A. C., L. Jin, A. Lewis and L. M. Loew (2003b). "Direct measurement of the voltage sensitivity of second-harmonic generation from a membrane dye in patch-clamped cells." Opt Lett **28**(14): 1221-3.

Mills, S. L. and S. C. Massey (1995). "Differential properties of two gap junctional pathways made by AII amacrine cells." Nature **377**(6551): 734-7.

Mitra, P. and M. M. Slaughter (2002). "Mechanism of generation of spontaneous miniature outward currents (SMOCs) in retinal amacrine cells." J Gen Physiol **119**(4): 355-72.

Nakajima, K., K. Harada, Y. Ebina, T. Yoshimura, H. Ito, T. Ban and R. Shingai (1993). "Relationship between resting cytosolic Ca2+ and responses induced by N-methyl-D-aspartate in hippocampal neurons." Brain Res **603**(2): 321-3.

Nelson, R. (1982). "AII amacrine cells quicken time course of rod signals in the cat retina." J Neurophysiol **47**(5): 928-47.

Nelson, R. and H. Kolb (1985). "A17: a broad-field amacrine cell in the rod system of the cat retina." J Neurophysiol **54**(3): 592-614.

Nemet, B. A., V. Nikolenko and R. Yuste (2004). "Second harmonic imaging of membrane potential of neurons with retinal." J Biomed Opt **9**(5): 873-81.

Newell, E. W. and L. C. Schlichter (2005). "Integration of K+ and Cl- currents regulate steady-state and dynamic membrane potentials in cultured rat microglia." J Physiol **567**(Pt 3): 869-90.

Ngo-Anh, T. J., B. L. Bloodgood, M. Lin, B. L. Sabatini, J. Maylie and J. P. Adelman (2005). "SK channels and NMDA receptors form a Ca2+-mediated feedback loop in dendritic spines." Nat Neurosci **8**(5): 642-9.

Oesch, N., T. Euler and W. R. Taylor (2005). "Direction-selective dendritic action potentials in rabbit retina." Neuron **47**(5): 739-50.

Orio, P., P. Rojas, G. Ferreira and R. Latorre (2002). "New disguises for an old channel: MaxiK channel beta-subunits." News Physiol Sci **17**: 156-61.

Palmer, M. J. (2006a). "Functional segregation of synaptic GABAA and GABAC receptors in goldfish bipolar cell terminals." J Physiol **577**(Pt 1): 45-53.

Palmer, M. J. (2006b). "Modulation of Ca(2+)-activated K+ currents and Ca(2+)-dependent action potentials by exocytosis in goldfish bipolar cell terminals." J Physiol **572**(Pt 3): 747-62.

Partin, K. M., D. K. Patneau, C. A. Winters, M. L. Mayer and A. Buonanno (1993). "Selective modulation of desensitization at AMPA versus kainate receptors by cyclothiazide and concanavalin A." Neuron **11**(6): 1069-82.

Petreanu, L., D. Huber, A. Sobczyk and K. Svoboda (2007). "Channelrhodopsin-2-assisted circuit mapping of long-range callosal projections." Nat Neurosci **10**(5): 663-8.

Protti, D. A. and I. Llano (1998). "Calcium currents and calcium signaling in rod bipolar cells of rat retinal slices." J Neurosci **18**(10): 3715-24.

Qian, H. and J. E. Dowling (1995). "GABAA and GABAC receptors on hybrid bass retinal bipolar cells." J Neurophysiol **74**(5): 1920-8.

Raffaelli, G., C. Saviane, M. H. Mohajerani, P. Pedarzani and E. Cherubini (2004). "BK potassium channels control transmitter release at CA3-CA3 synapses in the rat hippocampus." J Physiol **557**(Pt 1): 147-57.

Rotaru, D. C., D. A. Lewis and G. Gonzalez-Burgos (2007). "Dopamine D1 receptor activation regulates sodium channel-dependent EPSP amplification in rat prefrontal cortex pyramidal neurons." J Physiol **581**(Pt 3): 981-1000.

Shapley, R. (1997). "Retinal physiology: adapting to the changing scene." Curr Biol **7**(7): R421-3.

Shen, J. B., B. Jiang and A. J. Pappano (2000). "Comparison of L-type calcium channel blockade by nifedipine and/or cadmium in guinea pig ventricular myocytes." J Pharmacol Exp Ther **294**(2): 562-70.

Shevchenko, T., R. Teruyama and W. E. Armstrong (2004). "High-threshold, Kv3-like potassium currents in magnocellular neurosecretory neurons and their role in spike repolarization." J Neurophysiol **92**(5): 3043-55.

Sikora, M. A., J. Gottesman and R. F. Miller (2005). "A computational model of the ribbon synapse." J Neurosci Methods **145**(1-2): 47-61.

Singer, J. H. and J. S. Diamond (2003). "Sustained Ca2+ entry elicits transient postsynaptic currents at a retinal ribbon synapse." J Neurosci **23**(34): 10923-33.

Singer, J. H. and J. S. Diamond (2006). "Vesicle depletion and synaptic depression at a mammalian ribbon synapse." J Neurophysiol **95**(5): 3191-8.

Singer, J. H., L. Lassova, N. Vardi and J. S. Diamond (2004). "Coordinated multivesicular release at a mammalian ribbon synapse." Nat Neurosci **7**(8): 826-33.

Skinner, L. J., V. Enee, M. Beurg, H. H. Jung, A. F. Ryan, A. Hafidi, J. M. Aran and D. Dulon (2003). "Contribution of BK Ca2+-activated K+ channels to auditory neurotransmission in the Guinea pig cochlea." J Neurophysiol **90**(1): 320-32.

Smith, R. G. and N. Vardi (1995). "Simulation of the AII amacrine cell of mammalian retina: functional consequences of electrical coupling and regenerative membrane properties." Vis Neurosci **12**(5): 851-60.

Sterling, P. and L. A. Lampson (1986). "Molecular specificity of defined types of amacrine synapse in cat retina." J Neurosci **6**(5): 1314-24.

Sterling, P. and G. Matthews (2005). "Structure and function of ribbon synapses." Trends Neurosci **28**(1): 20-9.

Strettoi, E., E. Raviola and R. F. Dacheux (1992). "Synaptic connections of the narrow-field, bistratified rod amacrine cell (AII) in the rabbit retina." J Comp Neurol **325**(2): 152-68.

Stuart, G., N. Spruston, B. Sakmann and M. Hausser (1997). "Action potential initiation and backpropagation in neurons of the mammalian CNS." Trends Neurosci **20**(3): 125-31.

Sun, X., X. Q. Gu and G. G. Haddad (2003). "Calcium influx via L- and N-type calcium channels activates a transient large-conductance Ca2+-activated K+ current in mouse neocortical pyramidal neurons." J Neurosci **23**(9): 3639-48.

Takashima, A. and M. Takahata (2008). "Effects of active conductance distribution over dendrites on the synaptic integration in an identified nonspiking interneuron." PLoS ONE **3**(5): e2217.

Tamalu, F. and S. Watanabe (2007). "Glutamatergic input is coded by spike frequency at the soma and proximal dendrite of AII amacrine cells in the mouse retina." Eur J Neurosci **25**(11): 3243-52.

Taylor, W. R., S. Mittman and D. R. Copenhagen (1996). "Passive electrical cable properties and synaptic excitation of tiger salamander retinal ganglion cells." Vis Neurosci **13**(5): 979-90.

Treiman, M., C. Caspersen and S. B. Christensen (1998). "A tool coming of age: thapsigargin as an inhibitor of sarco-endoplasmic reticulum Ca(2+)-ATPases." Trends Pharmacol Sci **19**(4): 131-5.

Trevelyan, A. J. and J. Jack (2002). "Detailed passive cable models of layer 2/3 pyramidal cells in rat visual cortex at different temperatures." J Physiol **539**(Pt 2): 623-36.

Trong, P. K. and F. Rieke (2008). "Origin of correlated activity between parasol retinal ganglion cells." Nat Neurosci.

Tukker, J. J., W. R. Taylor and R. G. Smith (2004). "Direction selectivity in a model of the starburst amacrine cell." Vis Neurosci **21**(4): 611-25.

Vaney, D. I. (1986). "Morphological identification of serotonin-accumulating neurons in the living retina." Science **233**(4762): 444-6.

Veruki, M. L. and E. Hartveit (2002a). "AII (Rod) amacrine cells form a network of electrically coupled interneurons in the mammalian retina." Neuron **33**(6): 935-46.

Veruki, M. L. and E. Hartveit (2002b). "Electrical synapses mediate signal transmission in the rod pathway of the mammalian retina." J Neurosci **22**(24): 10558-66.

Veruki, M. L., S. H. Morkve and E. Hartveit (2003). "Functional properties of spontaneous EPSCs and non-NMDA receptors in rod amacrine (AII) cells in the rat retina." J Physiol **549**(Pt 3): 759-74.

Vigh, J., G. L. Li, C. Hull and H. von Gersdorff (2005). "Long-term plasticity mediated by mGluR1 at a retinal reciprocal synapse." Neuron **46**(3): 469-82.

Vigh, J. and H. von Gersdorff (2005). "Prolonged reciprocal signaling via NMDA and GABA receptors at a retinal ribbon synapse." J Neurosci **25**(49): 11412-23.

Volgyi, B., D. Xin and S. A. Bloomfield (2002). "Feedback inhibition in the inner plexiform layer underlies the surround-mediated responses of AII amacrine cells in the mammalian retina." J Physiol **539**(Pt 2): 603-14.

Wallner, M., P. Meera and L. Toro (1999). "Molecular basis of fast inactivation in voltage and Ca2+-activated K+ channels: a transmembrane beta-subunit homolog." Proc Natl Acad Sci U S A **96**(7): 4137-42.

Wang, G. Y., D. W. Robinson and L. M. Chalupa (1998). "Calcium-activated potassium conductances in retinal ganglion cells of the ferret." J Neurophysiol **79**(1): 151-8.

Wang, Y. W., J. P. Ding, X. M. Xia and C. J. Lingle (2002). "Consequences of the stoichiometry of Slo1 alpha and auxiliary beta subunits on functional properties of large-conductance Ca2+-activated K+ channels." J Neurosci **22**(5): 1550-61.

Warrier, A., S. Borges, D. Dalcino, C. Walters and M. Wilson (2005). "Calcium from internal stores triggers GABA release from retinal amacrine cells." J Neurophysiol **94**(6): 4196-208.

Williams, S. R. and G. J. Stuart (2003). "Voltage- and site-dependent control of the somatic impact of dendritic IPSPs." J Neurosci **23**(19): 7358-67.

Womack, M. D. and K. Khodakhah (2003). "Somatic and dendritic small-conductance calcium-activated potassium channels regulate the output of cerebellar purkinje neurons." J Neurosci **23**(7): 2600-7.

Woodruff, M. L., A. P. Sampath, H. R. Matthews, N. V. Krasnoperova, J. Lem and G. L. Fain (2002). "Measurement of cytoplasmic calcium concentration in the rods of wild-type and transducin knock-out mice." J Physiol **542**(Pt 3): 843-54.

Xu, J. W. and M. M. Slaughter (2005). "Large-conductance calcium-activated potassium channels facilitate transmitter release in salamander rod synapse." J Neurosci **25**(33): 7660-8.

Yang, L., Y. Su, W. Liu, X. Jin and J. Wu (2002). "Sugar interaction with metal ions. The coordination behavior of neutral galactitol to Ca(II) and lanthanide ions." Carbohydr Res **337**(16): 1485-93.

Yasuda, R., E. A. Nimchinsky, V. Scheuss, T. A. Pologruto, T. G. Oertner, B. L. Sabatini and K. Svoboda (2004). "Imaging calcium concentration dynamics in small neuronal compartments." Sci STKE **2004**(219): pl5.

Zhang, F., L. P. Wang, E. S. Boyden and K. Deisseroth (2006). "Channelrhodopsin-2 and optical control of excitable cells." Nat Methods **3**(10): 785-92.

Zhang, J., W. Li, E. B. Trexler and S. C. Massey (2002). "Confocal analysis of reciprocal feedback at rod bipolar terminals in the rabbit retina." J Neurosci **22**(24): 10871-82.

Zipfel, W. R., R. M. Williams and W. W. Webb (2003). "Nonlinear magic: multiphoton microscopy in the biosciences." Nat Biotechnol **21**(11): 1369-77.